ornl

OAK RIDGE NATIONAL LABORATORY

LOCKHEED MARTIN

ORNL/TM-11825

Evaluation of ^{28,29,30}Si Neutron Induced Cross Sections for ENDF/B-VI

D. M. Hetrick, D. C. Larson, N. M. Larson,
L. C. Leal, and S. J. Epperson

MANAGED AND OPERATED BY
LOCKHEED MARTIN ENERGY RESEARCH CORPORATION
FOR THE UNITED STATES
DEPARTMENT OF ENERGY

ORNL-27 (3-96)

DISCLAIMER

DISCLAIMER

ORNL/TM-11825

Evaluation of ^{28,29,30}Si Neutron Induced Cross Sections for ENDF/B-VI

D. M. Hetrick, D. C. Larson,
N. M. Larson, L. C. Leal, and S. J. Epperson
Oak Ridge National Laboratory

April 1997

Prepared by the
OAK RIDGE NATIONAL LABORATORY
Oak Ridge, Tennessee 37831
managed by
LOCKHEED MARTIN ENERGY RESEARCH CORP.
for the
U.S. DEPARTMENT OF ENERGY
under contract DE-AC05-96OR22464

CONTENTS

CONTENTS (cont.)

LIST OF TABLES

LIST OF FIGURES

LIST OF FIGURES (cont.)

LIST OF FIGURES (cont.)

ABSTRACT

Separate evaluations have been done for the three stable isotopes of silicon for ENDF/B-VI. The evaluations are based on analysis of experimental data, supplemented by results of nuclear model calculations. The computational methods and the parameters required as input to the nuclear model codes are reviewed. Discussion of the evaluated data given for resonance parameters, neutron induced reaction cross sections, associated angular and energy distributions, and gamma-ray production cross sections is included. Extensive comparisons of the evaluated cross sections to measured data are shown in this report. The evaluations include all necessary data to allow KERMA (Kinetic Energy Released in MAterials) and displacement cross sections to be calculated directly. These quantities are fundamental to studies of neutron heating and radiation damage.

1. INTRODUCTION

Silicon is an important semiconductor material, so understanding neutron-induced radiation damage effects is very important. There is considerable interest in the cross sections for secondary charged particle production (including recoil nuclei) for radiation damage calculations in electronic components. Since silicon is a major constituent of concrete and soils, neutron and gamma-ray transport information is also important. For these reasons, much effort was put into the ENDF/B-VI evaluations for the three stable isotopes of silicon. The evaluations are based on analysis of experimental data, supplemented by results of nuclear model calculations which reproduce the experimental data.

Evaluated data are given for resonance parameters, neutron induced reaction cross sections, associated angular and energy distributions, and gamma-ray production cross sections. Since very little information exists for the energy distributions of secondary neutrons, and there are no available data for secondary proton and alpha energy distributions (except for the lowest discrete states), nuclear model calculations were relied on to provide the necessary data. The primary code used for the evaluation work was TNG (FU88, SH86), an advanced multistep Hauser-Feshbach code which includes precompound and compound contributions to cross sections in a self-consistent manner, provides correlated angular and energy distributions, calculates gamma-ray production, and conserves angular momentum in all steps. Extensive model calculations were performed for each isotope with the goal of simultaneously reproducing measured data for that isotope using a consistent set of parameters. Internal consistency and energy conservation within each evaluation is ensured.

The new File 6 format of ENDF/B is used to represent energy-angle correlated data and recoil spectra, both present for the first time in the silicon evaluations. Also, for the first time, all necessary nuclear data are given to allow KERMA (Kinetic Energy Released in MAterials) and displacement cross sections to be calculated directly from information available in the evaluation, dependent only upon the quality of the evaluated data. These quantities are fundamental to studies of neutron heating and neutron radiation damage.

This report documents the structure of the evaluations, notes important measured data utilized, gives a summary of the model codes used, and shows the calculations compared to measured data. Preliminary results for radiation damage show the overall quality of the silicon evaluation is much improved over ENDF/B-V and should meet the present needs of the user community.

2. COMPUTATIONAL METHODS AND PROCEDURES

Nuclear model calculations play an important role in modern evaluations for the interpolation and extrapolation of cross sections to energy regions where no data exist, and for predictions of reaction cross sections for which there are few or no experimental data. However, in order to ensure internal consistency, the model calculations should simultaneously reproduce as much of the experimental information as possible for as many reaction channels as reliable data are available. As noted earlier, the primary code used for this evaluation work was TNG (FU88, SH86), an advanced multistep Hauser-Feshbach model. TNG includes precompound and compound contributions to cross sections in a self-consistent manner, provides correlated angular and energy distributions, calculates gamma-ray production, and conserves angular momentum in all steps. The code is capable of using variable energy bin widths for outgoing particle energies, i.e., smaller bins at low outgoing-particle energies and larger ones at high outgoing-particle energies. This capability has eliminated many energy balance problems that occurred previously in cross-section evaluations as a result of using uniform-width energy bins (SH86).

Calculations for ^{28}Si, ^{29}Si, and ^{30}Si at a number of incident energies from 0.01 to 20.0 MeV were performed. Parameters required as input to TNG are discussed in Section 3. Parameters required for the precompound mode of reaction were the same as determined previously (FU88) and were found to be satisfactory for the present calculations. TNG simultaneously computes cross sections for all energetically possible binary reactions and tertiary reactions, and also computes the resulting gamma-ray production cross sections, and outgoing particle spectra as required. The resulting cross-section sets are consistent and energy balance is ensured. The results from TNG are found to agree reasonably well with available data, and these comparisons are discussed in the following sections.

The resonance parameters are given in File 2 ENDF format for the evaluations. When sufficient cross-section data were available, they were evaluated and used directly in the evaluations in File 3 format of ENDF; otherwise calculations are used. The new File 6 ENDF format is used to represent the TNG computed energy-angle correlated data for each product of each reaction. Neutron, proton, alpha, recoil (for first time in the silicon evaluation), and gamma-ray spectra are represented. Angular distributions are given for the neutron emission spectra for ^{28}Si only and isotropy is assumed for the other isotopes and particles. Branching ratios for the discrete levels are given directly in File 12 format; i.e., the continuum and discrete gammas are given separately in the evaluations. Also, for the first time, all necessary nuclear data are given to allow KERMA (Kinetic Energy Released in MAterials) and displacement cross sections to be calculated directly from information available in the evaluation, dependent only upon the quality of the evaluated data. These quantities are fundamental to studies of neutron heating and neutron radiation damage.

The following sections review the important measured data considered in the evaluations, and examples of calculations compared to the data are given. Discussions of contents of the evaluations are included.

3. PARAMETER DETERMINATION

3.1. RESONANCE PARAMETERS

Resonance parameters for the three isotopes of silicon were determined by a new self-consistent analysis of relevant data, including both natural and isotopically-enriched samples. Oxygen data were also included in the analysis, since the isotopically-enriched samples were oxides rather than pure silicon. Thermal elastic and capture values were likewise included. The multilevel R-matrix code SAMMY (LA96) was used for the analysis, which incorporated both Doppler and resolution broadening as well as other measurement-specific effects.

Using results from Mughabghab et al. (MU81) and Weigmann et al. (WE87) as guidance, parameters were determined for 58 resonances in ^{28}Si, of which five resonances are negative-energy "dummies" (whose values determine the thermal cross sections) and nine lie above the cutoff energy of 1.75 MeV. Twenty-nine resonances are specified for ^{29}Si, of which three are at negative energies and two lie above the cutoff energy of 1.50 MeV. Twenty-nine resonances are given for ^{30}Si, of which two are at negative energies and two are above the cutoff of 1.50 MeV. The set of data used for the resonance region analysis is summarized in Table 1. The resonance parameters obtained, with assigned spin and parity values, are given for the isotopes of ^{28}Si, ^{29}Si, and ^{30}Si in Tables 2-4, respectively. More details and plots of the SAMMY fit are given in Section 4 for the total cross section; a full report describing the resonance analysis is in preparation (LE97).

3.2 NEUTRON OPTICAL-MODEL POTENTIAL

Since optical-model parameters are essential input for nuclear model codes, a series of optical model studies were performed in an attempt to generate a consistent set of neutron optical model parameters. Thirty four elastic scattering angular distributions from 4 to 14 MeV were used in a global search using the code GENOA (PE67) with the aim of fitting each angular distribution, the energy averaged total cross section, and the available nonelastic cross section. In order to speed up the searching and averaging over resonant effects, angular distributions measured at nearby energies were averaged, resulting in a set of eight distributions at 4.25, 4.80, 5.25, 5.80, 6.60, 7.75, 8.75, and 14.1 MeV. In addition, two single measurements at 9.8 and 10.95 MeV were used in the search. Details about the individual measurements are listed in Table 5.

In the global search by GENOA, a compound elastic term was included, the shape determined from preliminary Hauser-Feshbach calculations using an average set of parameters and including competition between the (n,n'), (n,p), and (n,α) channels. The shape of the compound elastic contribution at the energies of the averaged data sets were fed into GENOA, and the magnitude of the compound elastic contribution was searched on, in addition to the various parameters of the optical model. A series of searches resulted in a set of optical model parameters which provided a good overall fit to the averaged angular distributions as well as to the average total and nonelastic cross sections. The resulting magnitude of the compound elastic contribution was checked later against the compound elastic channel in the final stages of the Hauser-Feshbach calculations and the two results were found to be in agreement to better than 10%.

Details of the searching technique are similar to those used by C. Y. Fu (FU76) in the calcium evaluation, and will not be discussed further here. Table 6 presents the final set of neutron optical model parameters arrived at and used in the remainder of the evaluation. Figures 1 through 5 show the final fits obtained to the data sets at incident energies of 4.8, 5.8, 7.75, 9.8, and 14.1 MeV.

3.3 CHARGED-PARTICLE OPTICAL-MODEL PARAMETERS

Proton and alpha optical model parameters were also required for the Hauser-Feshbach analysis. The proton parameters were taken from the work of Perey (PE63, PE74). The alpha parameters were taken from the 5 MeV set given by S. S. So (SO66), with the real radius changed from 1.80 f to 1.70 f. The proton and alpha parameters are given in Table 6.

3.4 THE DIRECT REACTION MODEL AND PARAMETERS

The Distorted Wave Born Approximation (DWBA) program DWUCK (KU72) was used to calculate the direct-interaction component of the inelastic-scattering cross sections to a number of levels in ^{28}Si for which information was available. Inputs to this code were the neutron optical-model parameters of Table 6 and the deformation parameters, β^2_l, shown in Table 7. The value of the deformation parameter β^2_l for the 1.779 MeV level was found to yield the correct amount of direct interaction such that when combined with the compound reaction contribution, a good fit to the data was obtained as shown in Fig. 6 (note that the TNG calculation for this level was not used in ENDF/B-VI; see Section 8) . This value of β^2_l is higher than most found in the literature (e.g., see HA84, OB73, SE86, DE79, KL78, BO83, ST65a, HO69, CL64, and AL86) but is the same as that found by Crawley and Garvey (CR67) in the analysis of their 17.5 MeV (p,p') experiment, and was used successfully by Brandenberger et al. (BR72) for their analysis of 8 and 9 MeV neutron scattering. The β^2_l used for the 4.617 MeV level was obtained from Hohn et al. (HO69) and is also higher than other reported values (e.g., see HA84, SE86, and AL86), but the lower β^2_l's did not yield enough calculated direct interaction cross section (see Fig. 7 for the TNG calculation versus data for this level). For the higher lying levels, β^2_l values from available references (see Table 7) were averaged to obtain the values shown in Table 7.

The partial excitation functions ^{28}Si(n,p$_i$)^{28}Al were computed by TNG, but no direct interaction contributions were included because of lack of data. A direct reaction contribution was included for ^{28}Si(n,α_0)^{25}Mg and ^{28}Si(n,α_1)^{25}Mg, computed by taking the compound contribution for each level from a preliminary TNG calculation times 33 and 17 percent, respectively, as recommended by Hermsdorf (HE82a).

The resulting calculated direct interaction contributions, shown in Figure 8 for the inelastic excitation cross sections and Figure 9 for the lowest two states in ^{25}Mg, were used as input to the Hauser-Feshbach code TNG for the purpose of including the direct interaction effects in the gamma-ray cascade calculation. All TNG results were automatically scaled to maintain the same total reaction cross section.

3.5 DISCRETE ENERGY LEVELS AND LEVEL-DENSITY PARAMETERS

The statistical-model calculations with TNG require a complete description of the energy levels of the residual nuclei for the various open channels. The low-energy excitation region of these nuclei can be adequately described in terms of discrete levels for which we usually know the energy, spin and parity (J^{π}), and gamma-ray deexcitation branching ratios, hereinafter referred to as branching ratios. As the excitation energy increases, our knowledge of these levels becomes incomplete, and eventually, as their number increases, it is preferred to describe them in terms of a level density formula. In this section we give the discrete levels used in the calculations and discuss the level density formulae and parameters.

The reactions for which we need level information for the residual nuclei are: $^{28}Si(n,n')^{28}Si$, $^{28}Si(n,p)^{28}Al$, $^{28}Si(n,\alpha)^{25}Mg$, $^{28}Si(n,np)^{27}Al$, $^{28}Si(n,n\alpha)^{24}Mg$, $^{28}Si(n,2n)^{27}Si$, and $^{28}Si(n,\gamma)^{29}Si$ for ^{28}Si; $^{29}Si(n,n')^{29}Si$, $^{29}Si(n,p)^{29}Al$, $^{29}Si(n,\alpha)^{26}Mg$, $^{29}Si(n,np)^{28}Al$, $^{29}Si(n,n\alpha)^{25}Mg$, $^{29}Si(n,2n)^{28}Si$, and $^{29}Si(n,\gamma)^{30}Si$ for ^{29}Si; $^{30}Si(n,n')^{30}Si$, $^{30}Si(n,p)^{30}Al$, $^{30}Si(n,\alpha)^{27}Mg$, $^{30}Si(n,np)^{29}Al$, $^{30}Si(n,n\alpha)^{26}Mg$, $^{30}Si(n,2n)^{29}Si$, and $^{30}Si(n,\gamma)^{31}Si$ for ^{30}Si. The level energies, J^{π} values and gamma-ray branching ratios adopted for these nuclei are given in Tables 8 to 20 and were mostly taken from the compilation of Endt and Van der Leun (EN78) or the Table of Isotopes (BR78). There are a few levels where the energies are known, but J^{π} values or branching ratios are experimentally undetermined. These J^{π} values and branching ratios were assigned as indicated by the parentheses in the tables. In most cases, these values are as given in the references; others were estimated from systematics. It should be noted that excited states were reported having excitation energies larger than for levels shown in Tables 8 through 20. However, the branching ratios for these higher levels were not known and thus the levels were not explicitly used in the calculations.

To represent the continuum excitation energy region occurring above the highest-energy discrete level (continuum cutoff E_c), the level-density formulae as described by Fu (FU76, FU80) were used. The level-density parameters of the residual nuclei of all reactions analyzed are given in Table 21. Gilbert and Cameron (GI65) was referenced in obtaining these parameters, but several exceptions to using their parameters and formulae are now noted. It was found that for computing the spin-cutoff parameter "c" a formula due to Facchini and Saetta-Menichella (FA68) produced better results and was used for excitation energies greater than the tangency point (E_x). The spin cutoff parameter at E_c was based on the cumulative sum of the discrete values. In between E_x and E_c, the spin cutoff parameter was assumed to vary linearly with the excitation energy. Also, the parameter "a" for the residual nuclei ^{29}Al, ^{27}Mg, and ^{25}Mg was altered from those given in Gilbert and Cameron (GI65) so that calculated results from TNG gave better reproduction of the available data for the $^{29}Si(n,p)^{29}Al$, $^{30}Si(n,\alpha)^{27}Mg$, and $^{28}Si(n,\alpha)^{25}Mg$ reactions (see comparisons to data in Section 8).

3.6 GIANT DIPOLE RESONANCE PARAMETERS

The giant dipole resonance parameters used as input to TNG in this analysis are those reported by Fuller et al. (FU73). The resonance has a peak cross section of 52 mb, the width of the resonance is 5 MeV, and the energy of the resonance peak is 20.2 MeV.

4. THE TOTAL CROSS SECTION

The evaluation for the total cross section is based upon a resonance parameter analysis of available data for all three isotopes, as well as natural sample data (see Section 3.1). The analysis extended from 10^{-5} eV to 1.75 MeV, a convenient cutoff just below the first inelastic level of ^{28}Si. Above 1.75 MeV, recent 200-m high resolution total cross section data (HA93) for a sample of natural silicon were averaged and used in the evaluation for each isotope, since no data for the individual isotopes were available at the higher energies, and to ensure consistency of the isotopic data with the natural material. Tables 1-4 summarize the data used for the resonance region analysis and the resonance parameters obtained. Figures 10-11 present plots of the SAMMY fit to the various data sets. A brief discussion will now be given for each isotope.

4.1 ^{28}Si TOTAL CROSS SECTION

The experimental thermal scattering value was taken from Mughabghab (MU81), and given as 1.992±0.006 b. Five negative-energy resonances were included in the analysis, which gave a thermal value of 1.992 b and a good fit to available low energy cross section data. A total of 49 resonances were determined for ^{28}Si up to 1.75 MeV, and an additional 9 resonances were used to reproduce the average cross section above the cutoff energy.

4.2 ^{29}Si TOTAL CROSS SECTION

The experimental thermal scattering value was calculated from the scattering lengths in Mughabghab as 2.784±0.193 b. Three negative energy resonances were utilized in the fit and provided a thermal scattering value of 2.779 b. The data of Harvey et al. (HA96) starting at 100 keV also helped determine the three values of the negative energy scattering resonances. Since the data were from a silicon dioxide sample, the oxygen total cross section was also included in the SAMMY fit, which stopped at 1.50 MeV, corresponding to the end of the isotopic ^{29}Si data. A total of 24 resonances were identified from 10 keV to 1.5 MeV, and two additional resonances were utilized above the cutoff energy to reproduce the average cross section. The SAMMY calculation for ^{29}Si was used to bridge the gap from 1.5 to 1.75 MeV, above which energy the pointwise representation for the natural element was utilized. (Note: The cutoff energy in the evaluated file was set to 1.3 MeV to avoid inconsistencies with the threshold energy of the first inelastic level.)

4.3 ^{30}Si TOTAL CROSS SECTION

The experimental thermal scattering value of 2.49±0.04 b was taken from Mughabghab. Two negative energy resonances were utilized in the fit and provided a thermal scattering value of 2.50 b. The $^{30}SiO_2$ data of Harvey et al. (HA83) were used from 100 keV to 1.5 MeV in the analysis to identify the resonance parameters. A total of 25 resonances from 2 keV to 1.5 MeV were identified for ^{30}Si, and two resonances were utilized above the cutoff energy to reproduce the average cross section. As for ^{29}Si, the SAMMY calculation for ^{30}Si was used to bridge the gap from 1.5 to 1.75 MeV.

5. THE NONELASTIC CROSS SECTION

The nonelastic cross section represents the sum of all reaction processes except the elastic scattering. The available experimental data on the nonelastic cross section are very scarce and are shown in Fig. 12 versus the calculation from TNG (0.9221 * ^{28}Si + 0.047 * ^{29}Si + 0.0309 * ^{30}Si) and the ENDF/B-VI for ^{28}Si.

6. THE ELASTIC CROSS SECTION

Below 5 eV the elastic scattering cross section is taken as constant at 2.042 b (DI71). At energies above 5 eV, the evaluated elastic cross section is taken as the difference between the total cross section and the evaluated nonelastic cross section. The evaluated elastic cross section for ^{28}Si from 4 to 20 MeV is shown in Fig. 13 compared to available data for ^{nat}Si. The experimental data points were obtained by integration of angular distribution measurements. It should be noted that the energy resolution of the experimental data for elastic scattering in general is much poorer than the resolution available in modern transmission measurements. Thus the data do not verify the detailed structure in the evaluated curve, but on the average the agreement is quite good. At incident neutron energies above 10 MeV where the fluctuation of the total cross section is small, the evaluated elastic cross section is in good agreement with the results of the optical model calculations that were discussed in Section 3.2.

7. THE CAPTURE CROSS SECTION

Average values for capture widths corresponding to spins and parities of the resonances for each isotope were estimated from capture widths given in Mughabghab (MU81), and used for resonances which did not have experimentally determined values in Mughabghab. Thermal values were taken from Raman et al. (RA92), with the negative energy resonance capture values adjusted to reproduce the values obtained by Raman et al. Above the resonance region (1.75 MeV) for each isotope, the calculated capture shape from TNG was used and normalized to provide an approximate fit to available experimental data, including points around 14 MeV. Experimental and calculated thermal values from Raman et al. for ^{28}Si were (169±4, 169) mb, for ^{29}Si were (119±3, 120) mb and for ^{30}Si were (107±3, 107) mb.

8. THE (n,particle) REACTIONS

8.1 INELASTIC SCATTERING TO THE DISCRETE LEVELS

The inelastic scattering to the 1.779 MeV level was taken from the ENDF/B-V. This cross section was reevaluated from ENDF/B-IV from threshold to about 9 MeV based on data of Kinney and Perey (KI70), and high resolution data of Dickens et al. (DI70, DI74) and Perey et al. (PE71). These data were in good agreement up to about $E_n = 3.5$ MeV, where the Perey et al. data stops. The gamma-ray production data of Dickens for the 1.779 level goes up to $E_n = 9$ MeV. There is still structure above $E_n = 6$ MeV in the gamma-ray data, which is dominated by excitation of the 1.779 level directly. However, there is significant feeding from the higher levels to the 1.779 level above 6 MeV, as indicated by TNG calculations. Thus, the structure above 6 MeV was included for the 1.779 level, but a linear cross section sigma=aE+b was removed from the Dickens data, with a,b chosen so as to match other inelastic cross section data for the 1.779 MeV level which exist at about 9 MeV. Figure 14 presents the evaluation of the cross section for the 1.779 MeV level compared with measured data. The high resolution data is not shown for clarity, since it is essentially the same as the evaluated curve.

The inelastic cross section to the 4.617 MeV level was also taken from ENDF/B-V. The evaluation for this level was lowered from ENDF/B-IV in order to better fit the available data (see Fig. 15). Inelastic scattering data to higher lying states in ^{28}Si is much sparser than for the first two levels, but shows the same wide fluctuations in adjacent data points, assumed to be due to the underlying resonance structure. The evaluated cross sections for these levels are based on the results of the TNG analysis, using available data as a guide. As mentioned in Section 3, a direct interaction component was included for the 6.276, 6.879, and 6.889 levels. Comparisons to data for the 4.979 and 6.276 MeV levels are shown in Figs. 16-17, and for the sum of levels 6.879 and 6.889 in Fig. 18. Several additional inelastic levels up to 8 MeV in ^{28}Si were included in the evaluation and were taken from the TNG analysis, but without benefit of comparison to measurements.

Discrete inelastic levels up to 6.0 MeV in ^{29}Si and 5.0 MeV in ^{30}Si were included in the respective evaluations. The TNG analyses were used exclusively since there is no available data. A direct interaction component was not included.

8.2 THE ^{28}Si(n,p)^{28}Al REACTION

There is considerable interest in the cross section for secondary charged particles for radiation damage calculations in electronic components. For this reason, much effort was put into generating a consistent evaluation for the (n,p) and (n,α) reactions. The total (n,p) cross section for ^{28}Si is based on measurements from threshold up to $E_n = 9$ MeV, and then extrapolated via the TNG calculation from 9 MeV to 20 MeV, constrained by the scattered available data. The TNG energy distributions are given for the proton, ^{28}Al residual, and gamma rays in File 6 format. Prior to incorporation in File 6, the proton energy distributions from TNG were input to the RECOIL code (FU85), which converts the distributions from the center of mass to the laboratory frame, and computes the energy spectra of the heavy recoil nucleus. In addition, cross sections and angular distributions are given for individual

levels (n,p_i) up to 3 MeV in the residual nucleus ^{28}Al, again based on calculation and using the available data as a guide.

There is considerable (n,p) data available for silicon since it can serve simultaneously as a sample and detector. Data obtained in this manner is useful up to a neutron energy at which peaks from the (n,p) and (n,α) reactions overlap. However, the reaction product ^{28}Al is radioactive and β decays back 100% to the 1.779 MeV level in ^{28}Si, which then decays to the ground state. Hence either the resulting β or γ radiaton can be detected and used to obtain the (n,p) cross section at any neutron energy.

From threshold to 6 MeV, the evaluation is based on the β-decay data of Marion, Brugger, and Chapman (MA56). This was an activation experiment in which absolute beta counting techniques were employed. From 6 to 9 MeV the data of Bass et al. (BA66) were used, in which they also detected the resulting β-radiation. These were both relatively high resolution experiments which show much resonant structure, and were in substantial agreement with other available data. An excellent discussion of the relative merits of the various data sets available in this energy range can be found in Drake's description of his 1968 evaluation (DR68).

Above 9 MeV the evaluation is based on the results of the TNG calculations. The calculations were adjusted to reproduce cross sections to the low-lying groups of states p_{0+1} and p_{2+3} as measured by Mingay et al. (MI71), Andersson-Lindstrom and Zauzig (AN65), Grimes (GR69), Mainesbridge et al. (MA63), Shannon and Trice (SH66), Debertin et al. (DE67), Potenza et al. (PO63), and Robertson and Zieba (RO72). Above about 8 MeV, the cross sections agreed in magnitude on the average, with some differences in resonance peak locations (see Figs. 19 and 20). The calculations are a good average representation of the data. Cross sections to the higher lying states p_4, p_5, etc. were taken directly from the TNG results.

As noted earlier, up to $E_x = 3$ MeV in ^{28}Al, discrete levels were used in the Hauser-Feshbach analysis, while for $E_x > 3$ MeV a level density representation was employed. Final results for ^{28}Si(n,p)^{28}Al are shown in Fig. 21 and the TNG calculations (for $E_n > 9.0$ MeV) are a good compromise between the several discrepant data sets. From 14 MeV to 20 MeV, the tertiary reaction channels (n,pγ) and (n,pn) are open, but the measurements based on the β decay of ^{28}Al or the resulting gamma ray measure only the (n,pγ) component. These cross sections will be more fully discussed in the section on tertiary reactions.

8.3 THE ^{28}Si(n,d)^{27}Al REACTION

There have been no new measurements of the (n,d) reaction since the evaluation of Drake (DR68), so this evaluated cross section is adopted. The threshold for this reaction is 9.7 MeV, and the cross section rises to a maximum of 19 mb around 14 MeV and then decreases with energy up to 20 MeV. This cross section is very speculative, but in any case is not large.

8.4 THE $^{28}Si(n,\alpha)^{25}Mg$ REACTION

The $^{28}Si(n,\alpha)$ reaction leads to ^{25}Mg, which is stable. Consequently, the several measurements available are from detection of the alpha groups resulting from excitation of discrete levels in ^{25}Mg. A few MeV above the threshold (E_{th} = 2.75 MeV), the experimental resolution is insufficient to resolve the individual groups. A total helium production cross section measurement for Si at an incident energy of 14.8 MeV due to Kneff et al. (KN86) is the only cross section available at 14 MeV. We must therefore rely on the results of the TNG calculations for the (n,α) cross section above about 8 MeV. The TNG computed normalized distributions are given for the alpha, ^{25}Mg residual (as for the proton, the RECOIL code (FU85) was used), and gamma rays in File 6 format. In addition, cross sections and angular distributions are given for individual levels up to 4.8 MeV in the residual nucleus ^{25}Mg, based on calculation and using the available data as a guide.

From threshold to 8.4 MeV, the 1968 evaluation of Drake is adopted (DR68). This evaluation was compared with data available from Grimes (GR69) and Miller and Kavanagh (MI67) and excellent agreement both in structure and magnitude was found.

Above 8.4 MeV TNG results are used, as other alpha particle groups are contributing to the cross section, but can not be resolved. However, measurements for the low-lying groups α_0-α_5 are available and are shown versus the TNG calculations in Figs. 22-27. Alpha optical model parameters from So et al. (SO66) were used in the TNG calculations and were found to satisfactorily reproduce the measured cross sections to the low-lying states. The level density parameters were adjusted to reproduce the total helium production cross section of Kneff et al. (KN86). TNG calculations for the (n,α) and $(n,\alpha n)$ + $(n,n\alpha)$ reactions of the minor isotopes ^{29}Si and ^{30}Si are combined with ^{28}Si and shown in Fig. 28 versus Kneff's measured value. In addition, the gamma-ray production for photons arising from transitions in ^{25}Mg was checked and found to be in good agreement with the gamma-ray production data of Dickens et al. (DI70, DI73).

8.5 THE (n,p) AND (n,α) REACTIONS FOR ^{29}Si, ^{30}Si

TNG calculations are compared to available data for $^{29}Si(n,p)$, $^{29}Si(n,\alpha)$, and $^{30}Si(n,\alpha)$ in Figs. 29-31. The measurements are quite discrepant and the Hauser-Feshbach analysis offers a good compromise. The calculation for $^{30}Si(n,p)$ is shown in Fig. 32. The calculated results are adopted for the cross sections and normalized distributions for each of these reactions in the evaluations.

8.6 TERTIARY REACTION CROSS SECTIONS

Little or no data exist for the tertiary reaction cross sections of the isotopes of silicon with which to compare the TNG calculations and thus the TNG results are used in the evaluations. Measured ^{28}Al and ^{29}Al production cross sections are compared with computed values from TNG in Figs. 33 and 34. The good agreement allows confidence for the calculated (n,np)+(n,pn) cross sections for ^{29}Si and ^{30}Si. Note that the calculation for $^{29}Si(n,np)+(n,pn)$ is too small compared to the data of Ikeda et al. (IK88) as shown in Fig. 35.

No data were available for the (n,2n) or the (n,αn)+(n,nα) reactions. The (n,2n) and (n,αn)+(n,nα) cross sections calculated by TNG for the three Si isotopes are presented in Figs. 36 and 37, respectively.

The energy distributions for the outgoing particles were taken from the TNG calculations for the tertiary reactions. RECOIL (FU85) was used to convert the distributions from the center of mass to the laboratory frame, and to compute the energy spectra of the heavy nuclei. The distributions for particles from (n,np) and (n,pn) were weighted by their cross sections and combined for the evaluations, with a similar treatment for (n,nα) and (n,αn). Angular distributions are given only for the outgoing neutrons in ^{28}Si; isotropy is assumed for the other particles and gamma rays.

9. ANGULAR DISTRIBUTIONS

9.1 ELASTIC ANGULAR DISTRIBUTIONS

There is a large amount of neutron elastic scattering data from 40 keV to 15 MeV. Below 40 keV, the angular distribution is assumed to be isotropic, which was observed by Lane et al. (LA61, LA62).

From 40 keV to 800 keV, the distributions were taken from a R-function analysis of the data of Kinney and McConnell (KI76). The angular distribution data of Kinney and McConnell (thinned) were used between 800 keV and 3 MeV. The data at 3.1 MeV are from Popov (PO61) and those at 3.5 MeV are from Tanaka (TA64). As noted in Section 3.2, from 4 to 9 MeV, angular distributions measured at nearby energies were averaged, resulting in a set of seven distributions at 4.25, 4.8, 5.25, 5.8, 6.6, 7.75, and 8.75 MeV. The average distributions were obtained by fitting a Legendre series to each data set and averaging the coefficients to obtain the results used in the evaluation. The data sets which make up each averaged group are given in Table 5. The data at 9.8 MeV are from the work of Obst and Weil (OB73), and at 10.95 MeV from Nellis and Buchanan (NE72). From 11 to 20 MeV, the results of the optical model calculations from GENOA (PE67) are used to provide the recommended data set.

9.2 INELASTIC ANGULAR DISTRIBUTIONS

For the discrete levels 1.779, 4.617, 6.276, 6.879, and 6.8899 MeV of ^{28}Si, the angular distributions in ENDF/B-VI are a weighted sum of Legendre coefficients from the TNG and direct interaction (DWUCK) calculations. The angular distributions for all other levels of ^{28}Si, ^{29}Si, and ^{30}Si were taken from the TNG analyses. The calculated differential (n,n') cross sections for exciting selected low-lying discrete levels are compared with measurements in Figs. 38 through 49. The need for nuclear model analyses and better data can be seen from these figures for in many cases the measurements disagree with each other.

9.3 ANGULAR DISTRIBUTIONS OF NEUTRON-PRODUCTION CROSS SECTIONS

The computed angular distributions of neutron production cross sections for silicon at an incident energy of 14.5 MeV and for secondary energies of E'_n = 2.0-3.0, 4.0-5.0, 6.0-7.0, and 7.0-8.0 MeV are compared with experiments in Fig. 50. Again, discrepancies exist among the measured data sets. The results for E'_n = 7.0-8.0 MeV correspond to levels in the discrete region and include the sum of TNG and DWUCK calculations. For E'_n = 6.0-7.0 MeV, the results are also in the discrete region but are symmetric since there was no direct interaction contribution included and TNG computes the angular distributions for only the compound component of the discrete levels. The computed results lie below the data for the low outgoing energies and will be discussed further in the section on neutron emission below.

10. NEUTRON EMISSION SPECTRA

Neutron emission spectra were computed via TNG for 35 incident energies for each silicon isotope. However, measurements are available only for the incident energy range from 14.0 to 14.6 MeV. Comparison of the calculated neutron spectra at an incident energy of 14.5 MeV (weighted sum of ^{28}Si, ^{29}Si, and ^{30}Si) with the natural silicon experimental data is shown in Fig. 51. The data of Clayeux and Voignier (CL72) were measured at 90 degrees and the data of Hermsdorf et al. (HE75, HE82) and Takahashi et al. (TA83) are angle integrated. The calculation is angle integrated and includes the direct inelastic cross sections from DWUCK that were input to the TNG code. The figure shows the calculated total neutron emission spectra as well as the spectra associated with the individual contributing reactions.

It appears that the calculated neutron emission is too small at low outgoing energies. Experimentally, low energy neutrons form the largest part of the background, so background subtraction is especially difficult in this region of the spectrum. It has been observed that the data of Clayeux and Voignier (CL72) for several elements differ significantly at low outgoing neutron energy from the data of Hermsdorf et al. (HE75) and others (see HE79). In most cases, the energy-integrated neutron emission cross sections obtained from the data of Clayeux and Voignier are much larger than the calculated results, due to the large number of low energy neutrons indicated in their work. It has also been observed that the data of Takahashi et al. (TA83) is too large at low outgoing neutron energies (FU86). Finally, since there is good overall agreement between calculation and experiment in the nonelastic cross section, the various partial reaction cross sections, and gamma-ray production spectra (see below), and since energy conservation must be satisfied, the computed neutron emission compared to measurements as shown in Fig. 51 is judged to be acceptable.

In the ^{28}Si evaluation, the TNG computed angular distributions are given for the outgoing neutrons from each individual contributing reaction in File 6 format. Normalized distributions (isotropy is assumed) are given for ^{29}Si and ^{30}Si. Again, the neutron distributions from TNG were used as input to the RECOIL code (FU85) which converts the distributions from the center of mass to the laboratory frame, and computes the energy spectra of the heavy recoil nuclei.

11. GAMMA-RAY PRODUCTION CROSS SECTIONS

11.1 GAMMA-RAY EXCITATION FUNCTIONS

As discussed previously, a consistent and iterative Hauser-Feshbach analysis was employed to reproduce as faithfully as possible data from (n,n'), (n,p), and (n,α) reactions and the total cross section. The results of this analysis, coupled with the gamma ray branching ratios (see Tables 8-20), were used to calculate the resulting gamma ray production from these reactions. The computed excitation functions for four gamma rays of ^{28}Si, two gamma rays of ^{29}Si, and two gamma rays of ^{30}Si are shown in Figs. 52-59 compared to available measurements. Also, representative cross sections from the (n,pγ) and (n,aγ) reactions are compared to the calculations in Figs. 60-64. In general, the calculations are a good compromise for the discrepant data.

11.2 INTEGRATED YIELD OF SECONDARY GAMMA RAYS

The integrated yield of secondary gamma rays with $E_\gamma \geq 0.7$ MeV for the TNG calculations and measurement of Dickens et al. (DI73) are shown in Fig. 65. For clarity, the data of Dickens et al. were plotted at the midpoints of the incident neutron energy bins. The calculated yields agree quite well with the data.

11.3 GAMMA-RAY PRODUCTION CROSS SECTIONS AND SPECTRAL COMPARISONS

The calculated gamma-ray production cross sections are compared to the data measured by Dickens et al. (DI73) in Figs. 66 through 68. Although the measurement, as well as the calculations by TNG, were made at numerous incident energies, comparisons are shown only for energies of 5.5, 9.5, and 14.5 MeV. In each figure, the computed secondary spectra were smeared by a Gaussian function corresponding to the resolution of the detector for the data. The peak near $E_\gamma = 1.0$ MeV is from (n,pγ)+(n,αγ), the peak near $E_\gamma = 1.25$ MeV is (n,αγ), $E_\gamma = 1.78$ MeV is from (n,n'γ), $E_\gamma = 2.2$ MeV is from (n,pγ), $E_\gamma = 2.8$ MeV is from (n,n'γ), and the peaks near $E_\gamma = 4.5$, 5.0, and 7.0 MeV are from (n,n'γ). In general, the calculations provide a good reproduction of the experimental data, and in addition provide information on the cross sections for $E_\gamma < 0.7$ MeV. The calculated energy-dependent yield and the TNG normalized distributions for the gamma ray are given for each reaction using the File 6 format in ENDF/B-VI. For the discrete levels, the branching ratios are given directly in ENDF/B-VI in file 12 format and thus the continuum and discrete gammas are given separately in the evaluations.

Note that the energy dependence of the gamma ray cross sections is very useful as an independent check on the energy dependence of various partial cross sections, and frequently provide the bulk of the experimental information for some reactions. This is especially true when the neutron energies are high enough that tertiary reactions such as (n,np) are possible. There is frequently very little reliable data on such reactions, as direct measurements are difficult to untangle. However, the gamma rays associated with the residual nuclei show up clearly and reproducing the gamma ray cross sections with a model insures that the particle cross sections are at least approximately correct.

12. UNCERTAINTY INFORMATION

Uncertainty files are given for all cross sections in File 3, including inelastic scattering (levels and continuum), but not for the resonance parameters, energy distributions, angular distributions, or gamma-ray production. Fractional and absolute components, correlated only within a given energy interval, are based on data and estimates of uncertainties associated with the model calculations. Details of the approaches used are given in Hetrick et al. (HE91).

13. KERMA AND DAMAGE CALCULATIONS

Improvements to ENDF/B-VI for KERMA and damage calculations are discussed in detail by Larson et al. (LA91). In summary, prior to ENDF/B-VI, evaluations did not contain spectral distributions for outgoing charged particles, so only approximations could be made for heating and KERMA. Many evaluations in ENDF/B-V had serious problems with energy balance. In contrast, energy conservation is achieved for all reactions of silicon in ENDF/B-VI at all energies to better than 1%. Also, since most structural materials had elemental rather than isotopic evaluations in ENDF/B-V, average reaction Q-values had to be used, thereby introducing added inaccuracies. Therefore, the principal improvements in the ENDF/B-VI versus ENDF/B-V for Si regarding KERMA and damage calculations include (1) use of isotopic evaluations to eliminate the need for average Q values, (2) use of sophisticated nuclear model codes benchmarked against measured data to provide energy distributions for all outgoing charged particles, and (3) use of File 6 formats which allowed energy-angle correlated data to be stored, as well as recoil spectra. Thus, now KERMA can be calculated directly and depends only upon the quality of the nuclear data, and not on the severity of the approximation required to compute the average energy (LA91). Table 22 presents the ^{28}Si KERMA computed from ENDF/B-VI and the ^{nat}Si KERMA calculated from ENDF/B-V. The table shows that KERMA could not be computed from ENDF/B-V for several reactions.

14. SUMMARY AND CONCLUSIONS

Advanced nuclear model codes, an improved experimental data base, more flexible ENDF formats, and isotopic evaluations were used for the evaluation of silicon in ENDF/B-VI. Cross sections for all important reactions, with pre-equilibrium effects included, are given. Measurements are used to benchmark the model calculations. Neutron, charged particle (including recoil for the first time), and gamma-ray spectra are provided. Energy conservation is achieved to less than 1% for all reactions at all energies. For the first time, the required nuclear data are given to allow KERMA, heating, displacement cross sections, etc., to be calculated directly from information available in the evaluation. Thus, these quantities are derived without approximation and dependent only upon the quality of the evaluated data.

The silicon evaluation is much improved over ENDF/B-V. However, the evaluations would benefit from improving the data base further. For example, isotopic total cross section data need to be made available, particularly in the resonance region. Charged particle emission spectra are nonexistent and are needed to verify the model calculations, as well as neutron emission spectra at energies other than 14.5 MeV. Also, little or no data exist for the tertiary reactions with which to benchmark model calculations. Uncertainties should be given for important resonance parameters, as well as the angular and energy distributions.

15. ACKNOWLEDGMENTS

The authors acknowledge the comments and suggestions from Bob Roussin and Peter Fu who reviewed this report. We are also grateful to John White who uncovered some inconsistencies in the draft ENDF silicon files. Finally, many thanks go to Irene Rose for preparing this report for publication.

REFERENCES

AB73 Abbondanno, U., R. Giacomich, M. Lagonegro, and G. Pauli, J. Nucl. Energy 27, 227 (1973).

AL86 Alarcon, R. and J. Rapaport, Nucl. Phys. A458, 502 (1986).

AN64 Andersson-Lindstrom, G. and E. Roessle, Mem. Soc. Roy. Sci. Liege 10, 265 (1964).

AN65 Andersson-Lindstrom, G. and B. Zauzig, J. Annalen Der Physik 15, 287 (1965).

BA66 Bass, R., P. Haug, K. Kruger, and B. Staginnus, Report EANDC(E) 66"U" (1966).

BA85 Baba, M., M. Ono, N. Yabuta, T. Kikuti, and N. Hirakawa, "Scattering of 14.1-MeV Neutrons from ^{10}B, ^{11}B, C, N, O, F, and Si," Proc. of the Int. Conf. on Nuclear Data for Basic and Applied Science, Santa Fe, New Mexico 1, 223 (May 13-17, 1985).

BE80 Bezotosnyj, V. M., V. M. Gorbachjov, M. S. Shvetsov, and L. M. Surov, 5. All Union Conf on Neutron Phys., Kiev 2, 21 (Sept. 15-19, 1980).

BI63 Birk, M., G. Goldring, and P. Hillman, Nucl. Instrum. Methods in Phys. Res. 21, 197 (1963).

BO83 Bottcher, J., H. Blank, E. Finckh, C. Forstner, W. Jaumann, G. Schall, H. Scheuring, U. Schneidereit, K. Stauber, A. Weipert, W. Tornow, and E. Woye, J. Phys. G9, 165 (1983).

BR72 Brandenberger, J. D., A. Mittler, and M. T. McEllistrem, Nucl. Phys. A196, 65 (1972).

BR78 Browne, E., J. M. Dairiki, R. E. Doebler, A. A. Shihab-Eldin, L. J. Jardine, J. K. Tuli, A. B. Buyrn, Table of Isotopes, Seventh Edition, Edited by C. M. Lederer and V. S. Shirley, John Wiley and Sons, N. Y. (1978).

CH86 Chimoye, T., T. Vilaithong, and N. Chirapatpimol, Z. Phys. A235, 69 (1986).

CL64 Clarke, R. L. and W. G. Cross, Nucl. Phys. 53, 177 (1964).

CL72 Clayeux, G. and J. Voignier, CEA Report CEA-R-4279 (1972).

CO56 Cohen, A. V. and P. H. White, Nucl. Phys. 1, 73 (1956).

CO63 Colli, L., I. Iori, M. G. Marcazzan, and M. Milazzo, Nucl. Phys. 43, 529 (1963).

CO75 Connell, K. A. and A. J. Cox, Int. J. Appl. Radiat. Isotop. 26, 71 (1975).

CR67 Crawley, G. M. and G. T. Garvey, Phys. Rev. 160, 981 (1967).

REFERENCES (cont.)

CS86 Csikai, J., Zs. Lantos, and S. Sudar, Z. Phys. A325, 69 (1986).

DE61 Deuchars, Nature (London) 191, 995 (1961).

DE63 Devillers, D., Thesis, D.T.I.E.-14111 (Feb., 1963).

DE67 Debertin, K., H. Gunther, and E. Rossle, Nucl. Phys. A101, 473, (1967).

DI71 Dilg, W. and H. Vonach, Z. Naturforsch. A 26, 442 (1971).

DE79 D'Erasmo, L., Phys. Rev. C20, 1244 (1979).

DI70 Dickens, J. K., Phys. Rev. C2, 990 (1970).

DI73 Dickens, J. K., T. A. Love, and G. L. Morgan, ORNL-TM-4389 (1973).

DI74 Dickens, J. K. and G. L. Morgan, Phys. Rev. C10, 958 (1974).

DR68 Drake, M. K., Gulf General Atomic Report GA-8628 (1968).

DR69 Drake, D. M., J. C. Hopkins, C. S. Young, H.Conde, and A. Sattler, Nucl. Phys. A128, 209 (1969).

DR70 Drake, D. M., J. C. Hopkins, C. S. Young, and H. Conde, Nucl. Sci. Eng. 40, 294 (1970).

EN78 Endt, P. M. and C. Van der Leun, Nucl. Phys. A310, 1 (1978).

FA65 Fasoli, U., Inst. Naz. Fisica Nucleare Report BE-65, 6 (1965).

FA68 Facchini, U. and E. Saetta-Menichella, Energia Nucleare 15, 54 (1968).

FA70 Fasoli, U., G. Galeazzi, I. Scotoni, D. Toniolo, and G. Zago, Inst. Naz. Fisica Nucleare Report BE-70/10 (1970).

FL56 Flerov, N. N. and V. M. Talysin, Atomnaja Energija 1, 155 (1956).

FU73 Fuller, E. G., H. M. Gerstenberg, H. Vander Molen, and T. C. Dunn, "Photonuclear Reaction Data, 1973," U.S. Dept. of Commerce, National Bureau of Standards (March, 1973).

FU76 Fu, C. Y., At. Data and Nucl. Data Tables 17, 127 (1976).

REFERENCES (cont.)

FU80 Fu, C. Y., "A Consistent Nuclear Model for Compound and Precompound Reactions with Conservation of Angular Momentum," Proc. Int. Conf. Nuclear Cross Sections for Technology, Knoxville, TN, Oct. 22-26, 1979, NBS-594, p. 757, U.S. National Bureau of Standards. Also, ORNL/TM-7042 (1980).

FU85 Fu, C. Y. and D. M. Hetrick, Computer Code RECOIL, ORNL, Unpublished (1985).

FU86 Fu, C. Y. and D. M. Hetrick, "Evaluation and Testing of Double Differential Fe(n,n') Cross Sections," Trans. Am. Nucl. Society 53, 409 (1986).

FU88 Fu, C. Y., Nucl.Sci. Eng. 100, 61 (1988).

GA78 Garuska, U., J. Dresler, and H. Malecki, Polish Rept. INDC(POL)-9, 16 (1978).

GI65 Gilbert, A. and A. G. W. Cameron, Can. J. Phys. 43, 1446 (1965).

GR69 Grimes, S. M., Nucl. Phys. A124, 369 (1969).

HA83 Harvey, J. A., W. M. Good, R. F. Carlton, B. Castel, J. B. McGrory, and S. F. Mughabghab, "Neutron Spectroscopy as a High-Resolution Probe: Identification of the Missing 1/2+ States in ^{31}Si," Phys. Rev. C28, 24 (1983).

HA84 Haouat, G., Ch. Lagrange, R. de Swiniarski, F. Dietrich, J. P. Delaroche, and Y. Patin, Phys. Rev. C30, 1795 (1984).

HA93 Harvey, J. A., private communication (unpublished data taken in 1993).

HA96 Harvey, J. A., private communication (unpublished data).

HE75 Hermsdorf, D., A. Meister, S. Sassonoff, D. Seeliger, K. Seidel, and F. Shahin, Zentralinstitut fur Kernforschung Rossendorf Bei Dresden, ZfK-277 (U) (1975).

HE79 Hetrick, D. M., D. C. Larson, and C. Y. Fu, "Status of ENDF/B-V Neutron Emission Spectra Induced by 14-MeV Neutrons," ORNL/TM-6637, ENDF-280 (April, 1979).

HE80 Herman, M., A. Marcinkowski, J. Dresler, and U. Garuska, Inst. Badan Jadr (Nucl. Res.)-1871/I/PL/A, 13 (1980).

HE82 Hermsdorf, D., private communication to CSISRS Data Library, Brookhaven National Laboratory (1982).

HE82a Hermsdorf, D., "Consistent Interpretation of Neutron-Induced Charged-Particle Emission in Silicon," INDC(GDR)-22 (June, 1982).

REFERENCES (cont.)

HE91 Hetrick, D. M., D. C. Larson, and C. Y. Fu, "Generation of Covariance Files for the Isotopes of Cr, Fe, Ni, Cu, and Pb in ENDF/B-VI," ORNL/TM-11763, ENDF-350 (February, 1991).

HO69 Hohn, J., H. Pose, D. Seeliger, and R. Reif, Nucl. Phys. A134, 289 (1969).

IK88 Ikeda, I., C. Konno, K. Oishi, T. Nakamura, H. Miyade, K. Kawade, H. Yamamoto, and T. Katoh, "Activation Cross Section Measurements for Fusion Reactor Structural Materials at Neutron Energy from 13.3 to 15.0 MeV Using FNS Facility," JAERI 1312 (1988).

JA82 Janczyszyn, J., Int. Conf. on Nuclear Data for Sci. and Tech., Antwerp, 869 (Sept. 6-10, 1982).

JE63 Jeronymo, J. M. F., G. S. Mani, J. Olkowski, A. Sadeghi, and C. F. Williamson, Nucl. Phys. 47(1), 157 (1963).

KE59 Kern, B. D., W. E. Thompson, and J. M. Ferguson, Nucl. Phys. 10, 226 (1959).

KH65 Khurana, C. S. and I. M. Govil, Nucl. Phys. 69, 153 (1965).

KI70 Kinney, W. E. and F. G. Perey, ORNL 4517 (1970).

KI76 Kinney, W. E. and J. W. McConnell, Proc. Int. Conf. on Interactions of Neutrons with Nuclei, Lowell, Massachusetts, 2, 1319 (July 6-9, 1970).

KL78 Kliczewski, S. and Z. Lewandowski, Nucl. Phys. A304, 269 (1978).

KN67 Knitter, H.H. and M. Coppola, Z. Physik 207, 56 (1967).

KN86 Kneff, D. W., B. M. Oliver, H. Farrar IV, and L. R. Greenwood, Nucl. Sci. Eng. 92, 491-524 (1986).

KO63 Konijn, J. and A. Lauber, Nucl. Phys. 48, 191 (1963).

KO79 Kozma, P., P. Bem, and J. Vincour, 2. Int. Symp. on Neutron Induced Reactions, Smolenice, CSSR, published by Slovak Acad. of Sciences as 'Physics and Applications' 6, 113 (June 25-29, 1979).

KO80 Korzh, I. A., V. A. Mishchenko, and I. E. Sanzhur, Ukr. Fiz. Zh. 25(1), 109 (1980).

KU72 Kunz, P. D., "Distorted Wave Code DWUCK72," University of Colorado, unpublished (1972).

REFERENCES (cont.)

LA61 Lane, R. O., A. S. Langsdorf, Jr., J. E. Monahan, and A. J. Elwyn, Ann. Phys. (N. Y.) 12, 135 (1961).

LA62 Lane, R. O., A. J. Elwyn, and A. Langsdorf, Jr., Phys. Rev. 126, 1105 (1962).

LA76 Larson, D. C., C. H. Johnson, J. A. Harvey, and N. W. Hill, "Measurement of the Neutron Total Cross Section of Silicon from 5 eV to 730 keV," ORNL/TM-5618 (1976).

LA91 Larson, D. C., D. M. Hetrick, C. Y. Fu, and S. J. Epperson, in Proc. Seventh ASTM-EURATOM Symposium on Reactor Dosimetry, August 1990, Strasbourg, France (Edited by G. Tsotridis), (1991).

LA96 Larson, N. M., "Updated Users' Guide for SAMMY: Multilevel R-Matrix Fits to Neutron Data Using Bayes' Equations," ORNL/TM-9179 (1984). Also, ORNL/TM-9179/R1 (1985), ORNL/TM-9179/R2 (1989), ORNL/TM-9179/R3 (1996).

LE97 Leal, L. C., N. M. Larson, D. C. Larson, and D. M. Hetrick, "R-Matrix Evaluation of ^{28}Si, ^{29}Si, ^{30}Si up to 1.8 MeV," Abstract submitted to International Conference on Nuclear Data for Science and Technology, Trieste, Italy, (May 19-24, 1997).

MA56 Marion, J. B., R. M. Brugger, and R. A. Chapman, Phys. Rev. 101, 247 (1956).

MA63 Mainesbridge, B., T. W. Bonner, and T. A. Rabson, Nucl. Phys. 48, 83 (1963).

MA68 Martin, J., D. T. Stewart, and W. M. Currie, Nucl. Phys. A113, 564 (1968).

ME87 Meadows, J. W., D. L. Smith, M. M. Bretscher, and S. A. Cox, Ann. of Nucl. Energy 14, 489 (1987).

MI67 Miller, R. G. and R. W. Kavanagh, Nucl. Instr. and Meth. 48, 13 (1967).

MI71 Mingay, D. W., J. P. F. Sellschop, and P. M. Johnson, Nucl. Instr. and Meth. 94, 497 (1971).

MI73 Minetti, B., A. Pasquarelli, G. C. Bonazzola, T. Bressani, and E. Chiavassa, Lett. Nuovo Cimento 8, 249 (1973).

MU81 Mughabghab, S. F., M. Divadeenam, N. E. Holden, "Neutron Cross Sections, Vol. 1, Neutron Resonance Parameters and Thermal Cross Sections, part a: z=1-60," Academic Press, N.Y. (1981).

MU88 Murata, I., J. Yamamoto, and A. Takahashi, Int. Conf. on Nuclear Data for Sci. and Tech., Mito, Japan, 275 (May 30-June 3, 1988).

REFERENCES (cont.)

NE72 Nellis, D. O. and P. S. Buchanan, Report DNA 2716 (1972).

NG80 Ngoc, P. N., S. Gueth, F. Deak, and A. Kiss, "Investigations of (n,p), (n,α), and (n,2n) Reactions Around 14 MeV," Thesis Abstract, Eotvos Lorand Univ., Budapest (1980).

OB73 Obst, A. W. and J. L. Weil, Phys. Rev. C7, 1076 (1973).

PA53 Paul, E. B. and R. L. Clarke, Can. J. Phys. 31, 267 (1953).

PA67 Pasquarelli, A., Nucl. Phys. A93, 218 (1967).

PE63 Perey, F. G., Phys. Rev. 131, 745 (1963).

PE66 Petitt, G. A., S. G. Buccino, and C. E. Hollandsworth, Nucl.Phys. 79, 231 (1966).

PE67 Perey, F. G., Computer Code GENOA, ORNL, Unpublished (1967).

PE71 Perey, F. G., W. E. Kinney, and R. L. Macklin, "High Resolution Inelastic Cross Section Measurements for Na, Si, and Fe," Proc. of the Third Conference on Neutron Cross Sections and Technology, Univ. of TN, Knoxville, 191 (March 15-17, 1971).

PE72 Perey, F. G., T. A. Love, and W. E. Kinney, "A Test of Neutron Total Cross-Section Evaluations from 0.2 to 20 MeV for C, O, Al, Si, Ca, Fe, and SiO_2," ORNL-4823, ENDF-178 (1972).

PE74 Perey, C. M. and F. G. Perey, Atomic Data and Nuclear Data Tables 13, 293 (1974).

PE85 Pepelnik, R., B. Anders, B. M. Bahal, and M. Farooq, Reports rom CEC-Countries and CEC to NEANDC, NEANDC(E)-262U, (5), 32 (1985).

PO61 Popov, V. I., Book: Soviet Progress in Neutron Physics, Consultants Bureau, N. Y. (1966).

PO63 Potenza, R., R. Ricamo, and A. Rubbino, Nucl. Phys. 41, 298 (1963).

PR71 Prasad, R. and D. C. Sarkar, Nuovo Cimento A3(3), 467 (1971).

RA68 Ranakumar, N., E. Kondaiah, and R. W. Fink, Nucl. Phys. A122, 679 (1968).

RA92 Raman, S., E. T. Jurney, J. W. Starner, and J. E. Lynn, "Thermal-Neutron Capture by Silicon Isotopes," Phys. Rev. C46, 972 (1992).

RO64 Roturier, J., Nuclear Paris Congress, Paris, 2, 872 (July 2-8, 1964).

REFERENCES (cont.)

RO66 Roturier, J., Comptes Rendus, Series B, 262, 1736 (1966).

RO72 Robertson, W. and K. J. Zieba, Ann. of Nucl. Energy, 26(1), (1972).

RO73 Robertson, J. C., B. Audric, and P. Kolkowski, J. Nucl. Energy 27, 531 (1973).

RO75 Rogers, V. C., D. R. Dixon, C. G. Hoot, V. J. Orphan, C. G. Costello, and G. M. Sandquist, Trans. Amer. Nucl. Soc. 22, 817 (1975).

SC70 Schantl, W., Work not published because author deceased, information taken from an abstract communicated by Nuclear Data Section, IAEA, Vienna (1970).

SC77 Schweitzer, Th., D. Seeliger, and S. Unholzer, Kernenergie 20, 174 (1977).

SE86 Seeliger, D., D. Schmidt, and T. Streil, Nucl. Phys. A460, 265 (1986).

SH66 Shannon, J. A. and J. B. Trice, Nucl. Instrum. Methods in Phys. Res. 41, 255 (1966).

SH77 Shehebolev, V. T. and Z. A. Ramendik, Atomnaja Energija 43(1), 54 (1977).

SH86 Shibata, K. and C. Y. Fu, "Recent Improvements of the TNG Statistical Model Code," ORNL/TM-10093 (August, 1986).

SI70 Singh, J. J., Bull. Amer. Phys. Soc. 15, 1328 (1970).

SO66 So, S. S., C. Mayer-Boricke, and R. H. Davis, Nucl. Phys. 84, 641 (1966).

ST65 Strain, J. E. and W. J. Ross, ORNL-3672 (1965).

ST65a Stelson, P. H., R. L. Robinson, H. J. Kim, J. Rapaport, and G. R. Satchler, Nucl. Phys. 68, 97 (1965).

SU79 Sullivan, N. B., J. J. Egan, G. H. R. Kegel, and P. Harihar, Nucl. Sci. Eng. 70, 294 (1979).

TA64 Tanaka, S., J. Phys. Soc. Japan 19, 2249 (1964).

TA70 Tanaka, S., K. Tsukada, M. Maruyama, and Y. Tomita, Proc. Conf. Nuclear Data for Reactors, Helsinki (Vol. II) (1970).

TA83 Takahashi, A., J. Yamamoto, T. Murakami, K. Oshima, H. Oda, K. Fujimoto, M. Ueda, M. Fukazawa, Y. Yanagi, J. Miyaguchi, and K. Sumita, Octavian Report A-83-01, Osaka Univ., Japan (June, 1983).

REFERENCES (cont.)

TS61 Tsukada, K., S. Tanaka, M. Maruyama, and Y. Tomita, Proc. Reactor Physics Sem., Vienna, Austria 1, 75 (Aug. 3-11, 1961).

VE74 Velkley, D. E., D. W. Glasgow, J. D. Brandenberger, M. T. McEllistrem, J. C. Manthuruthil, and C. P. Poirier, Phys. Rev. C9, 2181 (1974) and private communication from D. E. Velkley.

VI81 Virdis, A., Centre D'Etudes Nucleaires Report Series R-5144 (December, 1981).

WE86 Wenguang, Z., T. Guoyou, B. Shanglian, S. Zhaomin, and C. Jinxiang, Chinese J. of Nucl. Phys. 8, 251 (1986).

WE87 Weigmann, H., P. W. Martin, R. Koehler, I. Van Parijs, F. Poortmans, and J. A. Wartena, Phys. Rev. C 36, 585 (1987).

Appendix A. Tables

Table 1. Silicon Data Included in the Resonance Parameter Analysis

- Total cross section data of Perey et al.(PE72) for natural silicon, measured on the 47-m flight path at the Oak Ridge Electron Linear Accelerator (ORELA) from 0.2 to 20 MeV (data used in the resonance parameter analysis were from 0.2 - 1.8 MeV)
- Transmission data of Harvey et al. (HA93) for natural silicon, measured on the 200-m flight path at ORELA from 0.3 to 20 MeV (data used in the resonance parameter analysis were from 0.3 - 1.8 MeV)
- Total cross section data of Larson et al. (LA76), measured on the 80- and 200-m flight paths at ORELA from 5.0 eV - 730 keV (data used in the resonance parameter analysis were from 5.0 eV - 700 keV)
- $^{29}SiO_2$ transmission data (HA96) from 300 keV - 1.8 MeV and $^{30}SiO_2$ transmission data (HA83) from 100 keV - 1.5 MeV, measured on the 80-m flight path at ORELA
- Elastic scattering thermal cross section for ^{28}Si (1.992±0.006 barns) from Mughabghab (MU81), and capture thermal cross section (0.169±0.004 barns) from Raman et al. (RA92). Values given by resonance parameters are 1.992 and 0.169 barns respectively.

Table 2. ^{28}Si resonance parameters. The analysis was performed with the following radii: 4.1364 fm for the $l = 0$ and 2 resonances and 4.9437 fm for the $l = 1$ resonances

Energy (keV)	l	J	Γ_n (eV)	Γ_γ (eV)
-3622.1	0	1/2	3.9362+6	145.36
-873.730	0	1/2	0.101510	1.0253
-365.290	0	1/2	0.030406	1.0
-63.1590	0	1/2	0.046894	1.0
-48.8010	0	1/2	0.0092496	1.0
31.7400	2	5/2	0.015667	1.0
55.6770	0	1/2	653.3100	1.5803
67.7330	1	3/2	2.658900	2.5
70.8000	2	5/2	0.029617	1.0
86.7970	1	3/2	0.726180	2.5
181.620	0	1/2	34894.00	5.6
298.700	2	5/2	9.886000	1.0
301.310	0	1/2	2.354800	3.6
354.590	2	5/2	14.46000	1.0
399.680	1	3/2	0.813610	0.66
532.660	1	3/2	532.8100	2.5
565.580	1	3/2	10953.00	2.9
587.170	1	1/2	199.1600	8.8
590.290	0	1/2	523.6600	3.6
602.470	2	3/2	50.49100	3.4
714.040	1	3/2	1.216500	2.5
771.710	2	5/2	53.13900	1.0
812.490	1	3/2	30100.00	9.7
845.230	2	3/2	397.9100	2.0
872.310	2	5/2	32.14000	1.3
910.040	1	3/2	3673.300	1.13
962.230	1	1/2	76614.00	16.0
1017.80	2	5/2	76.19200	1.0
1042.90	2	5/2	933.7000	1.0
1085.20	0	1/2	72.79400	3.6
1148.10	2	5/2	3.146900	1.0
1162.70	0	1/2	3013.600	3.8
1199.50	1	1/2	14914.00	7.6
1201.20	0	1/2	4601.200	3.6
1256.40	0	1/2	17383.00	3.6
1264.40	2	5/2	843.6400	1.0
1379.90	2	3/2	65.29900	2.4
1408.30	1	3/2	5198.300	2.7

Table 2. (continued)

Energy (keV)	l	J	Γ_n (eV)	Γ_γ (eV)
1479.90	2	3/2	3502.500	1.65
1482.40	1	1/2	0.886940	8.8
1512.30	2	5/2	91.49300	1.0
1528.70	2	3/2	2922.500	2.4
1580.60	2	3/2	1495.500	2.4
1592.80	1	1/2	11199.00	8.8
1597.20	2	3/2	4017.200	2.4
1639.60	2	5/2	15293.00	1.0
1651.10	2	5/2	21555.00	1.0
1658.60	1	1/2	1555.300	8.8
1665.00	2	3/2	215.9000	2.4
1785.00	2	3/2	192.9400	2.4
1805.70	1	3/2	1299.100	2.5
1850.70	2	5/2	35515.00	1.0
1852.40	1	3/2	70707.00	2.5
1923.70	2	5/2	1017.100	1.0
1968.90	2	5/2	5734.100	1.0
2248.70	0	1/2	444760.0	3.6
3007.30	0	1/2	289.9600	3.6
3067.80	0	1/2	422.2900	3.6

Table 3. ^{29}Si resonance parameters. The analysis was performed with a radius of 4.40 fm

Energy (keV)	l	J	Γ_n (eV)	Γ_γ (eV)
-2041.70	0	0	2061100.0	290.64
-859.350	0	0	35059.0	0.99981
-431.280	0	0	228510.0	1.00590
15.2820	1	1	10.0	1.646
38.8190	1	2	75.9260	2.40
159.680	1	1	1200.30	1.90
184.460	1	1	136.740	1.50
336.790	1	1	2512.80	0.80
385.760	0	1	24133.0	4.670
552.240	1	2	1298.90	5.70
566.560	1	1	70820.0	3.0
619.660	1	2	725.960	3.0
649.730	1	2	1095.90	3.0
653.060	1	1	19386.0	6.30
715.060	1	1	978.570	0.30
716.770	0	0	219300.0	3.0
802.260	2	1	9934.90	3.0
862.000	0	0	432930.0	3.0
872.480	1	1	17335.0	0.30
955.890	1	2	982.890	0.30
1098.40	2	1	57.7870	3.0
1113.80	1	1	76533.0	0.30
1122.30	1	2	4881.60	0.30
1178.60	0	1	8295.90	3.0
1192.30	1	1	375.060	0.30
1207.60	1	2	19795.0	0.30
1388.90	2	1	4271.40	3.0
1769.10	0	0	32.1360	3.0
2248.50	0	0	169.320	3.0

Table 4. ^{30}Si resonance parameters. The analysis was performed with a radius of 4.20 fm

Energy (keV)	l	J	Γ_n (eV)	Γ_γ (eV)
-1147.40	0	1/2	311750.0	912.97
-161.550	0	1/2	426.40	0.650
2.23500	1	3/2	0.932660	0.370
4.97700	1	1/2	1.1220	0.60
183.490	0	1/2	9997.60	6.0
235.230	2	3/2	115.410	0.80
302.840	1	3/2	274.430	0.370
413.140	1	1/2	1580.10	0.60
645.240	2	3/2	401.430	0.80
704.910	2	3/2	423.190	0.80
745.450	1	3/2	14735.0	0.370
796.950	1	1/2	469.320	0.60
807.380	1	1/2	274.330	0.60
810.800	1	1/2	419.310	0.60
844.670	1	3/2	3315.30	0.370
878.820	2	3/2	110.630	0.80
979.820	1	1/2	591.820	0.60
1182.20	0	1/2	5912.40	6.0
1217.80	2	3/2	1888.90	0.80
1274.90	1	1/2	2225.50	0.60
1302.00	2	3/2	304.790	0.80
1310.80	1	3/2	339.710	0.370
1338.00	1	1/2	4624.0	0.60
1356.00	1	3/2	12271.0	0.370
1383.60	1	1/2	25336.0	0.60
1401.00	2	3/2	1897.60	0.80
1412.10	1	3/2	668.620	0.370
1586.00	0	1/2	23644.0	6.0
2583.20	0	1/2	92076.0	6.0

Table 5. Summary of Elastic Scattering Data Used in Optical Model Search

Author(s)	Ref.	E_n	Ave. E_n	θ_{min}	θ_{max}	# angles
Knitter and Coppola	KN67	4.00		20	150	10
Drake et al.	DR69	4.00		40.4	136.5	6
Tanaka	TA64	4.20	4.25	15	160	9
Knitter and Coppola	KN67	4.25		20	150	10
Knitter and Coppola	KN67	4.50		20	150	10
Tanaka	TA64	4.50		15	160	9
Knitter and Coppola	KN67	4.71		20	150	10
Tanaka	TA64	4.80	4.80	15	160	9
Tanaka et al.	TA70	4.81		30	148	13
Knitter and Coppola	KN67	4.99		20	150	10
Knitter and Coppola	KN67	4.99		20	150	10
Knitter and Coppola	KN67	5.25	5.25	20	150	10
Kinney and Perey	KI70	5.44		25.4	115.9	22
Knitter and Coppola	KN67	5.50		20	150	10
Knitter and Coppola	KN67	5.75		20	150	10
Tanaka et al.	TA70	5.96	5.80	30	148	13
Martin et al.	MA68	6.00		28	153	15
Drake et al.	DR69	6.00		40.4	136.5	6
Kinney and Perey	KI70	6.37		23.3	119.8	23
Drake et al.	DR69	6.67	6.60	40.4	136.5	6
Tanaka et al.	TA70	7.02		30	148	13
Drake et al.	DR69	7.50		40.4	136.5	6
Kinney and Perey	KI70	7.55		15.5	136	23
Brandenberger et al.	BR72	7.71	7.75	30	150	16
Brandenberger et al.	BR72	7.96		30	145	13
Tanaka et al.	TA70	8.03		30	148	13
Velkley et al.	VE74	8.47		31	160.7	14
Kinney and Perey	KI70	8.56		15.5	136	19
Velkley et al.	VE74	8.92	8.75	31	160.7	27
Nellis and Buchanan	NE72	8.91		31	121.8	11
Brandenberger et al.	BR72	9.05		30	150	15
Obst and Weil	OB73	9.80	9.80	20.7	151	20
Nellis and Buchanan	NE72	10.95	10.95	31	121.8	10
Roturier	RO64	14.1	14.1	10.3	165.1	13

Table 6. Optical Model Parameters

Neutrons:				
	V (MeV)	= 47.91-0.267E	r_v (fm) = 1.254	a_v (fm) = 0.625
	W (MeV)	= 0.0		
	W_D(MeV)	= 12.95-0.053E	r_w (fm) = 1.096	a_w (fm) = 0.519
	U (MeV)	= 7.6	r_u (fm) = 1.254	a_u (fm) = 0.625
Protons:				
	V (MeV)	= 53.60-0.55E	r_v (fm) = 1.25	a_v (fm) = 0.65
	W (MeV)	= 0.0		
	W_D(MeV)	= 13.5	r_w (fm) = 1.25	a_w (fm) = 0.47
Alphas:				
	V (MeV)	= 110.0	r_v (fm) = 1.70	a_v (fm) = 0.48
	W (MeV)	= 5.0	r_w (fm) = 1.80	a_w (fm) = 0.48

E = incident energy (MeV),
V = real well depth,
W = imaginary well depth (Saxon-Woods),
W_D = Imaginary well depth (Saxon-Woods derivative),
U = spin-orbit potential depth,
r_v, r_w, r_u = radii for various potentials,
a_v, a_w, a_u = diffuseness for various potentials.

Table 7. Deformation parameters of ^{28}Si levels

Level (MeV)	J^{π}	β^2_l	Ref.
1.779	2^+	0.3300	CR67
4.617	4^+	0.1089	HO69
6.276	3^+	0.0400	SE86
6.879	3^-	0.1225	SE86, HO69
6.889	4^+	0.0961	SE86, HO69

Table 8. Energy levels and gamma-ray branching ratios (in %) of ^{27}Si

Initial State			Branching ratios to state N				
N	J^{π}	E (keV)	1	2	3	4	5
1	$5/2^+$	0					
2	$1/2^+$	780	100				
3	$3/2^+$	957	94	6			
4	$7/2^+$	2164	100				
5	$5/2^+$	2647	20	3	77		
6	$(3/2)^+$	2865	96	4			
7	$9/2^+$	2910	94			6	
8	$1/2^+$	3539		62	38		
9	$3/2^+$	3805	80	8			12

Table 9 . Energy levels and gamma-ray branching ratios (in %) of ^{28}Si

Initial State			Branching ratios to state N						
N	J^{π}	E (keV)	1	2	3	4	5	6	7
1	0^+	0							
2	2^+	1779	100						
3	4^+	4617		100					
4	0^+	4979		100					
5	3^+	6276		92	8				
6	0^+	6691		100					
7	3^-	6879	64	33	3				
8	4^+	6889		100					
9	2^+	7381	37	63					
10	2^+	7417	94	6					
11	3^+	7799		70	1		29		
12	2^+	7933	82	4	8	6			
13	2^+	8259	9	70	4	17			
14	1^+	8328	72	28					
15	4^-	8413		22	4				74
16	6^+	8543			100				
17	3^+	8589		94			6		
18	1^-	8904	47	53					

Table 10. Energy levels and gamma-ray branching ratios (in %) of ^{29}Si

Initial State			Branching ratios to state N							
N	J^{π}	E (keV)	1	2	3	4	5	6	7	8
1	$1/2^+$	0								
2	$3/2^+$	1273	100							
3	$5/2^+$	2028	94	6						
4	$3/2^+$	2426	87	13						
5	$5/2^+$	3067		80	20					
6	$7/2^-$	3623		2	89		9			
7	$7/2^+$	4080		68	32					
8	$9/2^+$	4741			93				7	
9	$1/2^+$	4840	90	10						
10	$5/2^+$	4895	18	50	32					
11	$3/2^-$	4934	94	5			1			
12	$9/2^-$	5255						100		
13	$7/2^+$	5286		11	76	13				
14	$9/2^+$	5652					41		47	12
15	$7/2^+$	5813			25	30	45			
16	$3/2^+$	5949	14	23	15	22	26			

Table 11. Energy levels and gamma-ray branching ratios (in %) of ^{30}Si

Initial State			Branching ratios to state N						
N	J^π	E (keV)	1	2	3	4	7	8	11
1	0^+	0							
2	2^+	2235	100						
3	2^+	3498	45	55					
4	1^+	3770	43	57					
5	0^+	3788		100					
6	2^+	4809	36	16	44	4			
7	3^+	4830		92	8				
8	3^+	5231		21	75		4		
9	4^+	5280		100					
10	0^+	5372		71		29			
11	3^-	5487		61	39				
12	2^+	5613		44		56			
13	4^+	5950	100						
14	4^-	6503					40	45	15
15	2^+	6537	31	20	35	14			

Table 12. Energy levels of ^{31}Si

N	J^π	E (keV)
1	$3/2^+$	0
2	$1/2^+$	752
3	$5/2^+$	1695
4	$3/2^+$	2317
5	$5/2^+$	2789
6	$7/2^-$	3134
7	$3/2^-$	3534

Table 13. Energy levels and gamma-ray branching ratios (in %) of ^{27}Al

Initial State			Branching ratios to state N							
N	J^{π}	E (keV)	1	2	3	4	5	6	7	8
1	$5/2^+$	0								
2	$1/2^+$	844	100							
3	$3/2^+$	1014	97	3						
4	$7/2^+$	2211	100							
5	$5/2^+$	2735	22	2	76					
6	$3/2^+$	2981	97	1	2					
7	$9/2^+$	3004	89			11				
8	$1/2^+$	3679	2	60	38					
9	$3/2^+$	3956	84	5	5		6			
10	$1/2^-$	4055		86	14					
11	$5/2^+$	4409	59		34	5	2			
12	$11/2^+$	4510				77			23	
13	$7/2^+$	4580	75			16	9			
14	$5/2^{(+)}$	4812	40		25	35				
15	$3/2^-$	5156	100							
16	$5/2^+$	5247	5		77	16		2		
17	$(5/2^-)$	5419				(100)				
18	$9/2^+$	5433							(100)	
19	$5/2^{(+)}$	5438	83				13	4		
20	$(11/2^+)$	5500				21			79	
21	$(3/2^+)$	5551	74		20	6				
22	$9/2^+$	5668	55						45	
23	$1/2^+$	5752		39	13			36		12
24	$(5/2^+)$	5827	15		85					
25	$7/2^{(-)}$	5960	35			42	23			

Table 14. Energy levels and gamma-ray branching ratios (in %) of ^{28}Al

Initial State			Branching ratios to state N							
N	J^{π}	E (keV)	1	2	3	4	5	6	7	10
1	3^+	0								
2	2^+	31	100							
3	0^+	972		100						
4	3^+	1014	37	63						
5	1^+	1373	5	55	40					
6	1^+	1620	6	92	2					
7	2^+	1623	100							
8	2^+	2139	43	50		7				
9	1^+	2202		79	16				5	
10	4^+	2272	100							
11	2^+	2485	22		6			61	11	
12	5^+	2582	95							5
13	4^+	2656	25			75				
14	$(3)^+$	2987	50						50	

Table 15. Energy levels and gamma-ray branching ratios (in %) of ^{29}Al

Initial State			Branching ratios to state N			
N	J^{π}	E (keV)	1	2	3	4
1	$5/2^+$	0				
2	$1/2^+$	1398	100			
3	$7/2^+$	1754	100			
4	$3/2^+$	2224	100			
5	$3/2^+$	2865	56	44		
6	$5/2^+$	3062	33		67	
7	$5/2^+$	3184	7	14	24	55
8	$1/2^+$	3433		83		17
9	$9/2^+$	3578	9		91	
10	$(5/2)^+$	3641	91		9	
11	$(3/2)^+$	3672	100			
12	$(7/2)^+$	3935	86			14
13	$(7/2^-)$	3985	100			
14	$(1/2^+)$	4057		50		50
15	$5/2^+$	4220			100	
16	$(5/2^+)$	4403	45		55	

Table 16. Energy levels and gamma-ray branching ratios (in %) of ^{30}Al

Initial State			Branching ratios to state N			
N	J^{π}	E (keV)	1	2	4	5
1	3^+	0				
2	(3^+)	250	100			
3	(1^+)	694	(50)	(50)		
4	(0^+)	(1000)	(100)			
5	(2^+)	1135	(75)		(25)	
6	(4^+)	1262	(50)			(50)

Table 17. Energy levels and gamma-ray branching ratios (in %) of ^{24}Mg

Initial State			Branching ratios to state N									
N	J^{π}	E (keV)	1	2	3	4	5	6	7	8	9	10
1	0^+	0										
2	2^+	1369	100									
3	4^+	4123		100								
4	2^+	4238	79	21								
5	3^+	5236		98		2						
6	4^+	6010		87		13						
7	0^+	6432		82		18						
8	2^+	7348	62	38								
9	1^-	7553	45	35		(20)						
10	3^-	7616	23	72	5							
11	1^+	7747	21	74		5						
12	(5^+)	7812			33		60	7				
13	6^+	8113			100							
14	3^-	8358	5	49			16	11		(6)	(6)	(7)
15	$(4)^+$	8437		63	23	7	6					1
16	1^-	8438	82	18								
17	2^+	8654		82		13			5			
18	2^-	8864		93		7						
19	2^+	9002	55	18	27							
20	1^-	9148	45	34		21						
21	2^+	9283		77	23							

Table 18. Energy levels and gamma-ray branching ratios (in %) of ^{25}Mg

Initial State			Branching ratios to state N									
N	J^{π}	E (keV)	1	2	3	4	5	6	7	8	9	10
1	$5/2^+$	0										
2	$1/2^+$	585	100									
3	$3/2^+$	975	51	49								
4	$7/2^+$	1612	100									
5	$5/2^+$	1965	26	47	27							
6	$1/2^+$	2564	3	80	17							
7	$7/2^+$	2738	6		87		7					
8	$3/2^+$	2801	22	39			39					
9	$9/2^+$	3405	19			81						
10	$3/2^-$	3414	10	76	14							
11	$5/2^+$	3908	11		66				13	10		
12	$7/2^-$	3971	79				21					
13	$9/2^+$	4060	60			39					1	
14	$1/2^-$	4277		5	79			12				4
15	$3/2^+$	4359		52	47			1				
16	$9/2^+$	4711					94		6			

Table 19. Energy levels and gamma-ray branching ratios (in %) of ^{26}Mg

Initial State			Branching ratios to state N								
N	J^{π}	E (keV)	1	2	3	5	6	8	10	13	14
1	0^+	0									
2	2^+	1809	100								
3	2^+	2938	10	90							
4	0^+	3588		100							
5	3^+	3941		38	62						
6	4^+	4320		100							
7	2^+	4332	8	82	10						
8	3^+	4350		55	45						
9	2^+	4835	11	4	81			4			
10	4^+	4901		91	9						
11	0^+	4972		7	93						
12	2^+	5291	2	7	91						
13	4^+	5474		16		29	55				
14	$1^{(+)}$	5690	10	61	29						
15	4^+	5715			19	38		37	6		
16	$(2)^+$	6125				10		90			
17	0^+	6256		93							7
18	(3^-)	6621							86	14	
19	2^+	6744		90	10						
20	3^-	6878		28	72						

Table 20. Energy levels and gamma-ray branching ratios (in %) of ^{27}Mg

Initial State			Branching ratios to state N					
N	J^{π}	E (keV)	1	2	3	4	5	6
1	$1/2^+$	0						
2	$3/2^+$	985	100					
3	$5/2^+$	1698	100					
4	$5/2^+$	1940	33	66	1			
5	$(7/2)^+$	3109		7	6	87		
6	$(5/2)^+$	3427		58	37	3	2	
7	$1/2^+$	3476	98	2				
8	$(3/2)^+$	3485	43	44	13			
9	$3/2^-$	3561	92	6	2			
10	$7/2^-$	3760			100			
11	$3/2^+$	3786	50	2	32	16		
12	$(9/2^+)$	3884			7	81	6	6

Table 21. Level density parameters

Residual Nuclei	T (MeV)	E_o (MeV)	a (MeV^{-1})	Δ (MeV)	c	E_c (MeV)	E_x (MeV)
^{24}Mg	2.384	1.9850	3.320	5.13	4.033	9.3	15.63
^{25}Mg	1.739	-0.0754	4.800	2.46	5.992	4.8	10.96
^{26}Mg	2.076	0.7308	4.080	4.26	5.228	7.0	14.68
^{27}Mg	1.274	0.7823	6.500	2.46	8.541	4.0	8.592
^{27}Al	2.375	-1.6920	3.450	1.80	4.533	6.0	13.00
^{28}Al	2.072	-2.5400	3.800	0.00	5.116	3.0	9.025
^{29}Al	2.897	-3.6220	3.000	1.67	4.134	4.5	16.92
^{30}Al	1.744	-1.8640	4.486	0.00	6.323	1.4	7.500
^{27}Si	2.596	-1.8430	3.178	2.09	4.176	4.0	14.49
^{28}Si	2.353	2.1350	3.050	3.89	4.106	9.0	12.22
^{29}Si	2.055	0.3677	3.570	2.09	4.920	6.0	9.762
^{30}Si	2.158	0.6527	3.810	3.76	5.371	5.0	14.00
^{31}Si	1.964	-0.3579	4.050	2.09	5.835	3.6	10.83

T = nuclear temperature
E_o= parameter for matching lower energy level density to the higher one
a = $\pi^2 g/6$ (g=density of uniformly spaced single particle states)
Δ = pairing energy correction
c = spin cutoff parameter
E_c= continuum cutoff
E_x= tangency point

Table 22. ^{28}Si KERMA (MeV-barns) Calculated from ENDF/B-VI and ^{nat}Si KERMA (MeV-barns) Calculated from ENDF/B-V (in parentheses)

Reaction		E_n (MeV) 8		14		20	
MT=2 (elastic)	recoil	0.144	(0.174)	0.175	(0.182)	0.241	(0.238)
MT=16 (n,2n)	recoil	0.0	(0.0)	0.0	(0.0)	0.003	(0.224)
MT=22 (n,nα)	α	0.0		0.034		0.733	
	recoil	0.0		0.012		0.205	
	sum	0.0	(0.0)	0.046	(0.10)	0.938	(1.539)
MT=28 (n,np)	p	0.0		0.050		0.922	
	recoil	0.0		0.036		0.325	
	sum	0.0	(0.0)	0.086	(0.198)	1.247	(1.572)
MT=51-67 (n,n') discrete	recoil	0.326		0.185		0.171	
MT=91 (n,n') continuum	recoil	0.0		0.147		0.153	
MT=51-91	sum	0.326	(0.359)	0.332	(0.233)	0.324	(-0.617)
MT=102 (capture)		1.62E-4	(1.52E-4)	2.44E-4	(2.14E-4)	3.07E-4	(2.60E-4)
MT=104 (n,d)		0.0	(0.0)	0.088	(0.088)	0.007	(0.007)
MT=600-613	p	0.578		0.474		0.10	
(n,p) discrete	recoil	0.104		0.053		0.01	
MT=649	p	0.0		0.838		0.425	
(n,p) continuum	recoil	0.0002		0.027		0.014	
MT=600-649	sum	0.6822	(0.913)	1.392	(1.541)	0.549	(0.636)
MT=800-815	α	0.836		0.698		0.04	
(n,α) discrete	recoil	0.182		0.151		0.008	
MT=849	α	0.0		0.309		0.117	
(n,α) continuum	recoil	0.0		0.080		0.028	
MT=800-849	sum	1.018	(0.680)	1.238	(1.265)	0.193	(0.426)
Total KERMA		2.170	(2.126)	3.357	(3.607)	3.502	(4.025)
Recoil KERMA		0.756		0.866		1.158	
(n,n') KERMA		0.326	(0.359)	0.332	(0.233)	0.324	(-0.617)
Proton KERMA		0.578		1.362		1.447	
α KERMA		0.836		1.041		0.890	

Appendix B. Figures

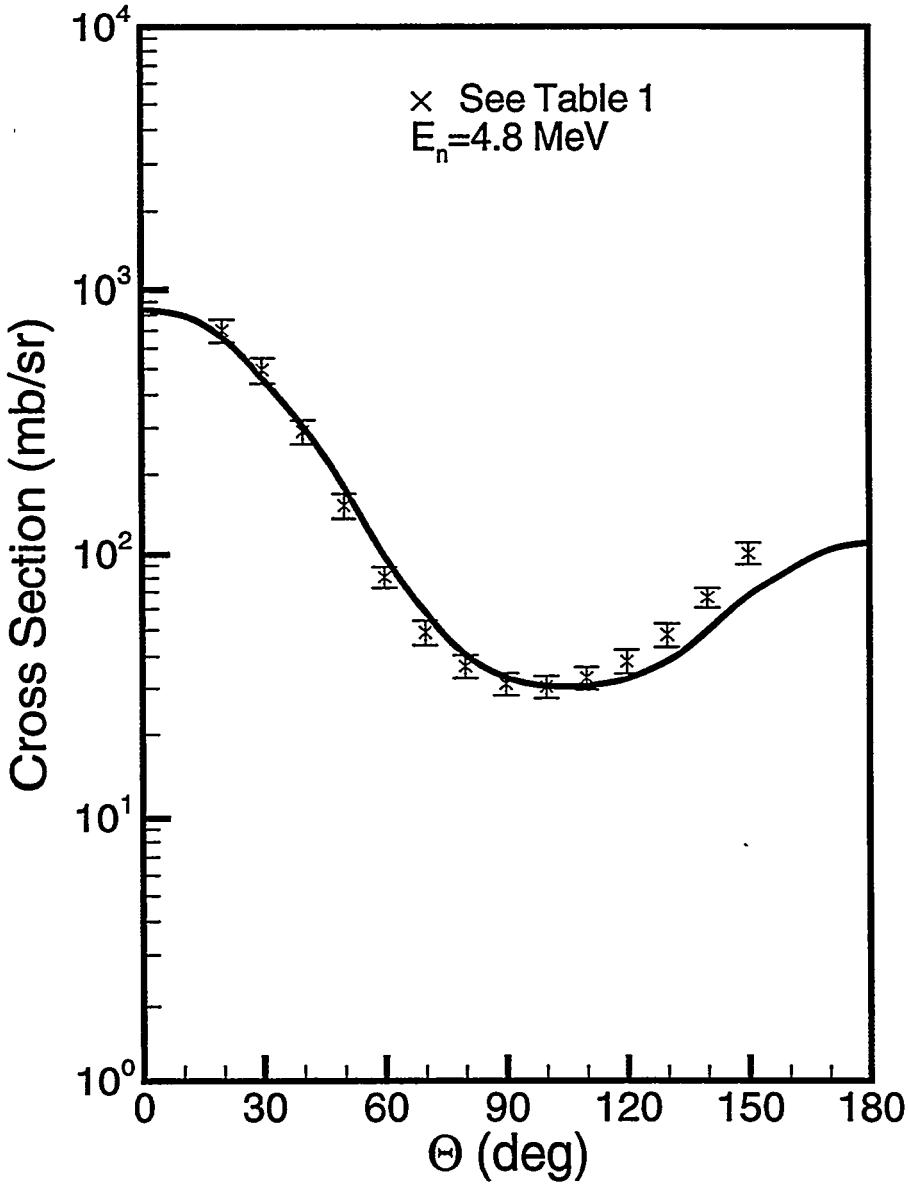

Fig. 1. Comparison of calculated and experimental differential elastic scattering cross sections for ^{28}Si at $E_n = 4.8$ MeV.

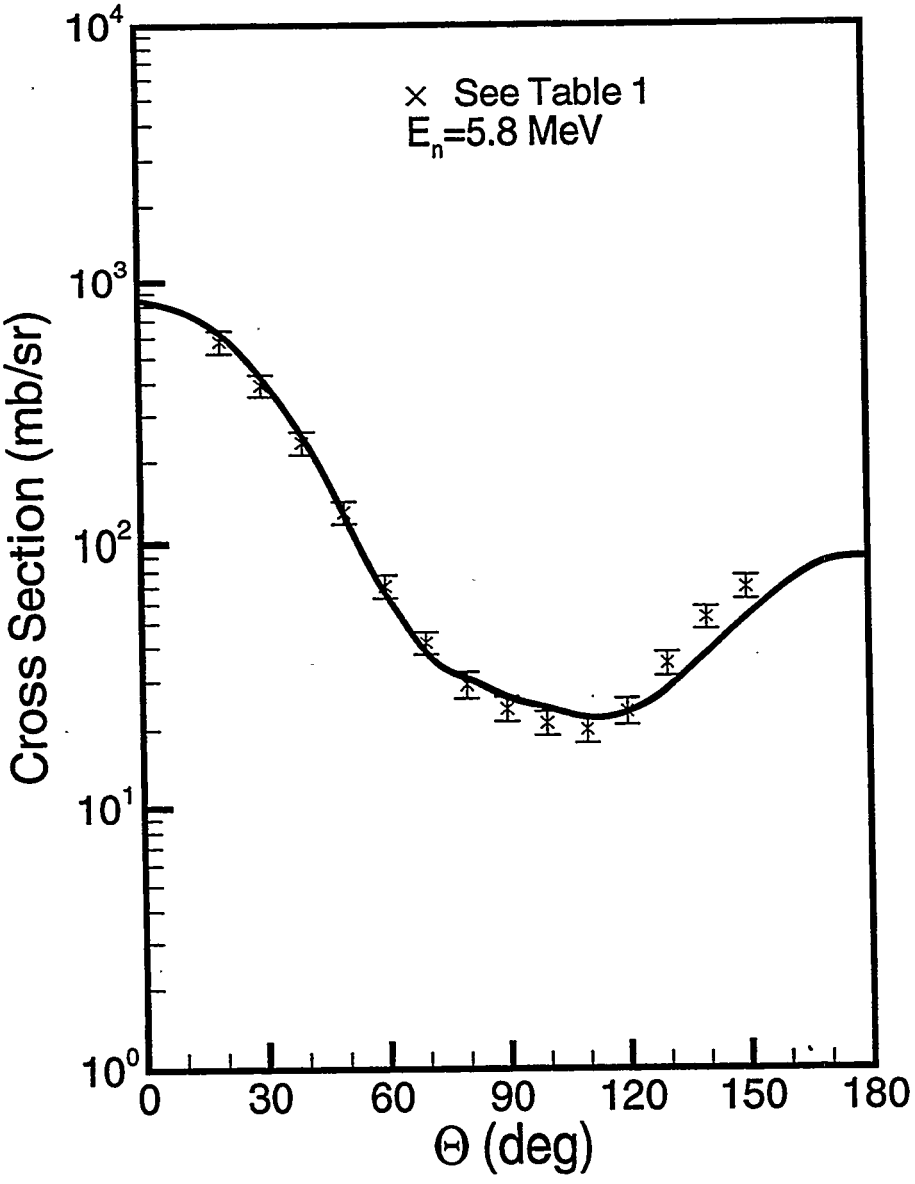

Fig. 2. Comparison of calculated and experimental differential elastic scattering cross sections for ^{28}Si at E_n = 5.8 MeV.

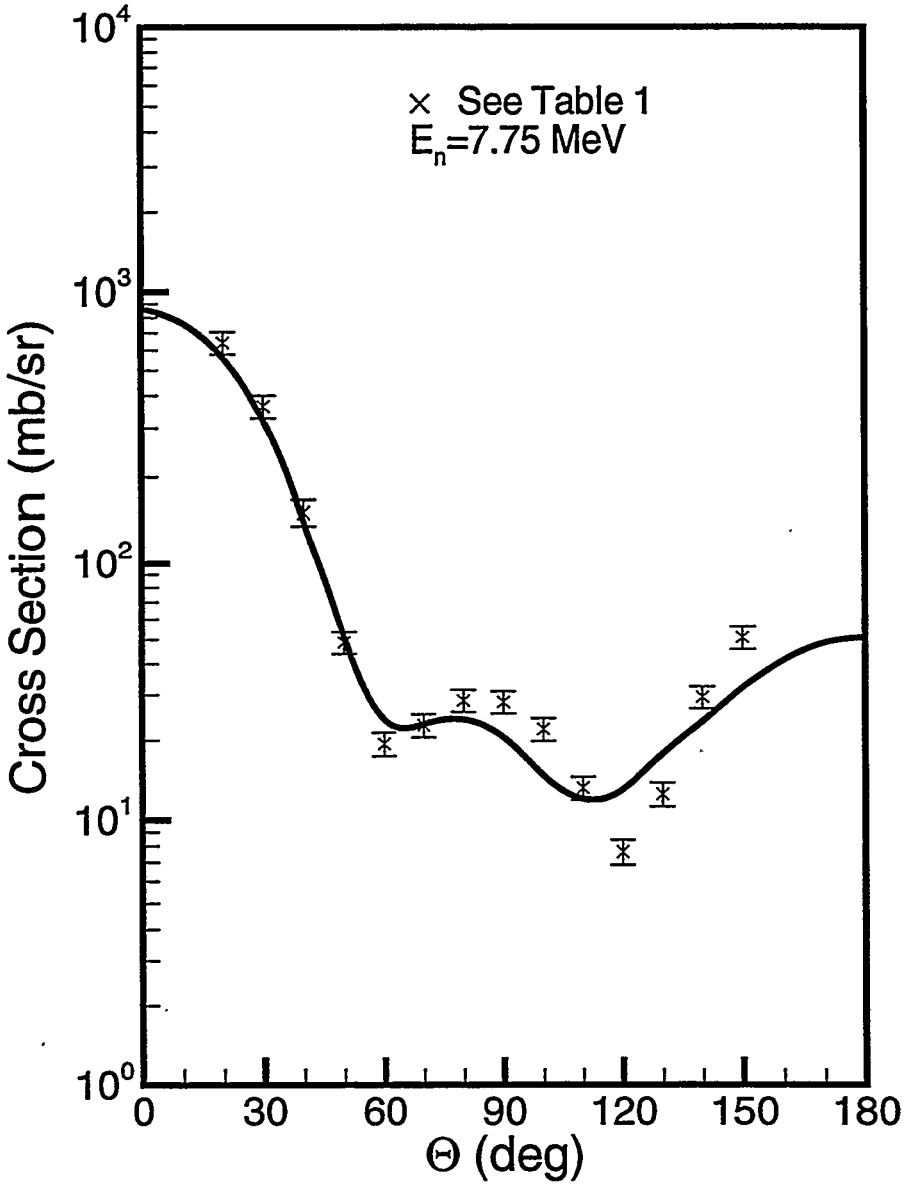

Fig. 3. Comparison of calculated and experimental differential elastic scattering cross sections for ^{28}Si at $E_n = 7.75$ MeV.

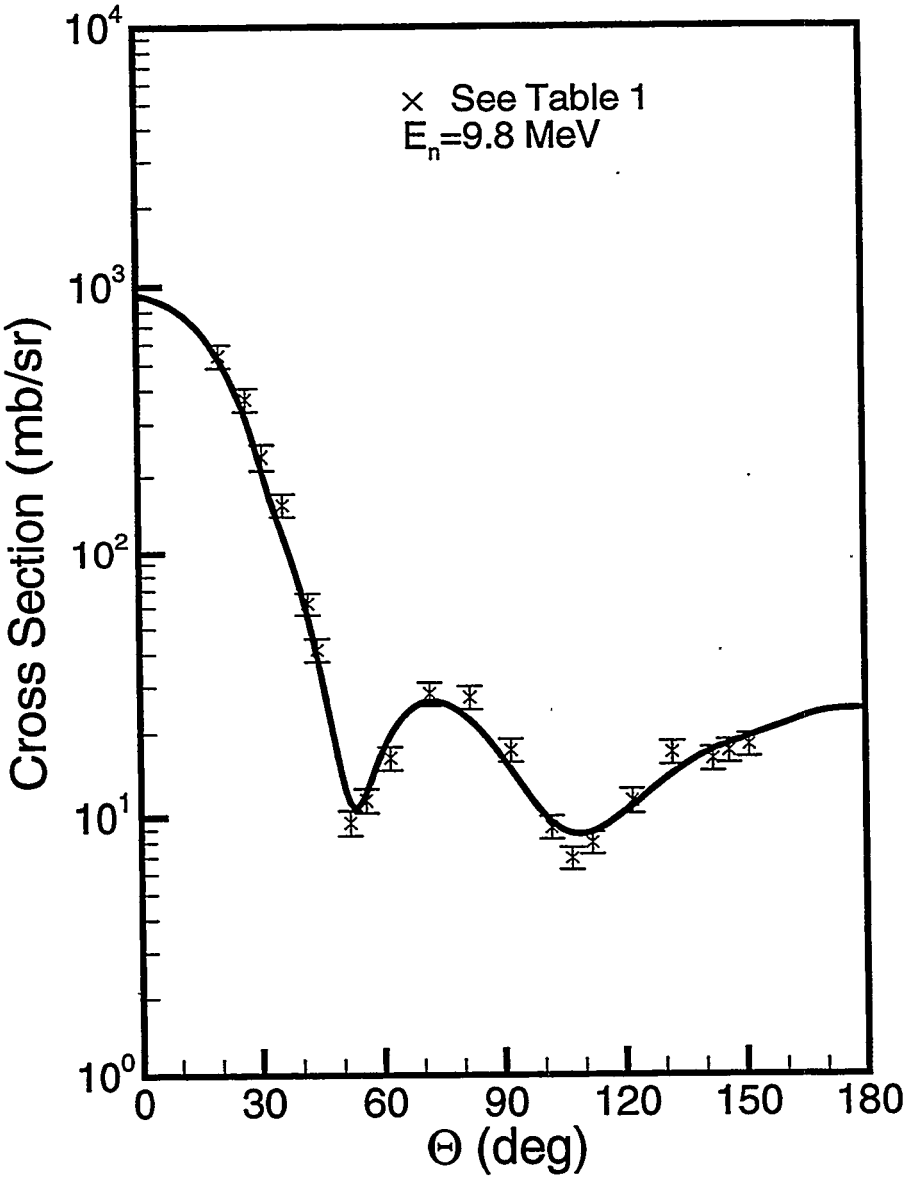

Fig. 4. Comparison of calculated and experimental differential elastic scattering cross sections for ^{28}Si at $E_n = 9.8$ MeV.

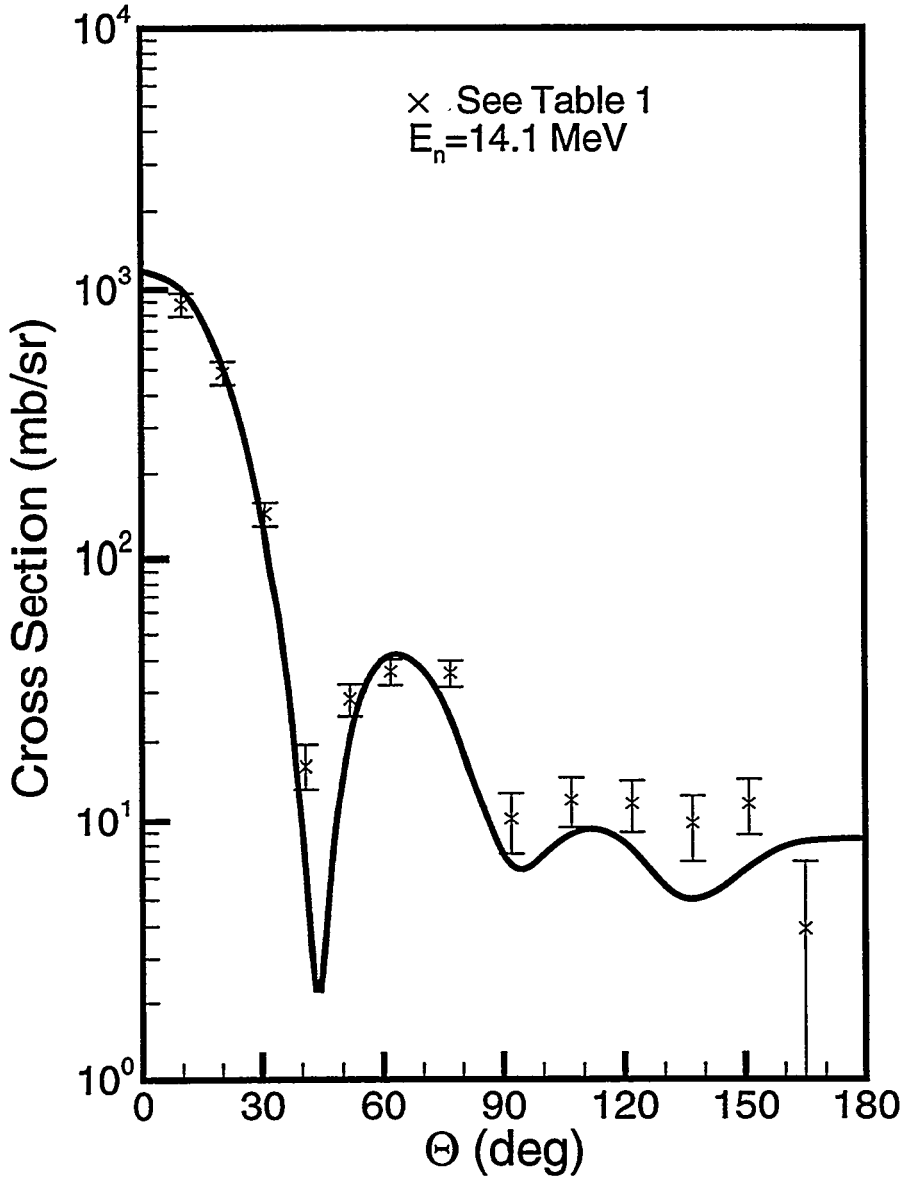

Fig. 5. Comparison of calculated and experimental differential elastic scattering cross sections for ^{28}Si at $E_n = 14.1$ MeV.

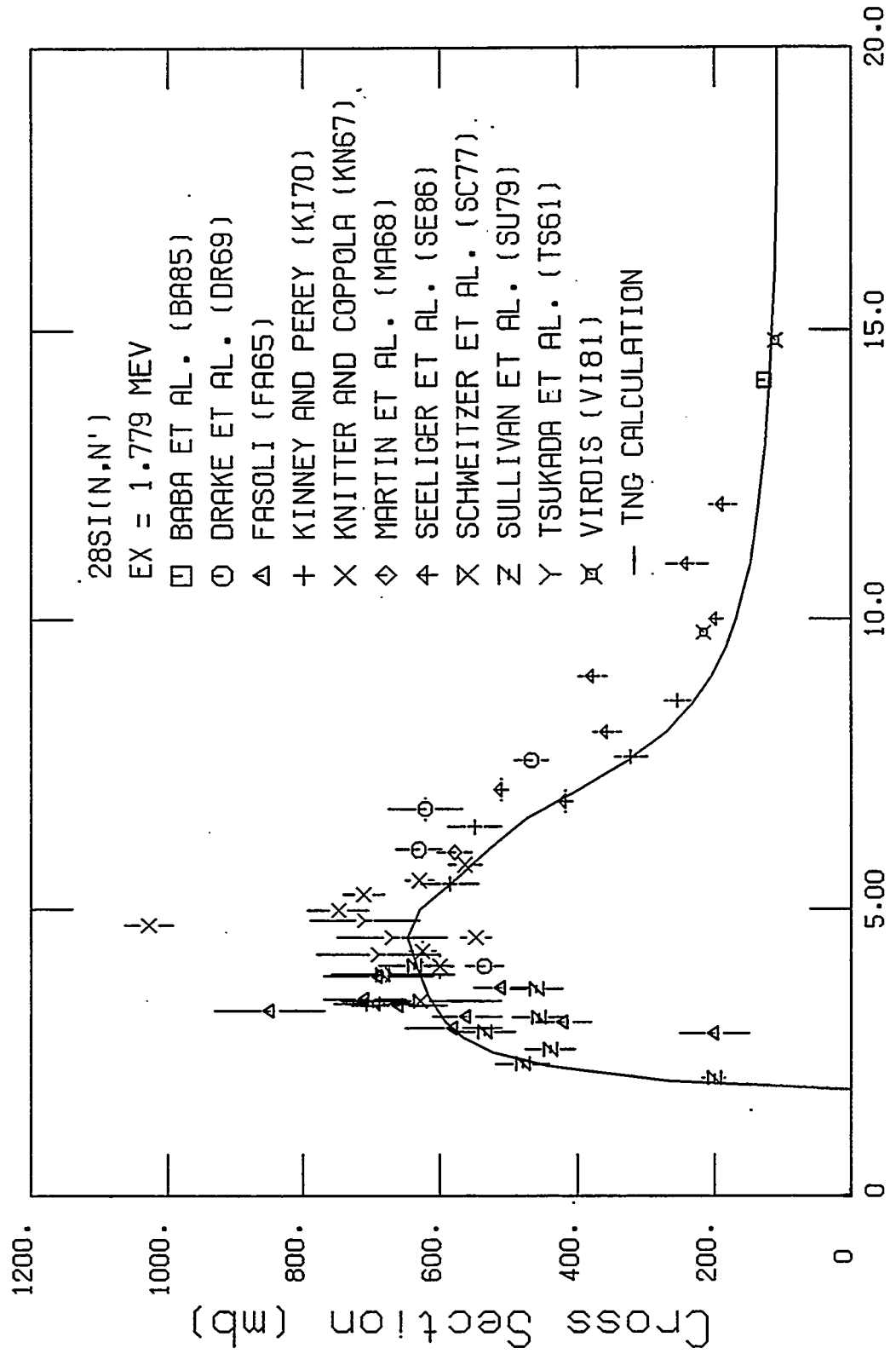

Fig. 6. Comparison of calculated and experimental $^{28}Si(n,n')$ cross sections for exciting the 1.779-MeV level.

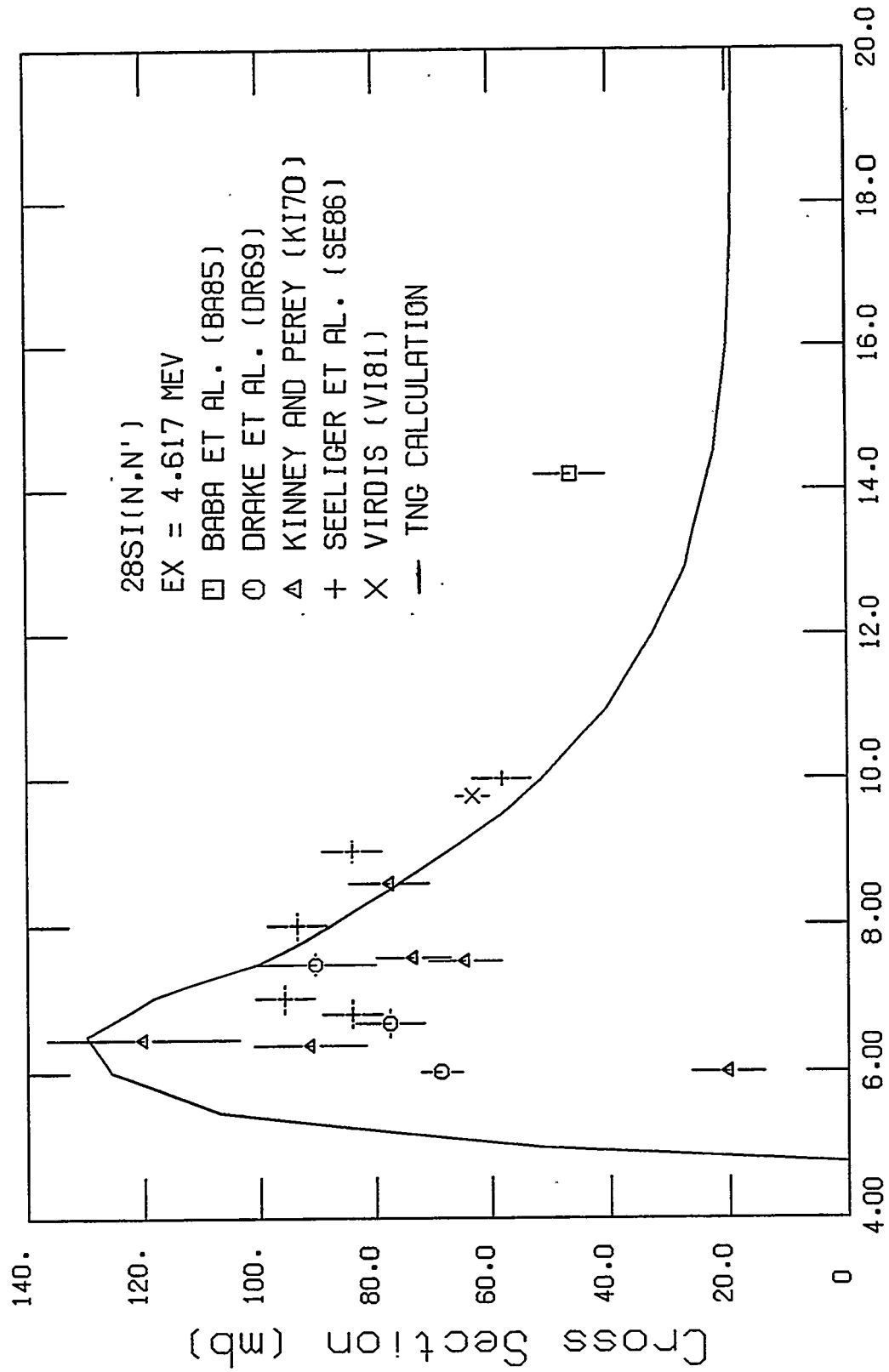

Fig. 7. Comparison of calculated and experimental ^{28}Si(n,n') cross sections for exciting the 4.617-MeV level.

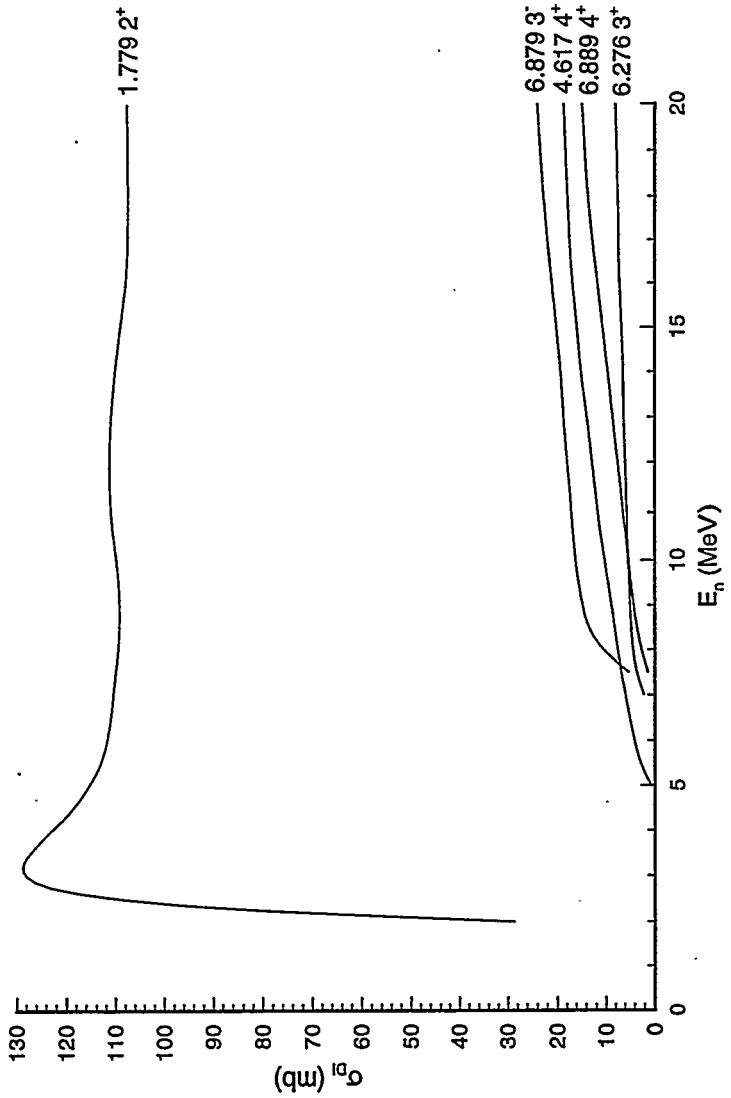

Fig. 8. Calculated direct inelastic excitation cross sections for ^{28}Si.

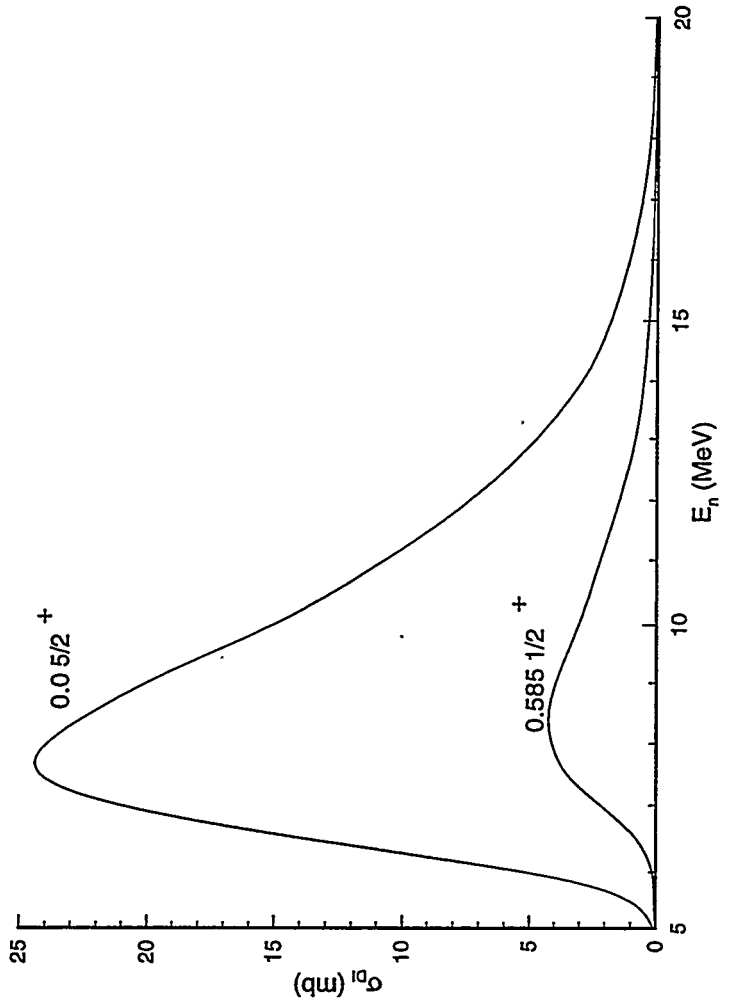

Fig. 9. Direct reaction contributions to the $^{28}Si(n,\alpha_i)$ cross sections.

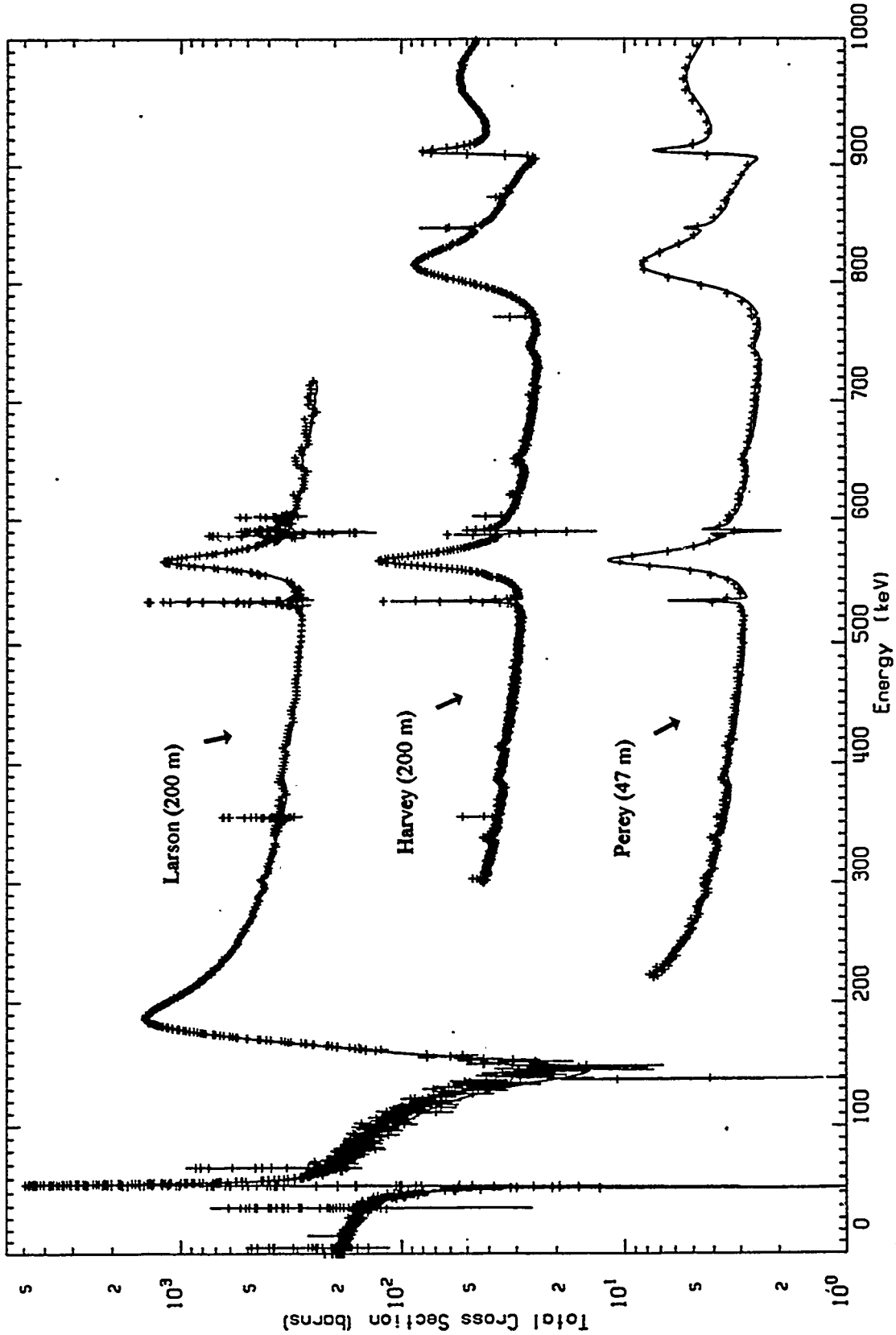

Fig. 10. Comparison of SAMMY fit to various data sets for the total cross section for E_n up to 1000 keV. The data are summarized in Table 1. For clarity, Larson data are displaced upward by two decades, whereas Harvey data are shifted by one decade.

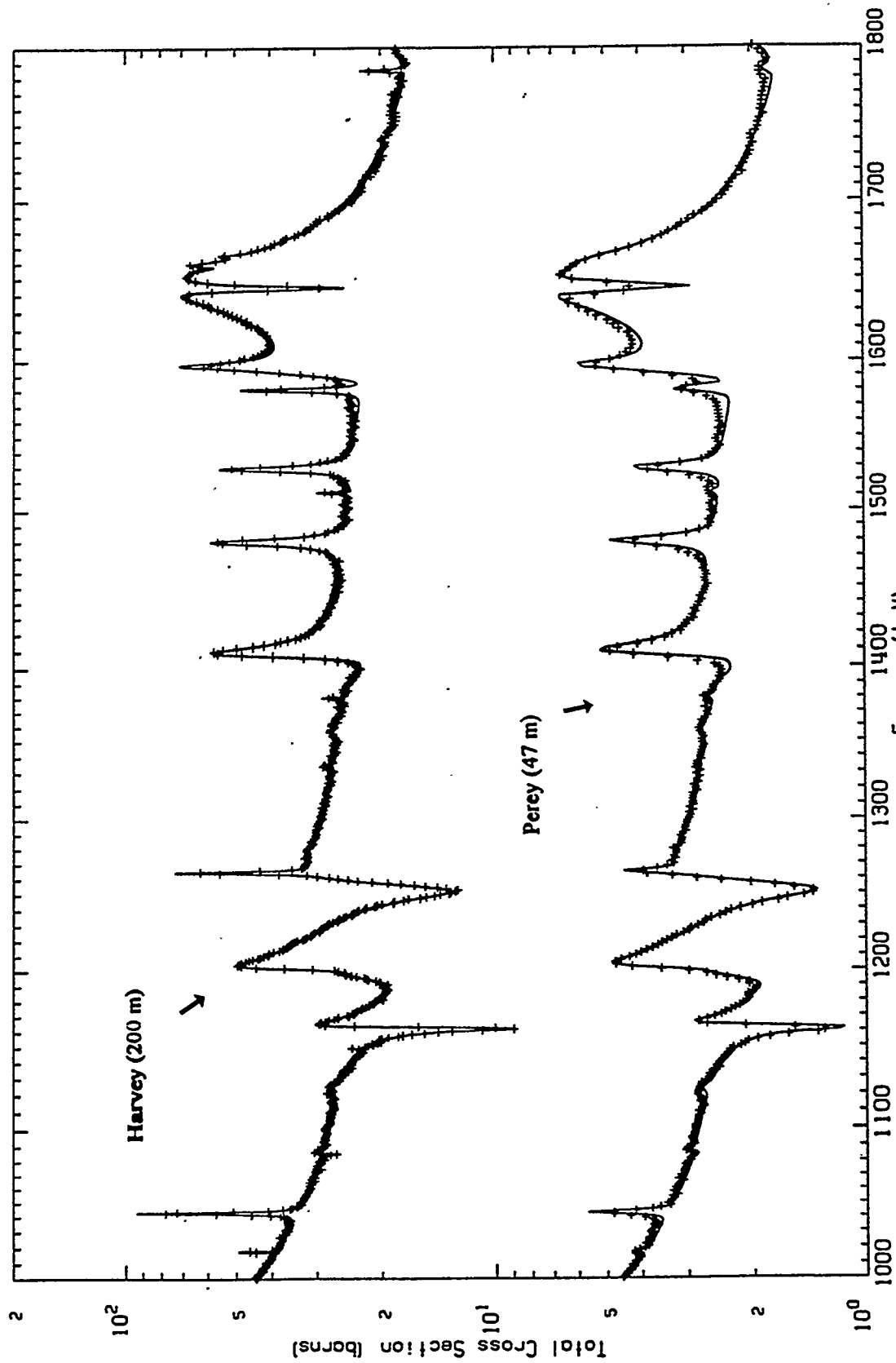

Fig. 11. Comparison of SAMMY fit to various data sets for the total cross section for E_n from 1000–1800 keV. The data are summarized in Table 1. For clarity, Harvey data are displaced upward by one decade.

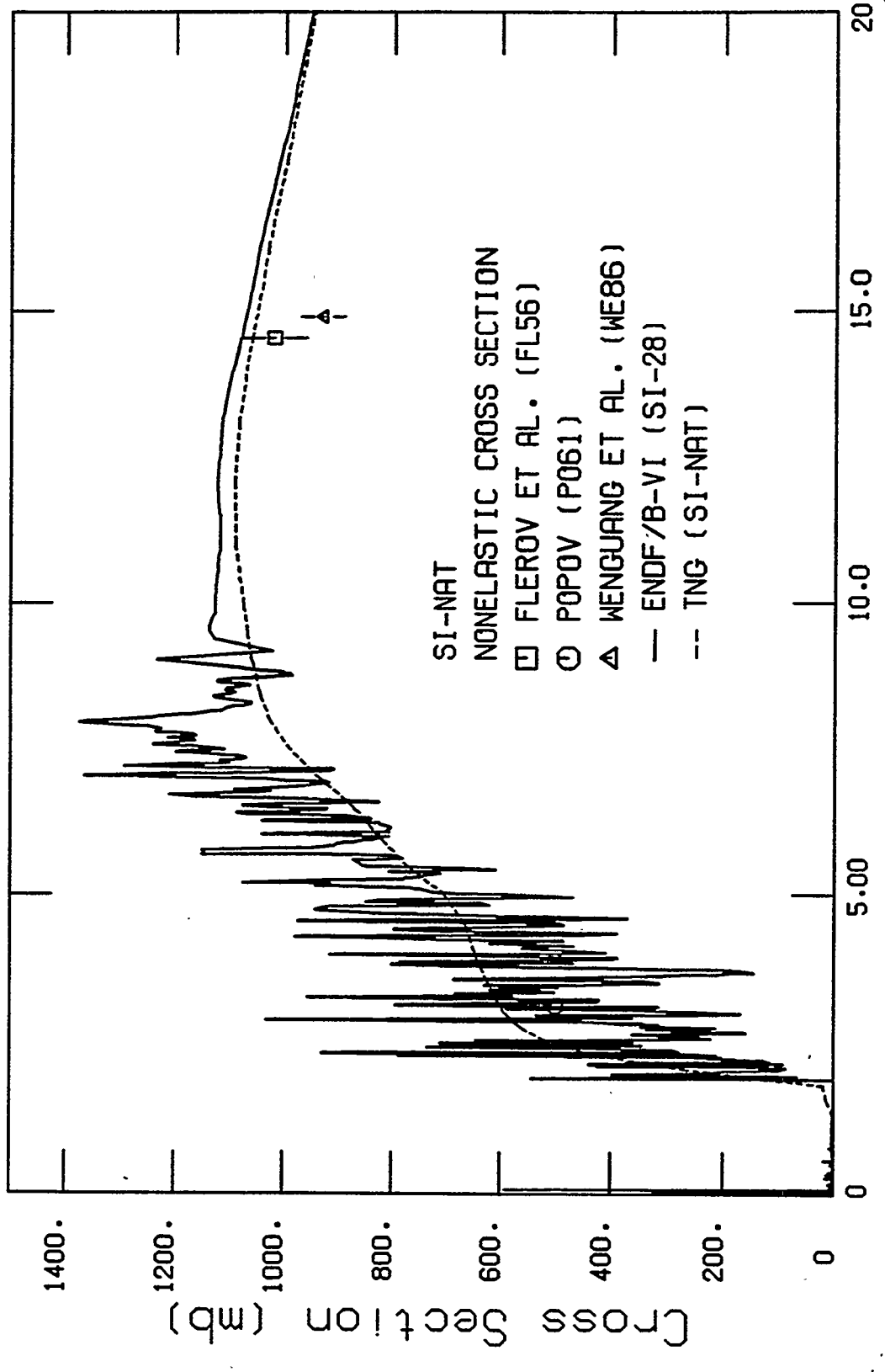

Fig. 12. Comparison of TNG calculated and ENDF/B-VI nonelastic cross sections with experimental data for ^{nat}Si.

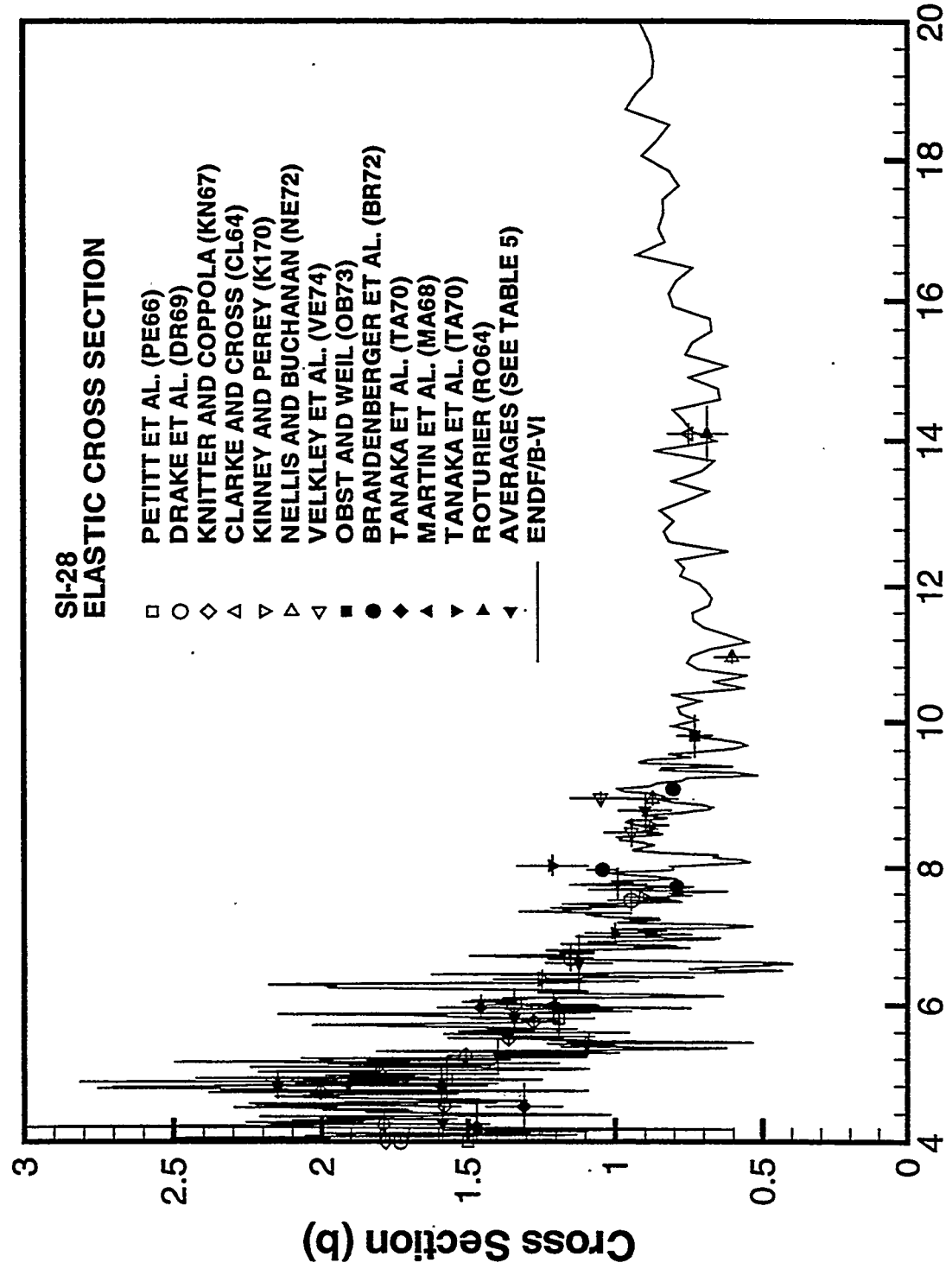

Fig. 13. Comparison of elastic cross section from ENDF/B-VI for ^{28}Si and experimental data for ^{nat}Si from 4.0 to 20.0 MeV.

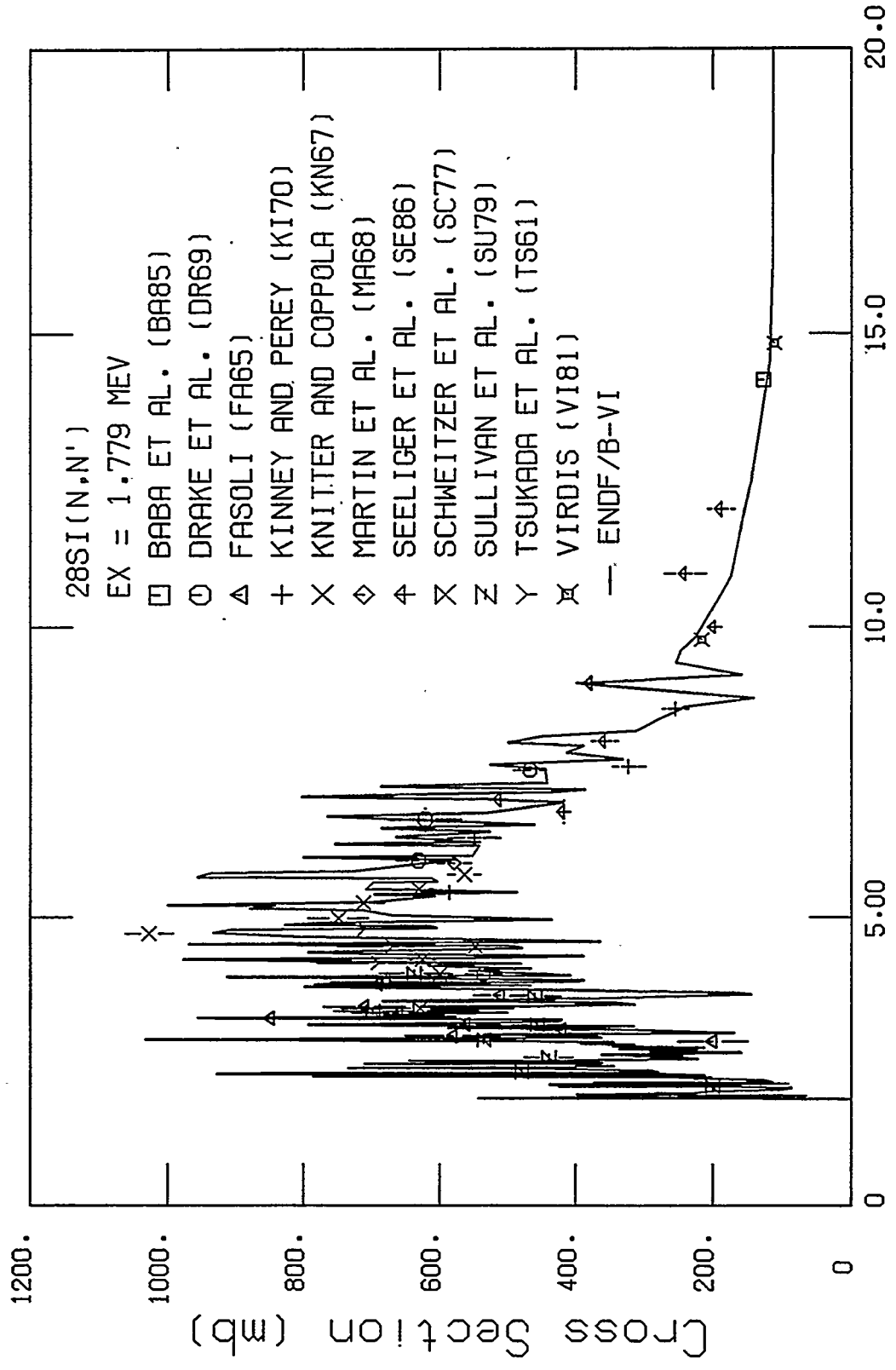

Fig. 14. Comparison of ENDF/B-VI and experimental ^{28}Si(n,n') cross sections for exciting the 1.779-MeV level.

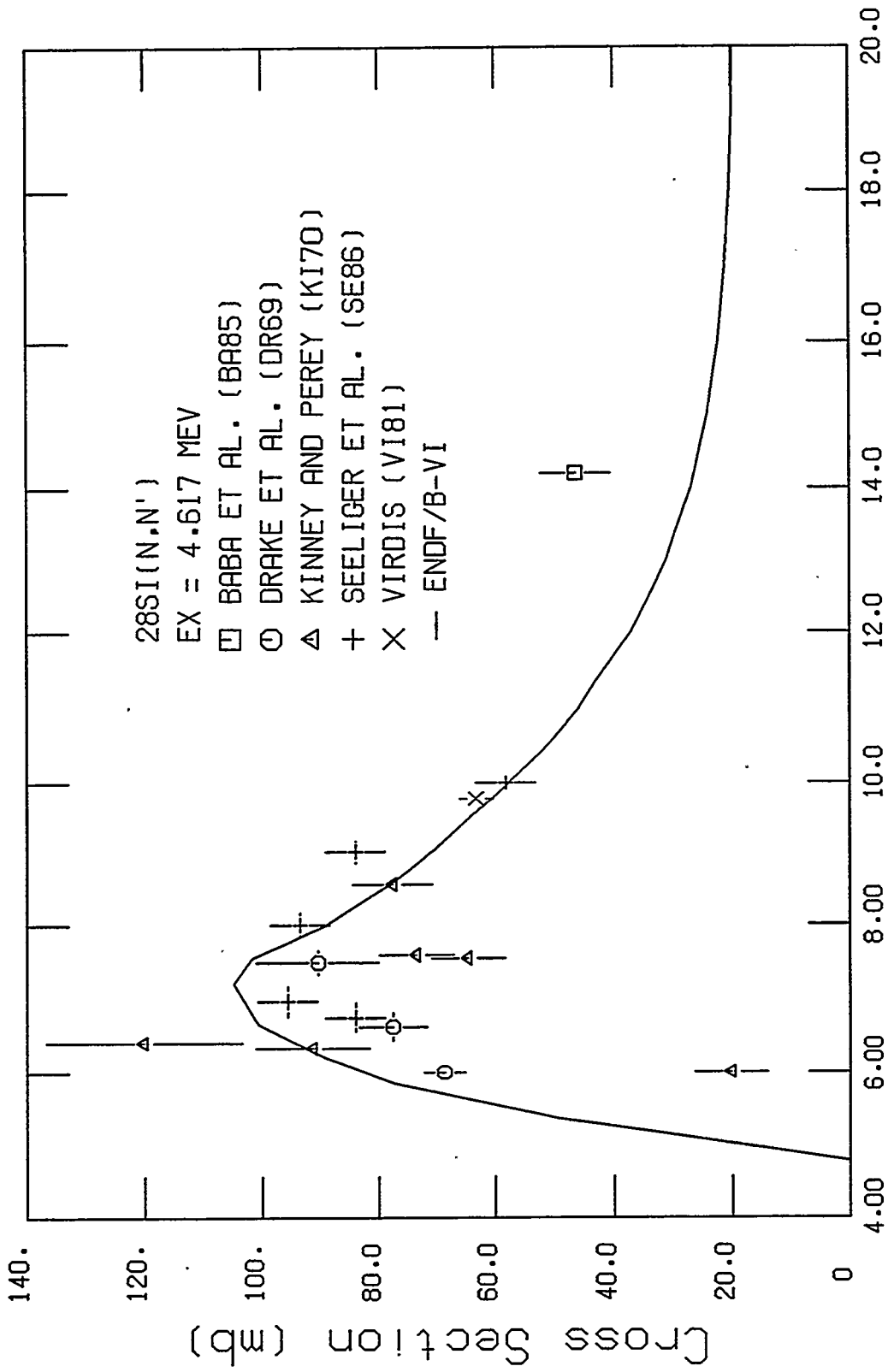

Fig. 15. Comparison of ENDF/B-VI and experimental $^{28}Si(n,n')$ cross sections for exciting the 4.617-MeV level.

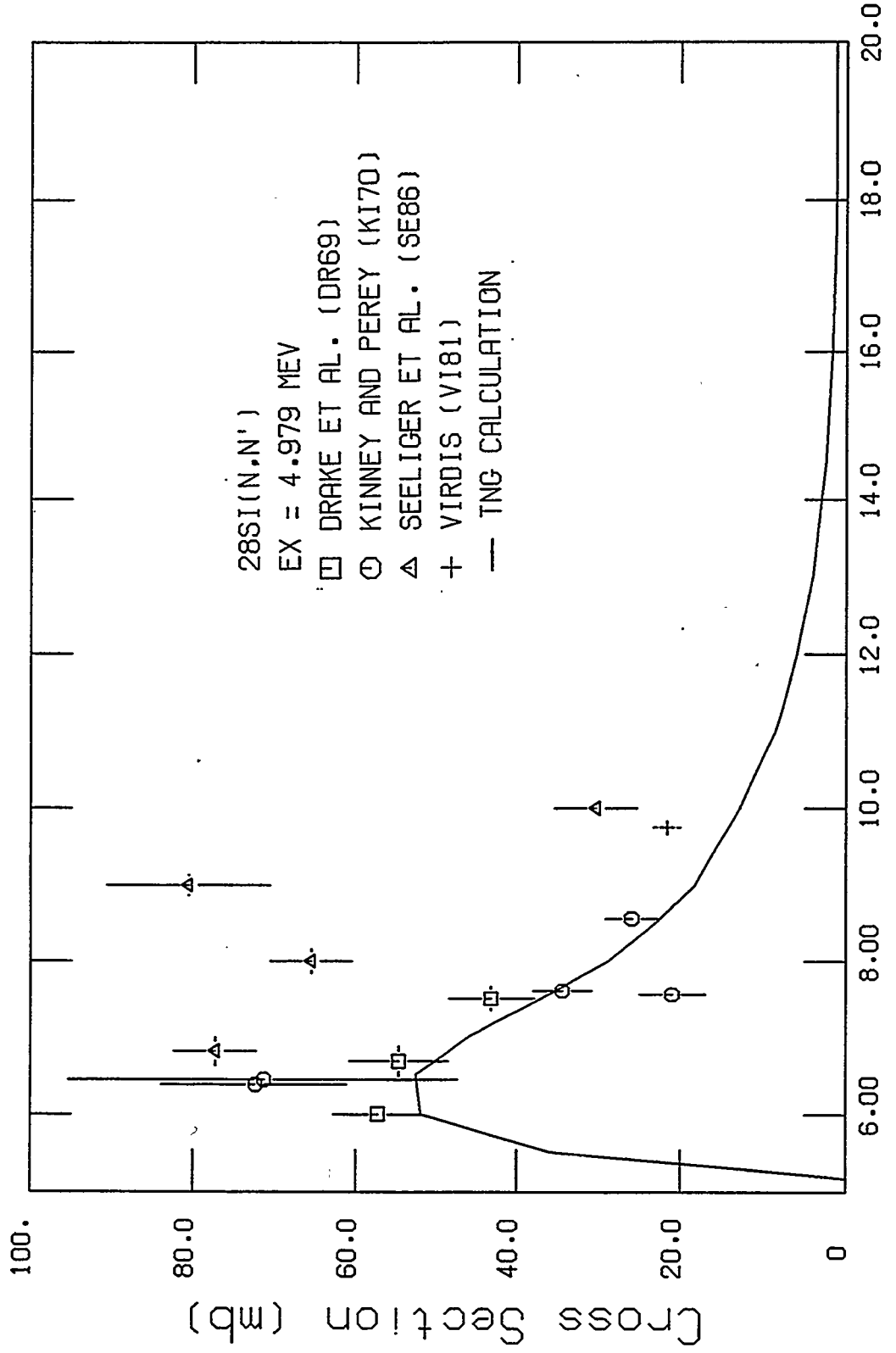

Fig. 16. Comparison of ENDF/B-VI and experimental ^{28}Si(n,n') cross sections for exciting the 4.979-MeV level.

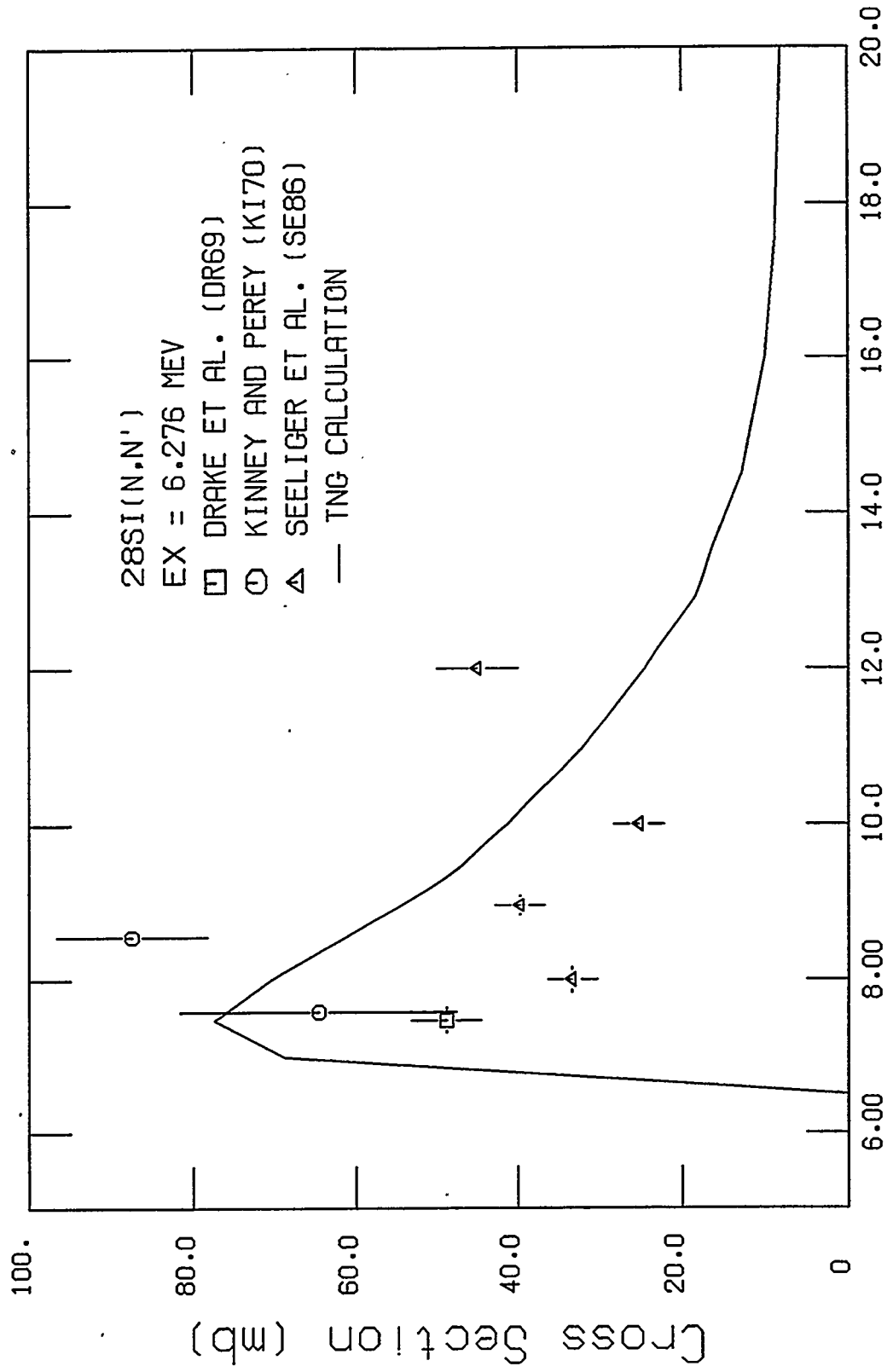

Fig. 17. Comparison of ENDF/B-VI and experimental $^{28}Si(n,n')$ cross sections for exciting the 6.276-MeV level.

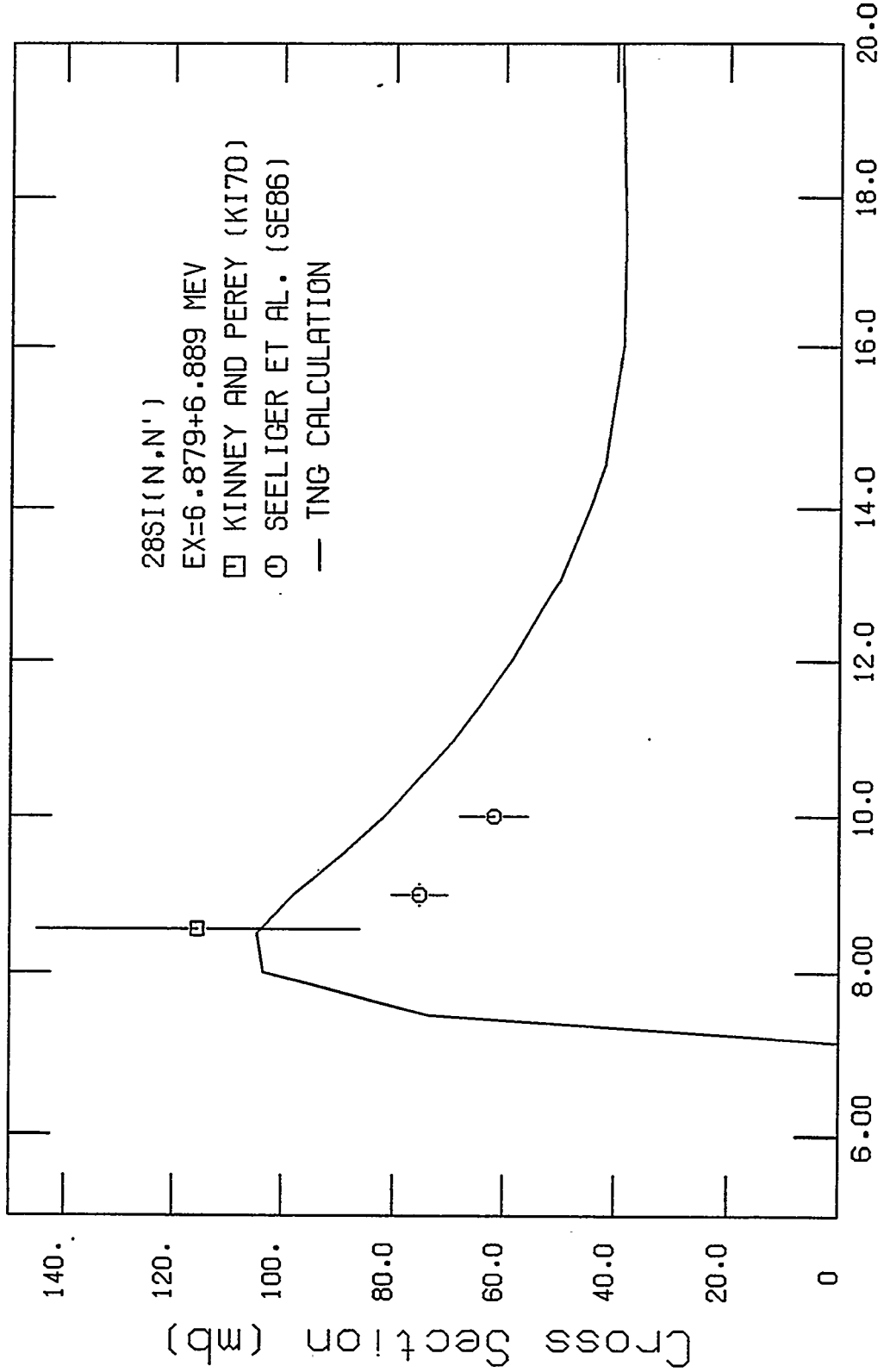

Fig. 18. Comparison of ENDF/B-VI and experimental $^{28}Si(n,n')$ cross sections for exciting the 6.879+6.889-MeV levels.

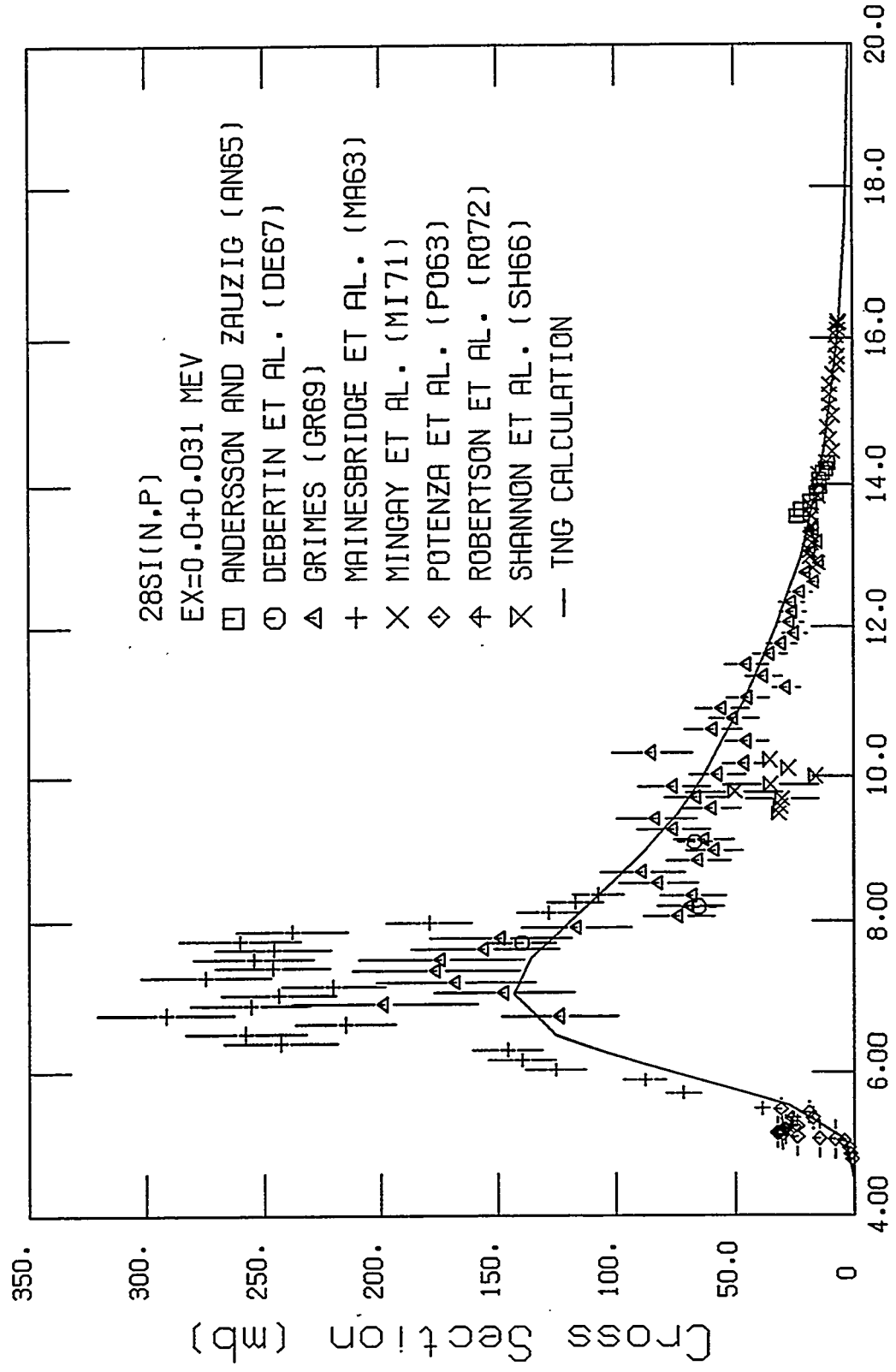

Fig. 19. Comparison of calculated and experimental $^{28}Si(n,p_{0+1})$ cross sections.

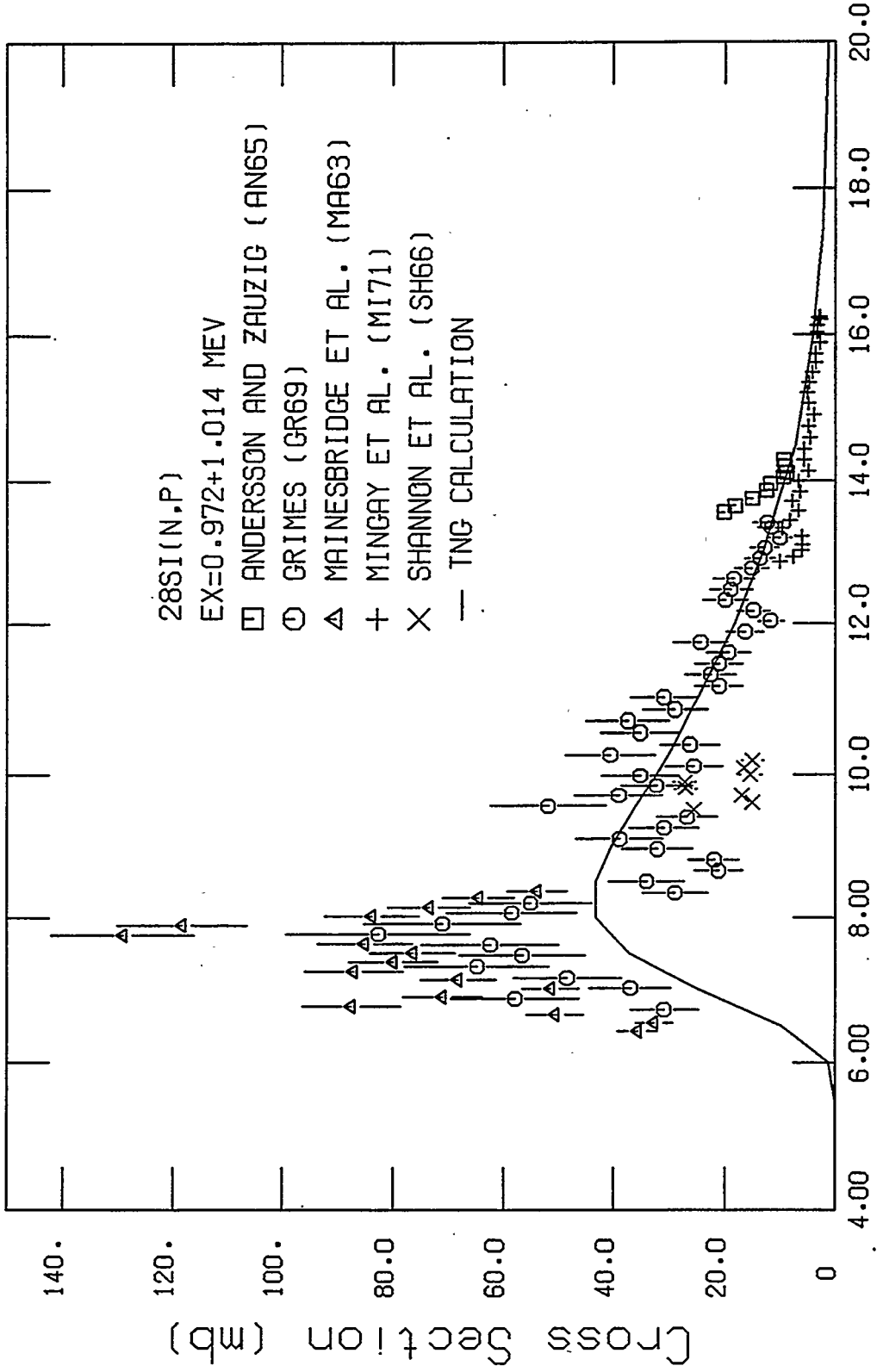

Fig. 20. Comparison of calculated and experimental $^{28}Si(n,p_{2+3})$ cross sections.

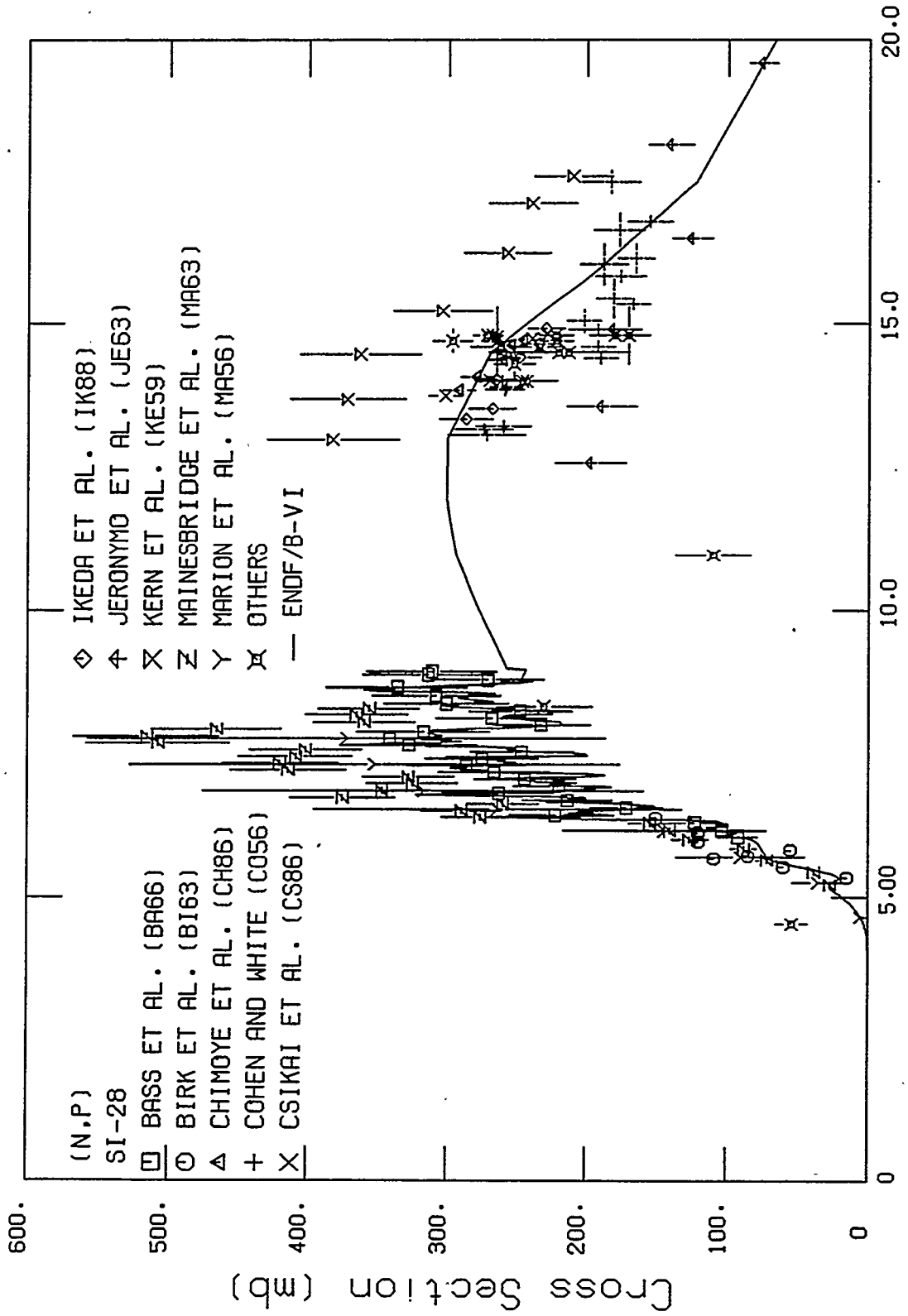

Fig. 21. Comparison of calculated and experimental ^{28}Si(n,p) cross sections.

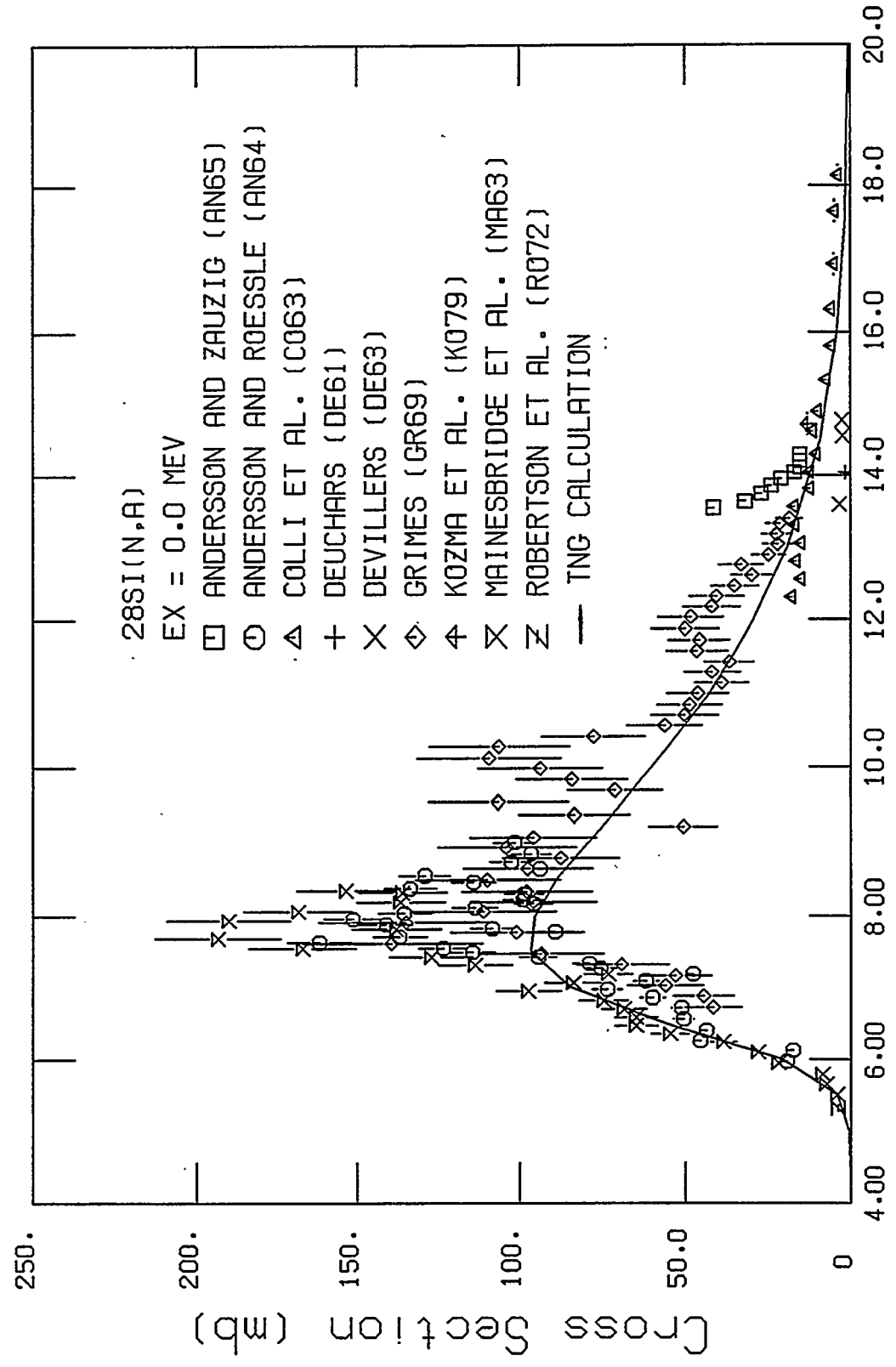

Fig. 22. Comparison of calculated and experimental $^{28}Si(n,\alpha_0)$ cross sections.

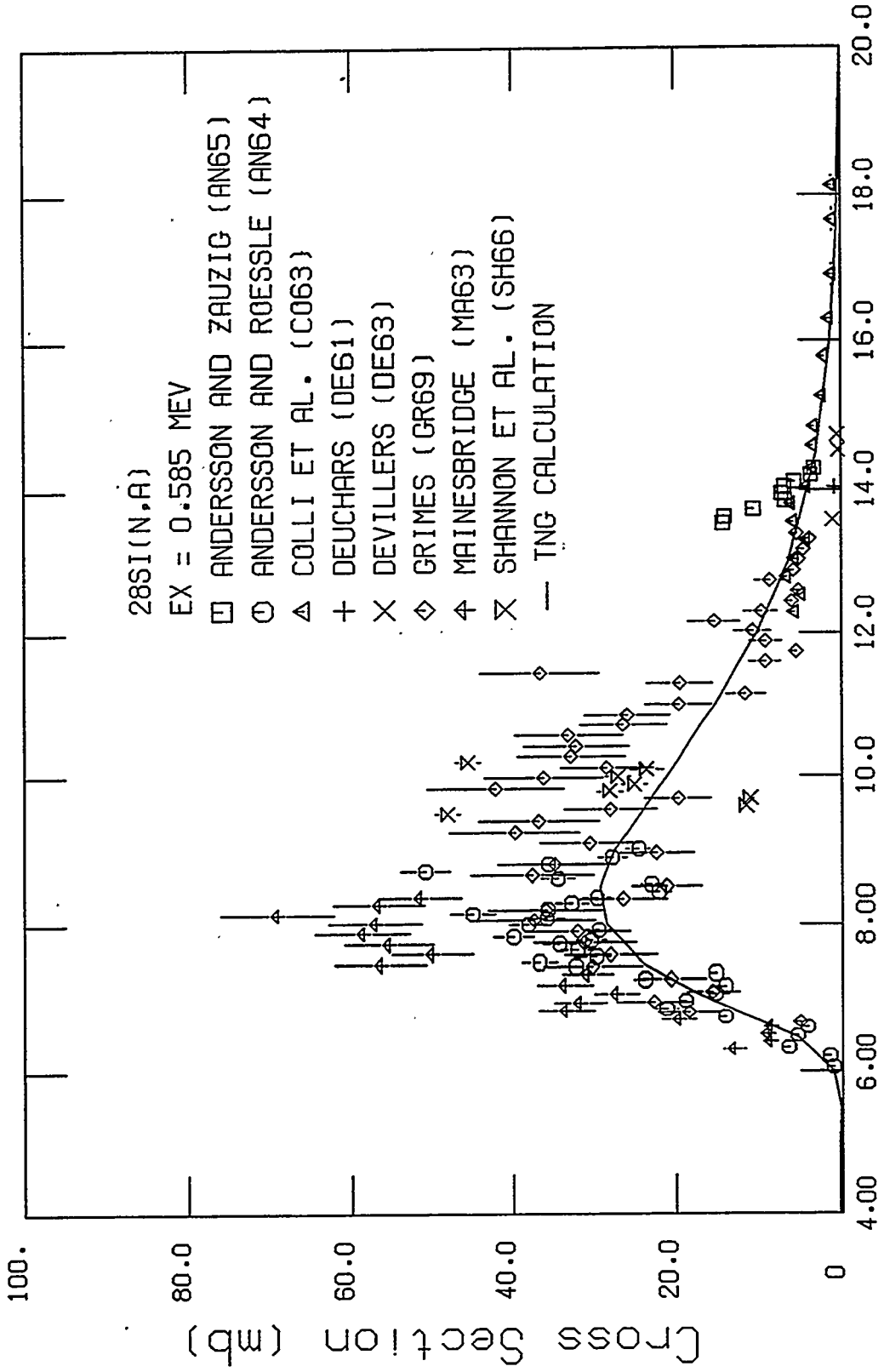

Fig. 23. Comparison of calculated and experimental $^{28}Si(n,\alpha_1)$ cross sections.

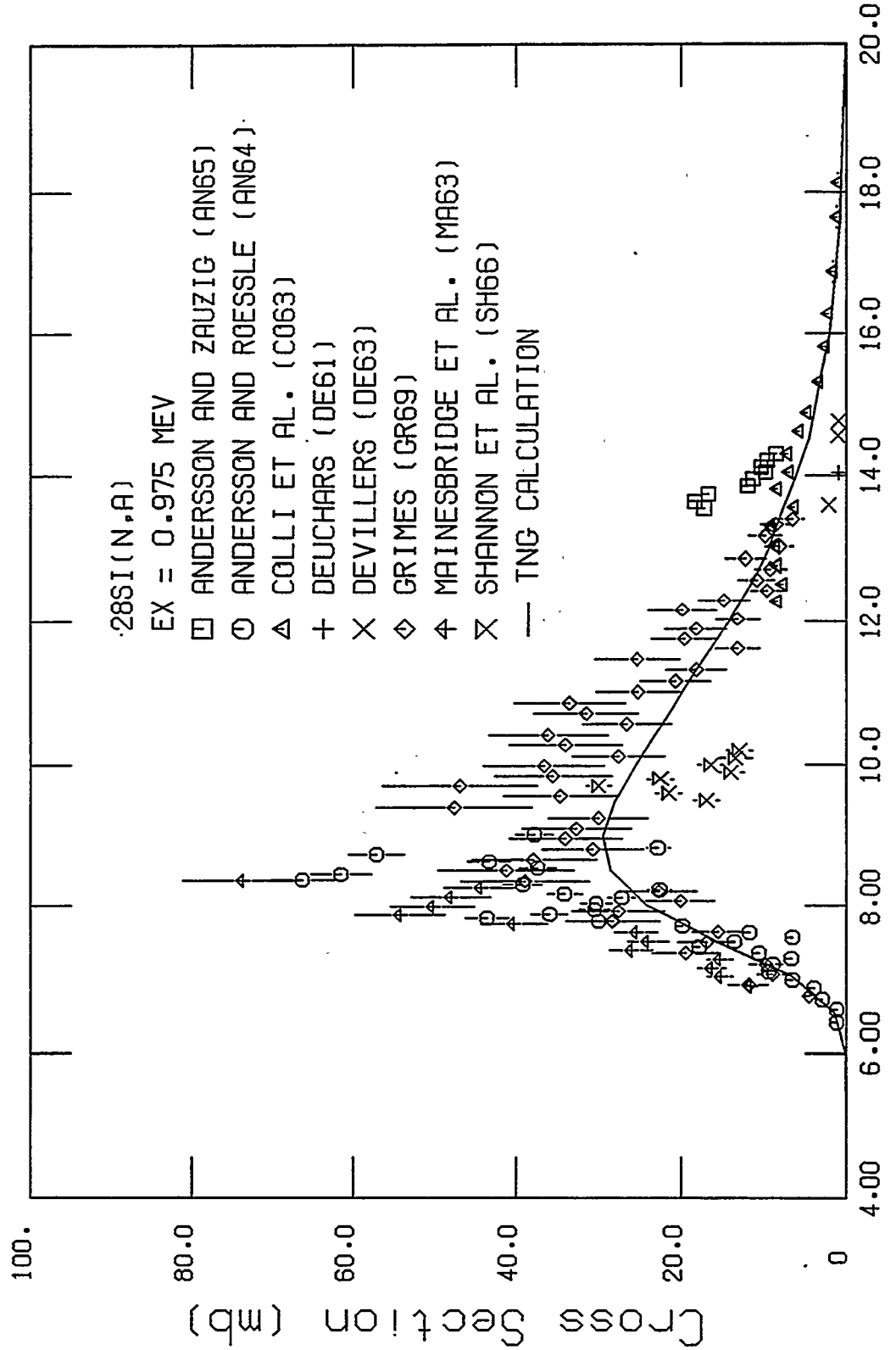

Fig. 24. Comparison of calculated and experimental $^{28}Si(n,\alpha_2)$ cross sections.

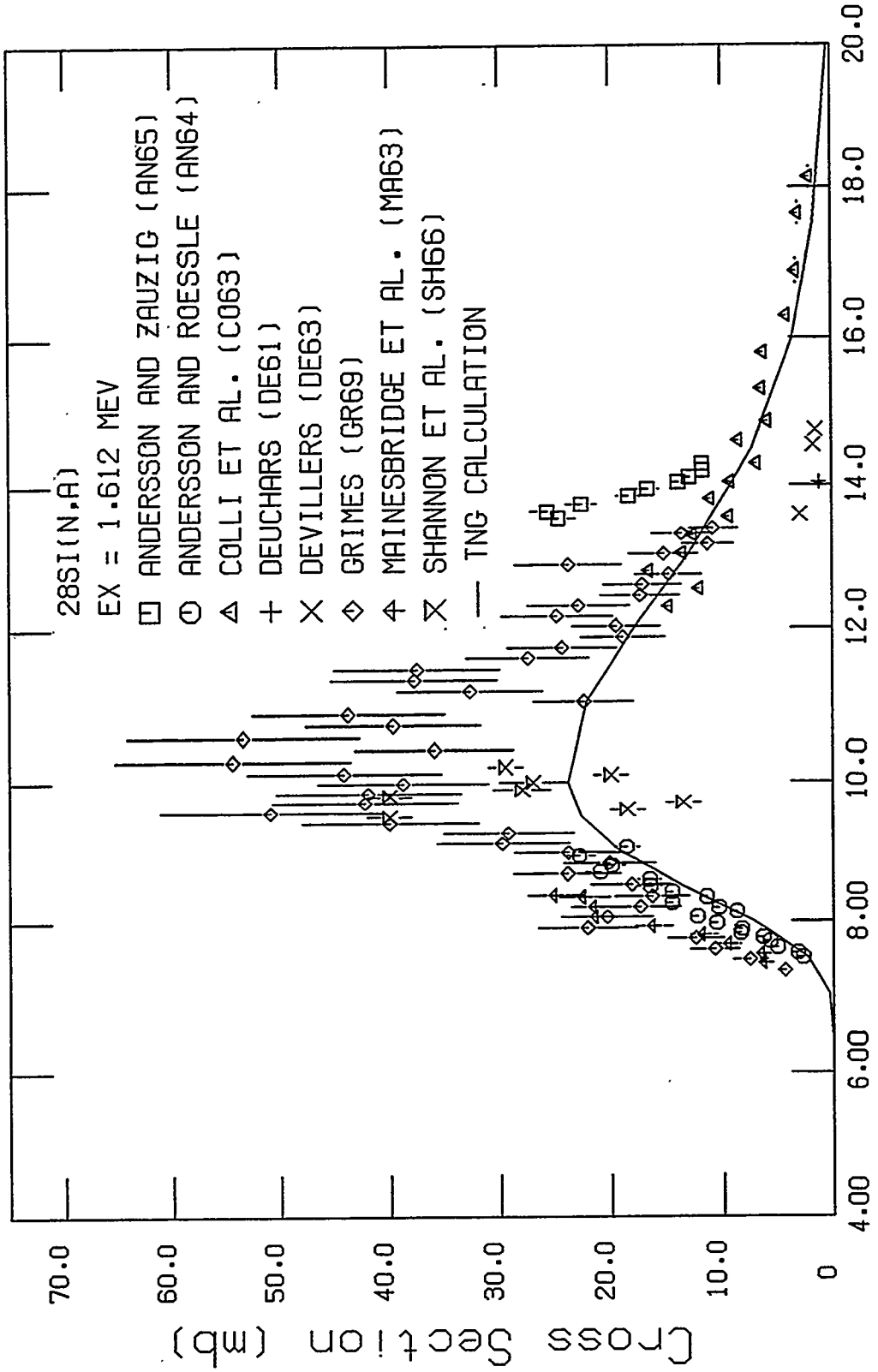

Fig. 25. Comparison of calculated and experimental $^{28}Si(n,\alpha_3)$ cross sections.

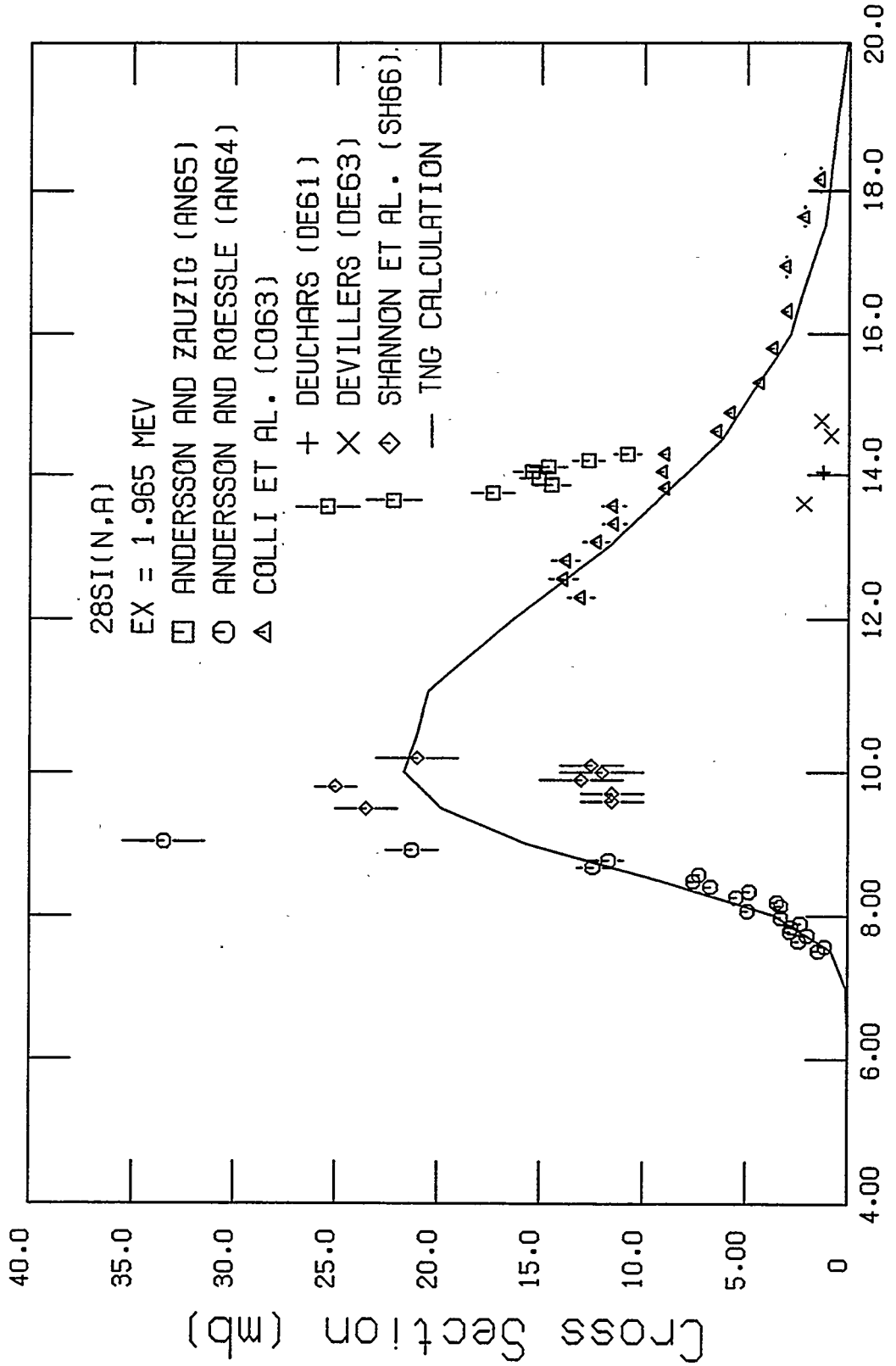

Fig. 26. Comparison of calculated and experimental $^{28}Si(n,\alpha_4)$ cross sections.

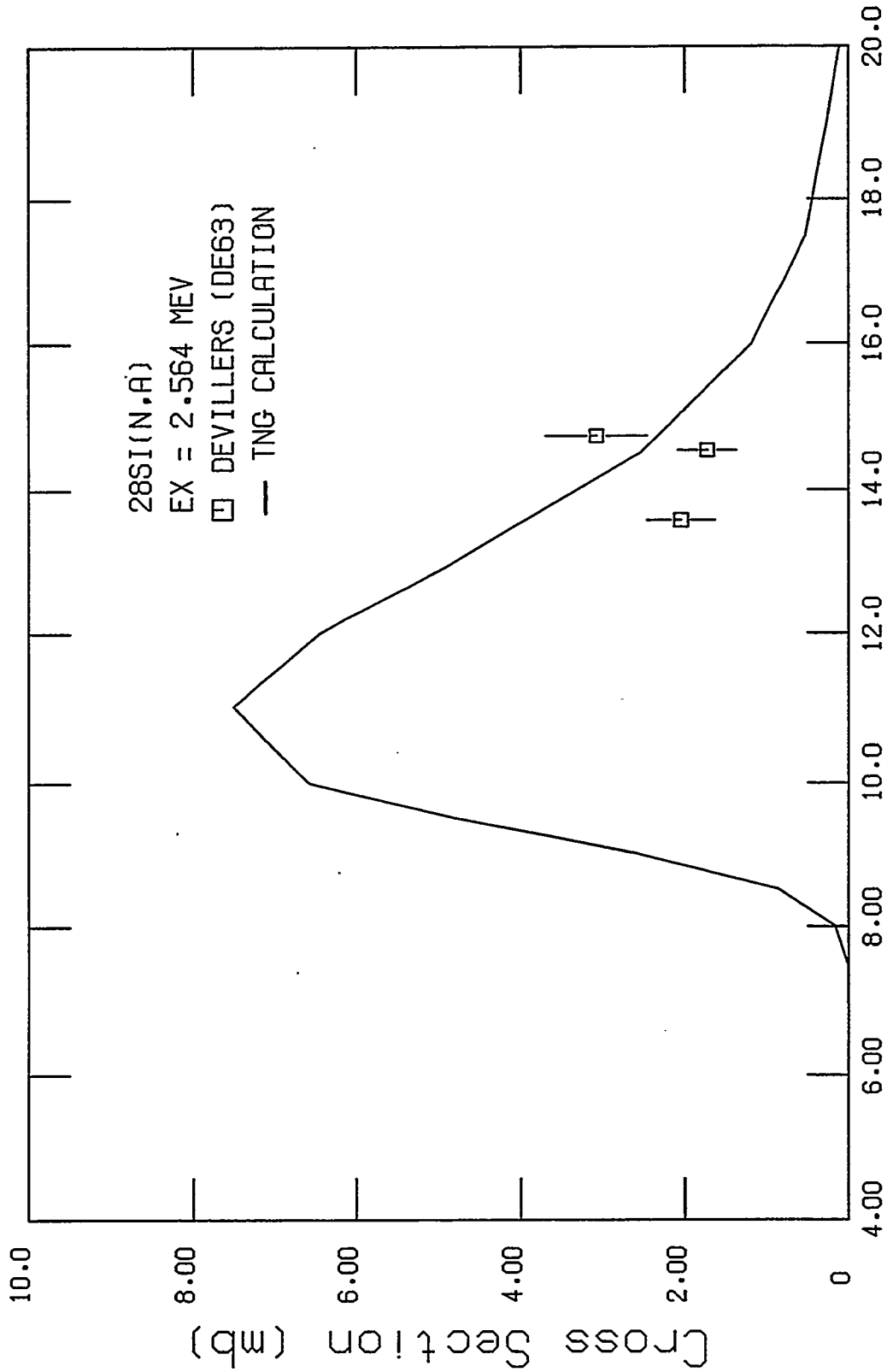

Fig. 27. Comparison of calculated and experimental $^{28}Si(n,\alpha_5)$ cross sections.

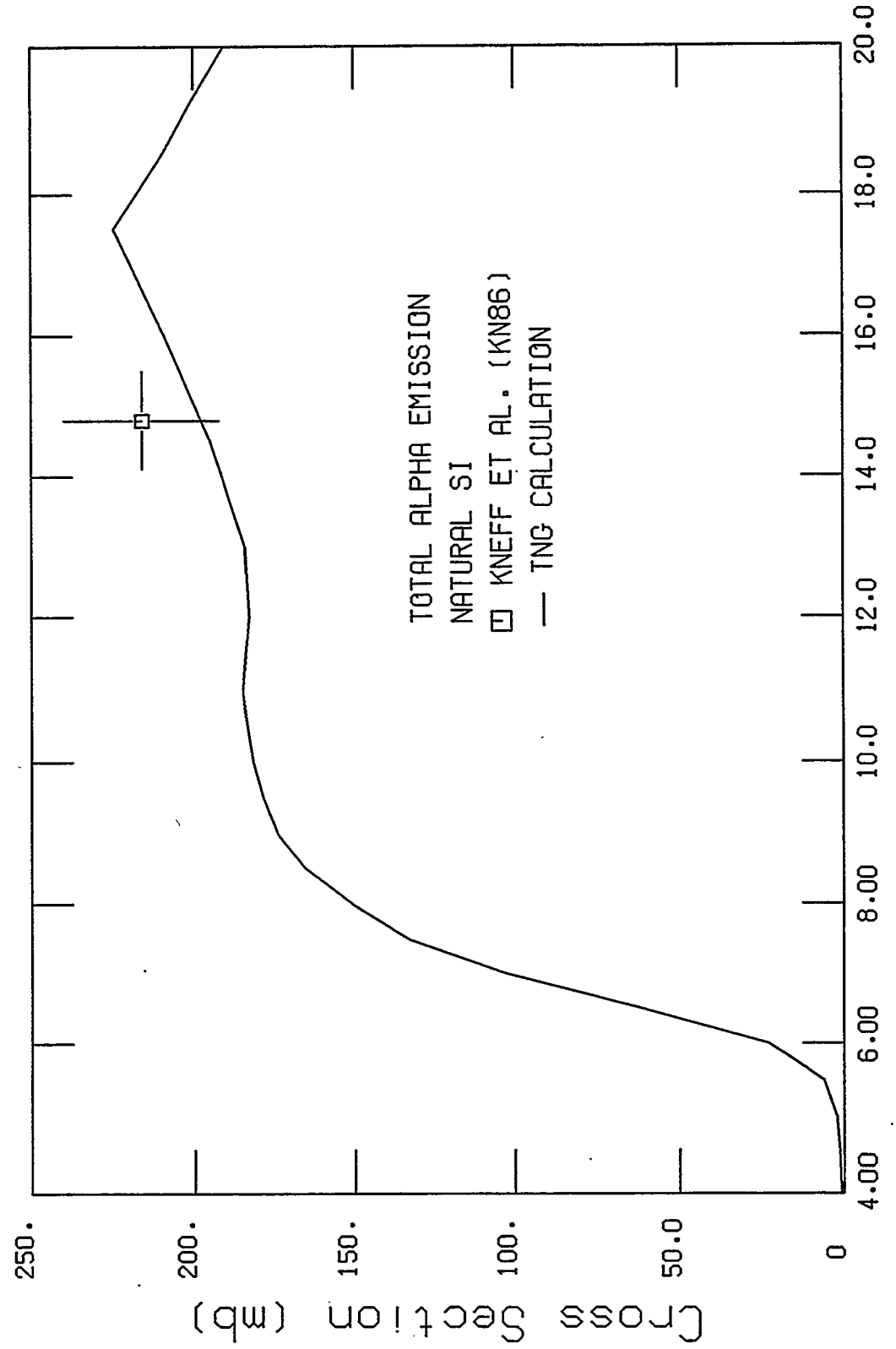

Fig. 28. Comparison of calculated and experimental cross sections for the total alpha emission of ^{nat}Si.

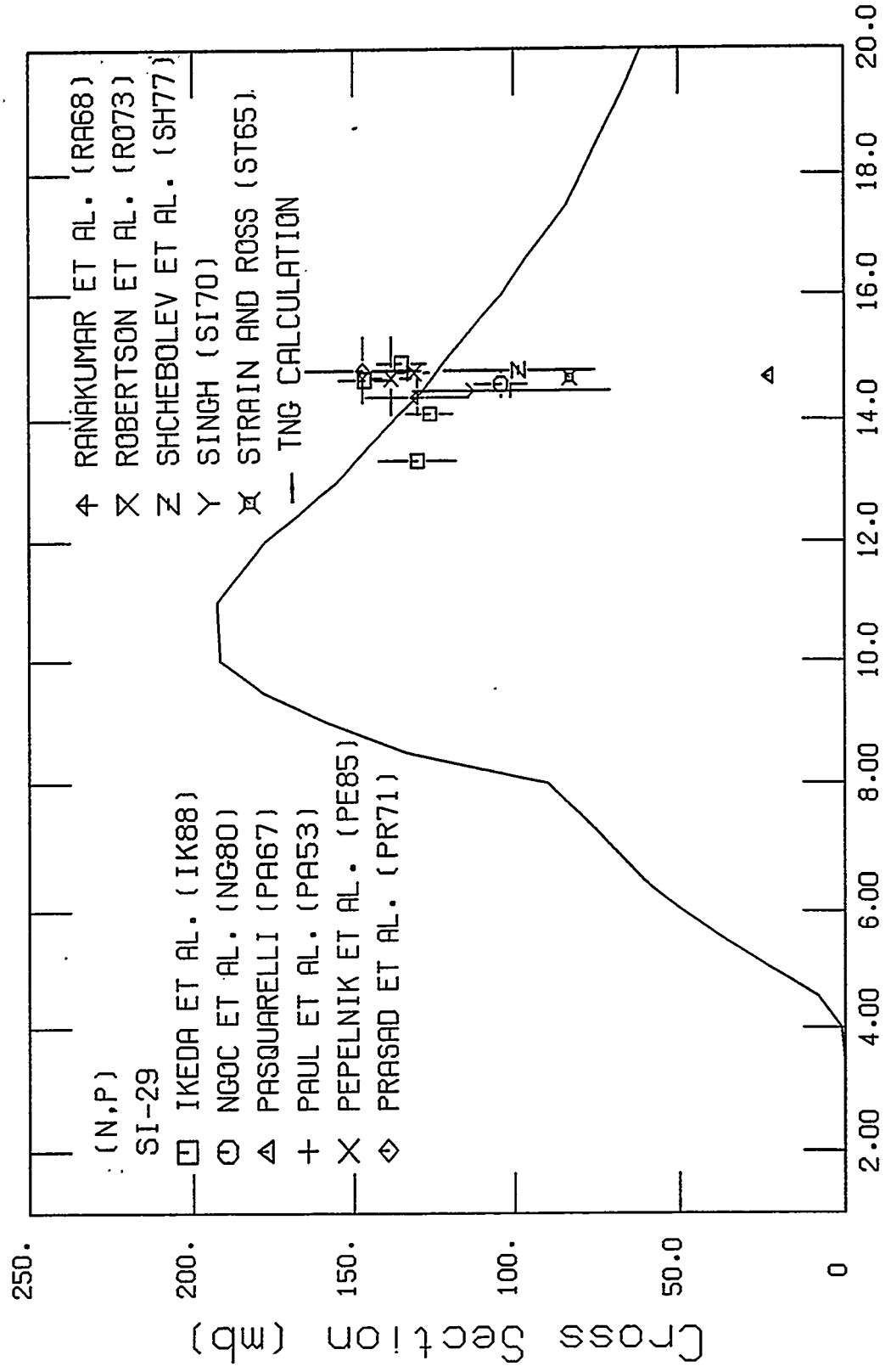

Fig. 29. Comparison of calculated and experimental ^{29}Si(n,p) cross sections.

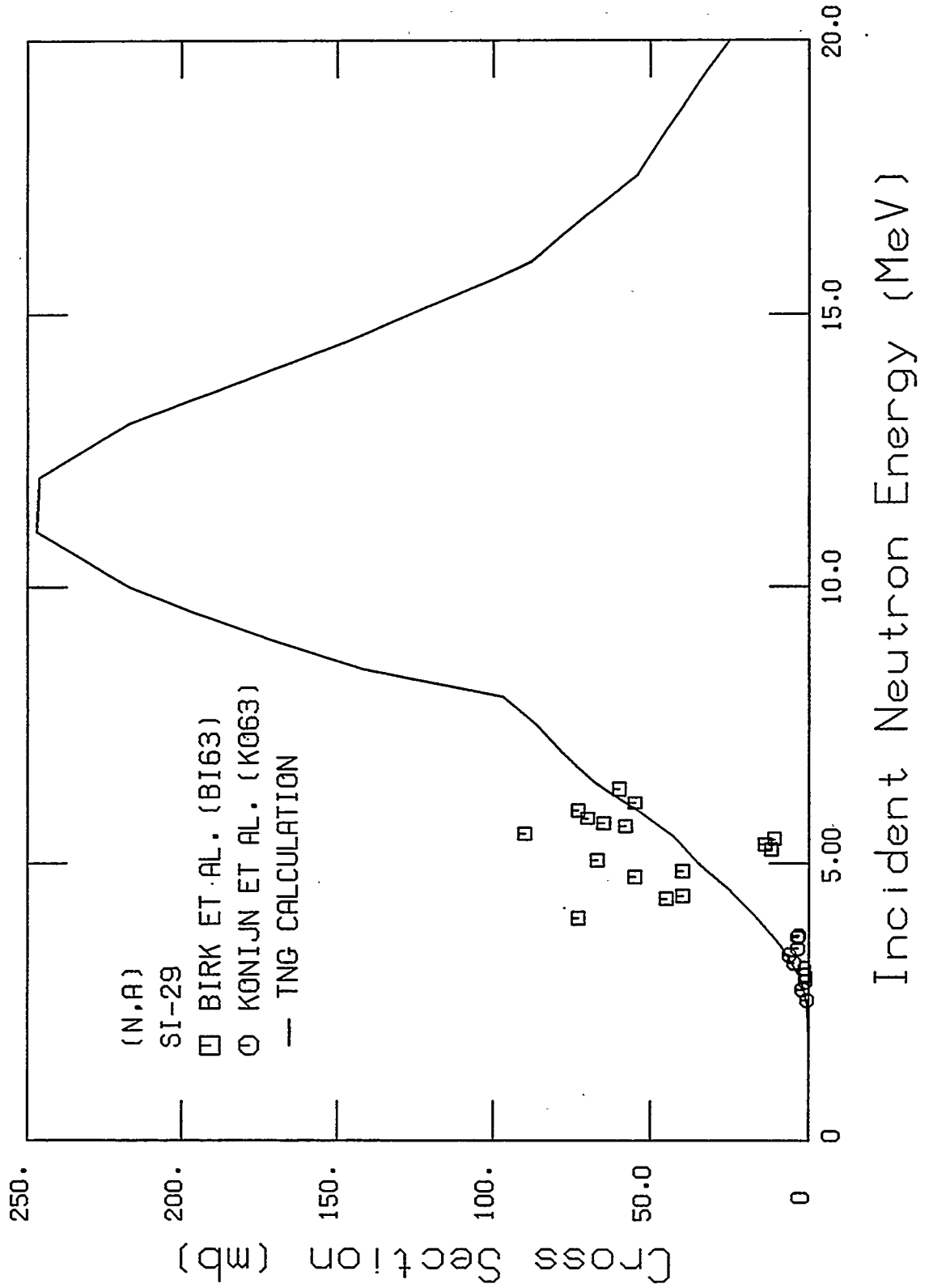

Fig. 30. Comparison of calculated and experimental $^{29}Si(n,\alpha)$ cross sections.

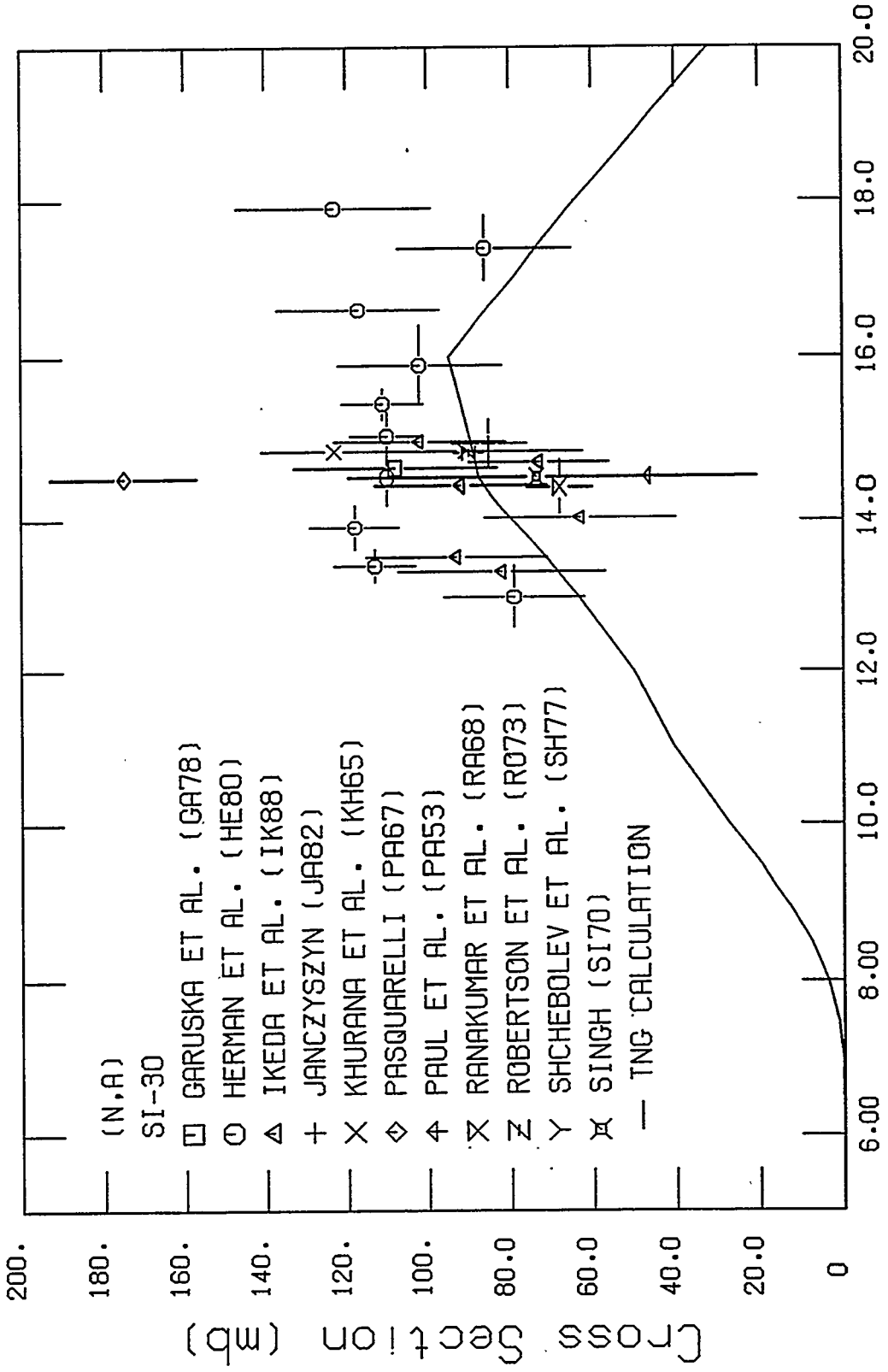

Fig. 31. Comparison of calculated and experimental $^{30}Si(n,\alpha)$ cross sections.

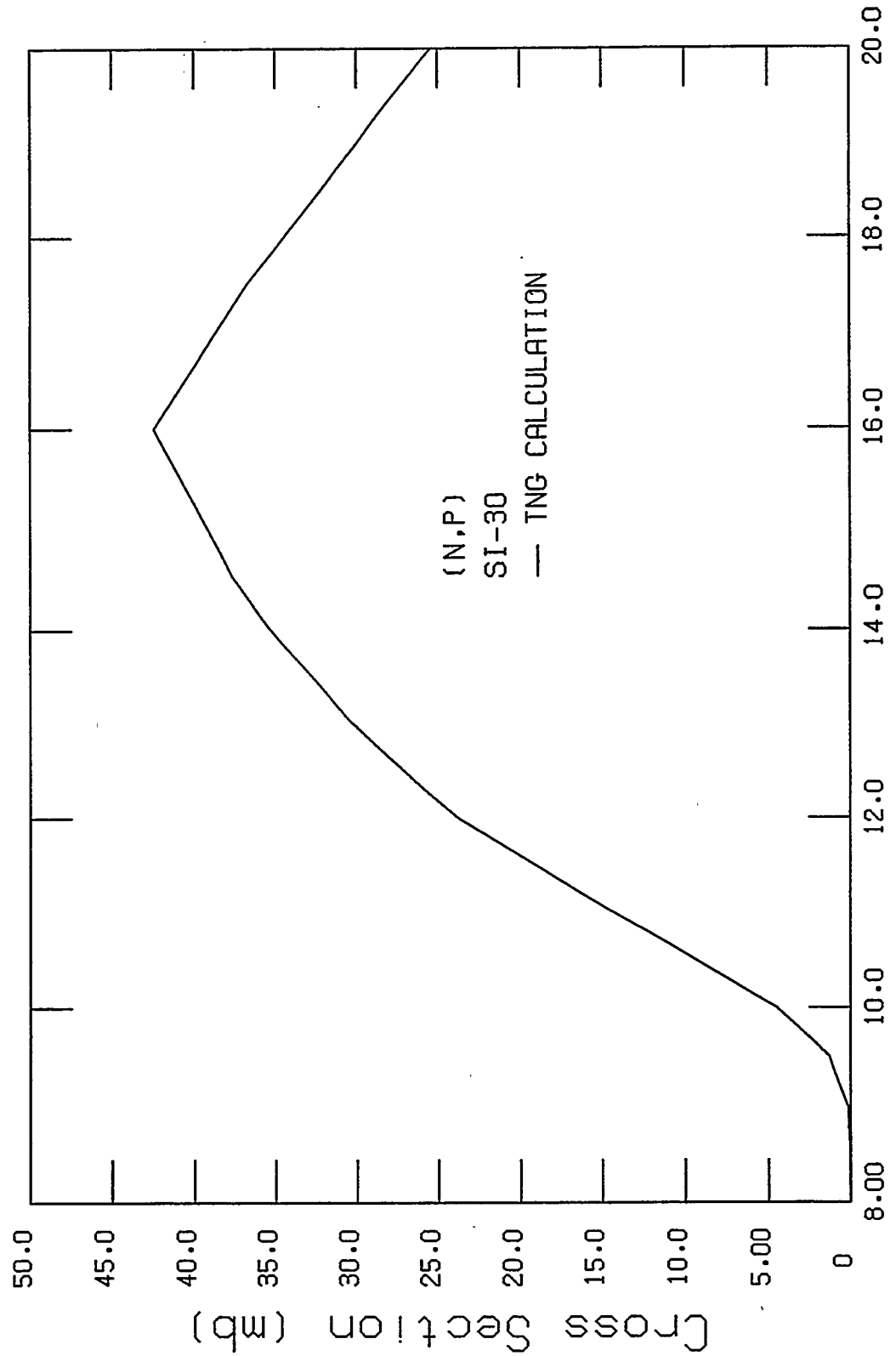

Fig. 32. TNG calculated cross section for ^{30}Si(n,p).

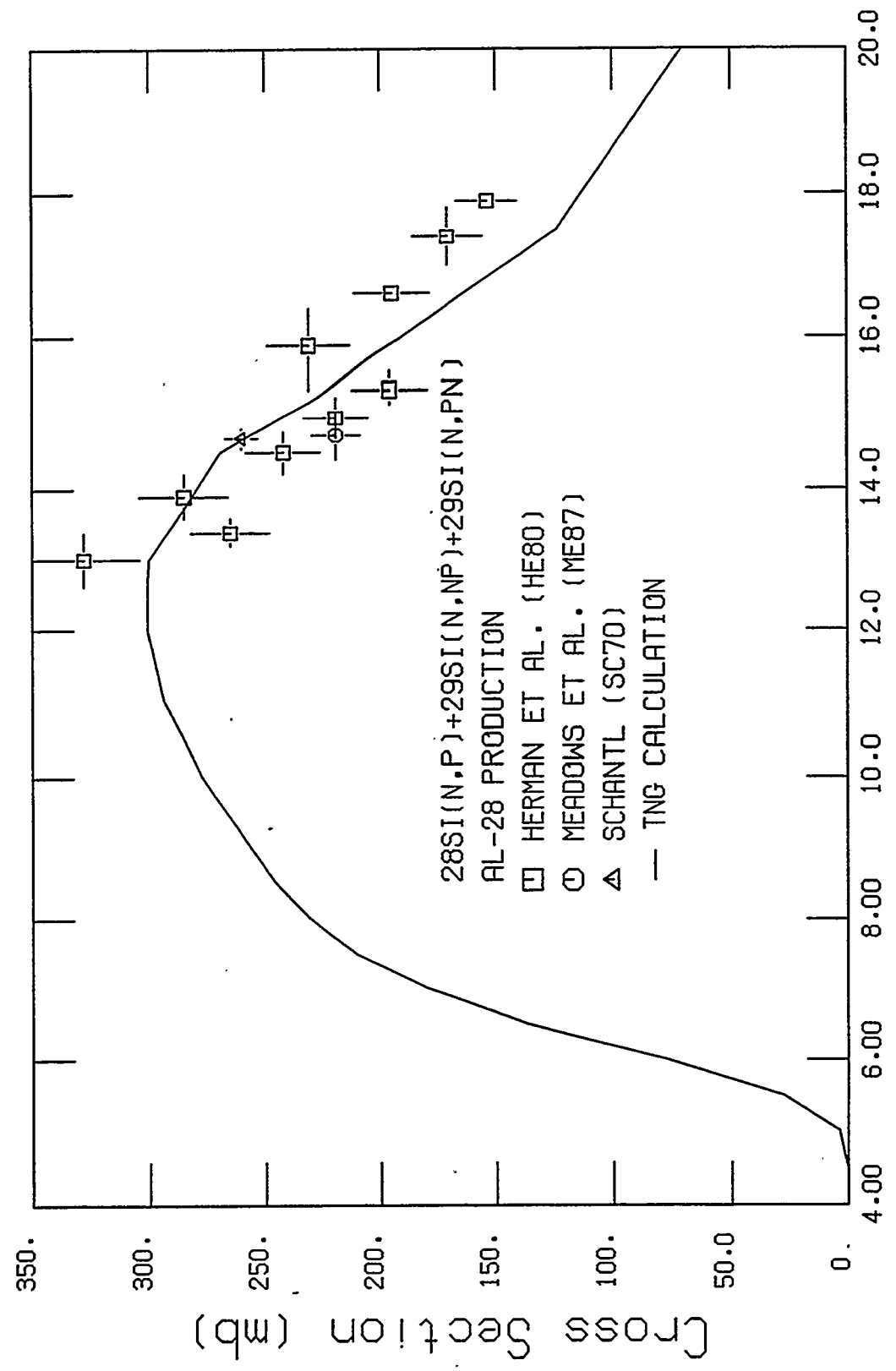

Fig. 33. Comparison of calculated and experimental $^{28}Si(n,p)+^{29}Si(n,np)+^{29}Si(n,pn)$ cross sections.

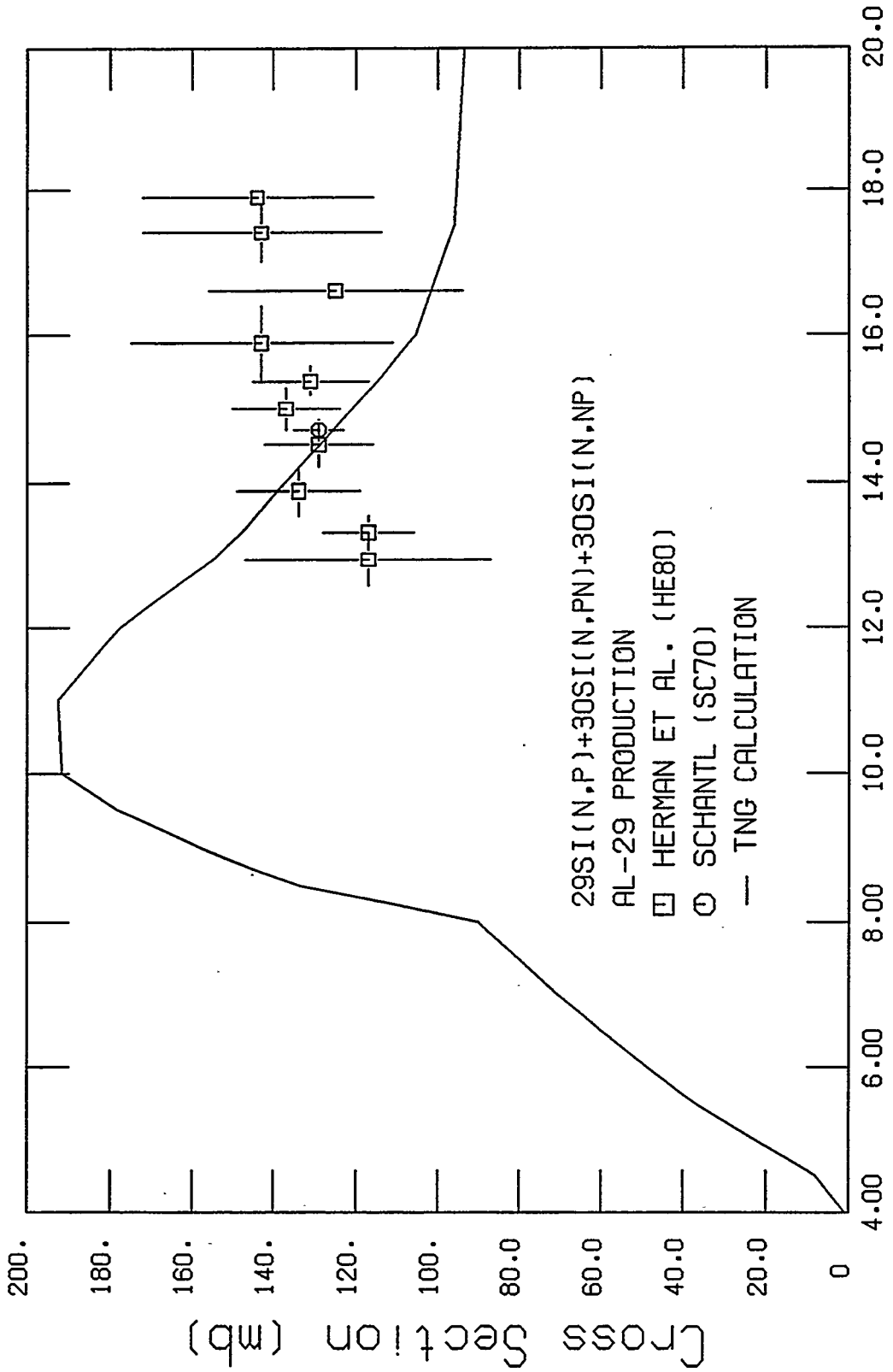

Fig. 34. Comparison of calculated and experimental $^{29}Si(n,p)+^{30}Si(n,np)+^{30}Si(n,pn)$ cross sections.

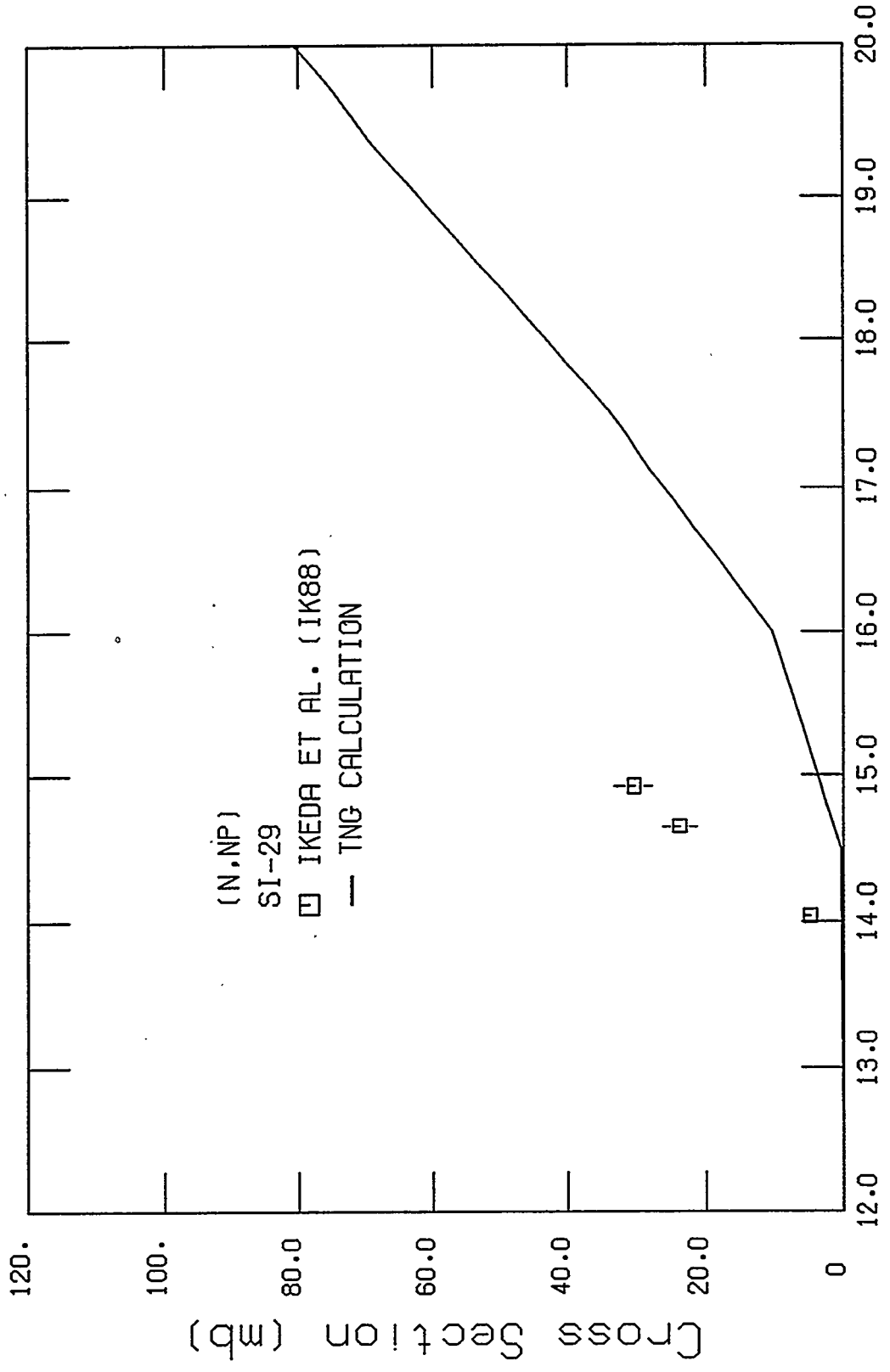

Fig. 35. Comparison of calculated and experimental ^{29}Si(n,np)+(n,pn) cross sections.

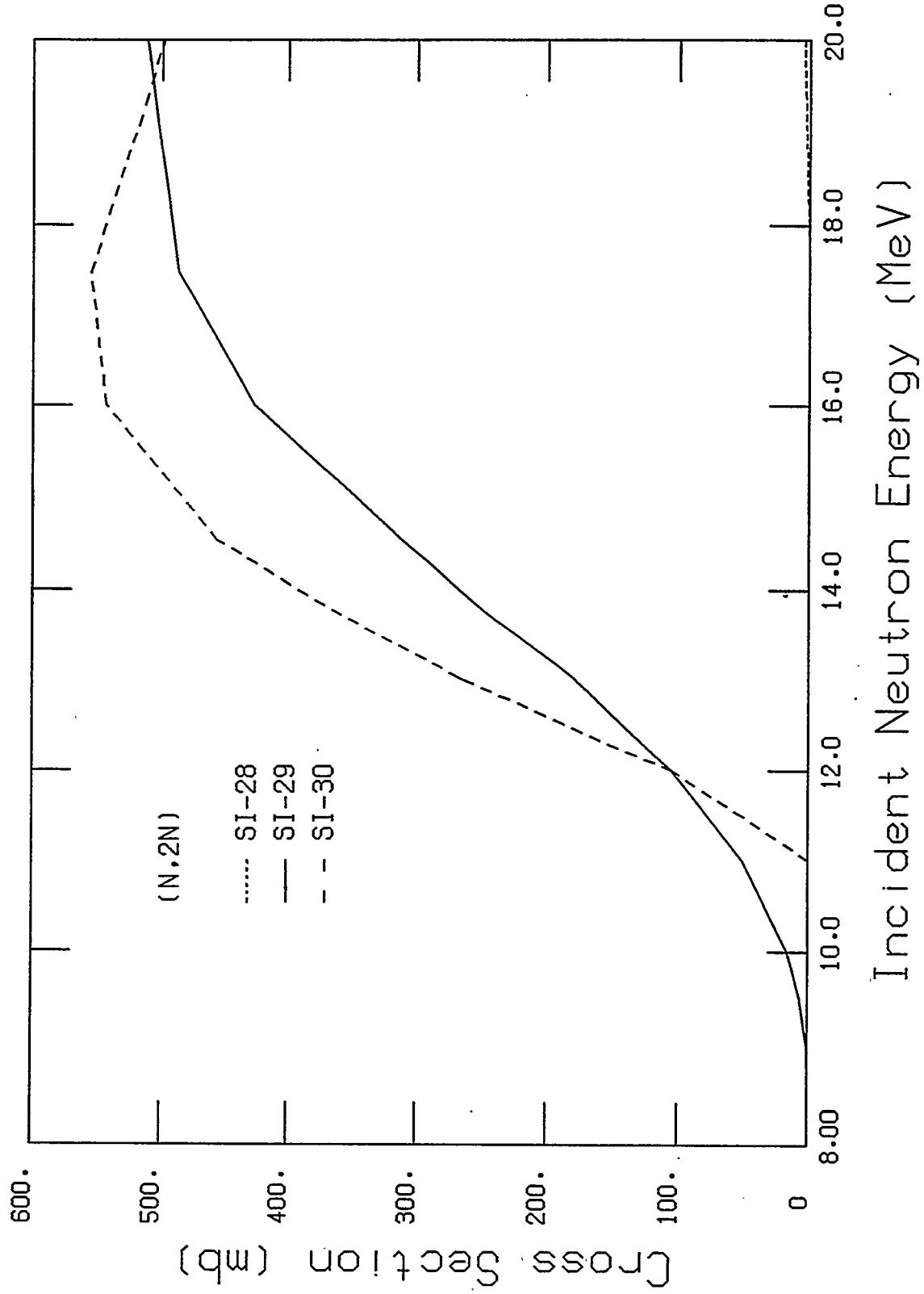

Fig. 36. TNG calculated cross section for ^{28,29,30}Si(n,2n).

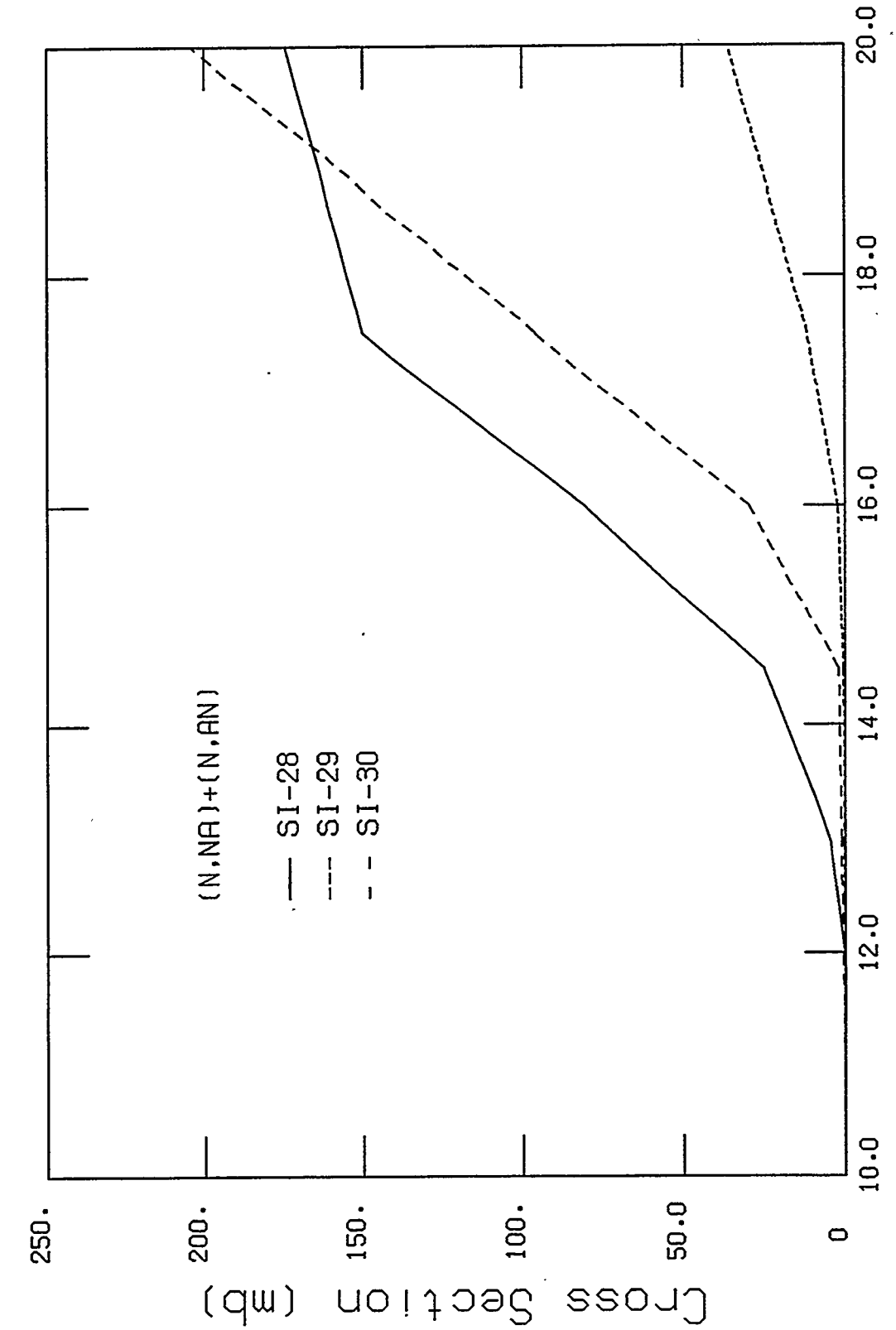

Fig. 37. TNG calculated cross section for ^{28,29,30}Si(n,nα)+(n,αn).

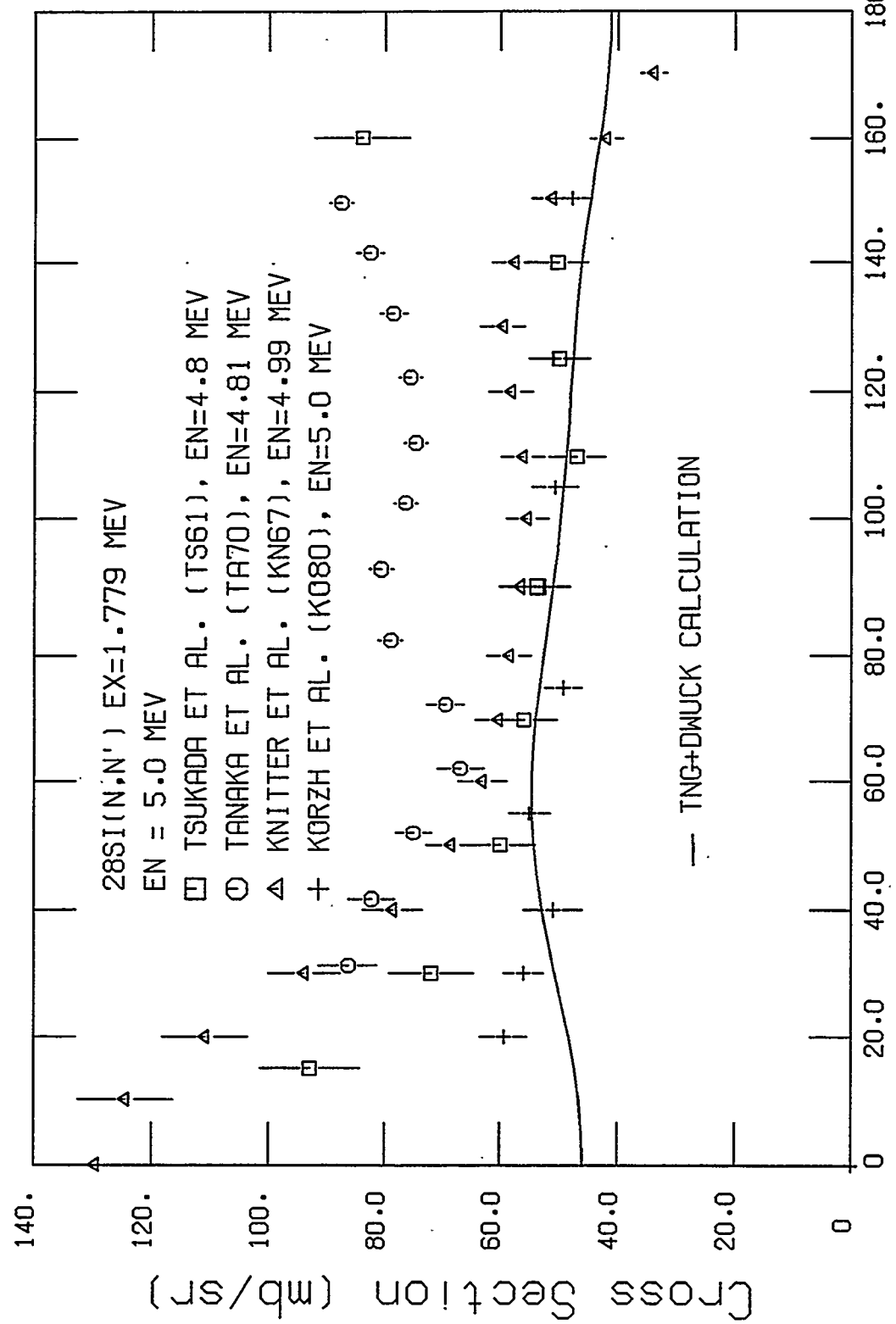

Fig. 38. Comparison of calculated and experimental differential cross sections for exciting the 1.779-MeV level at E_n = 5.0 MeV.

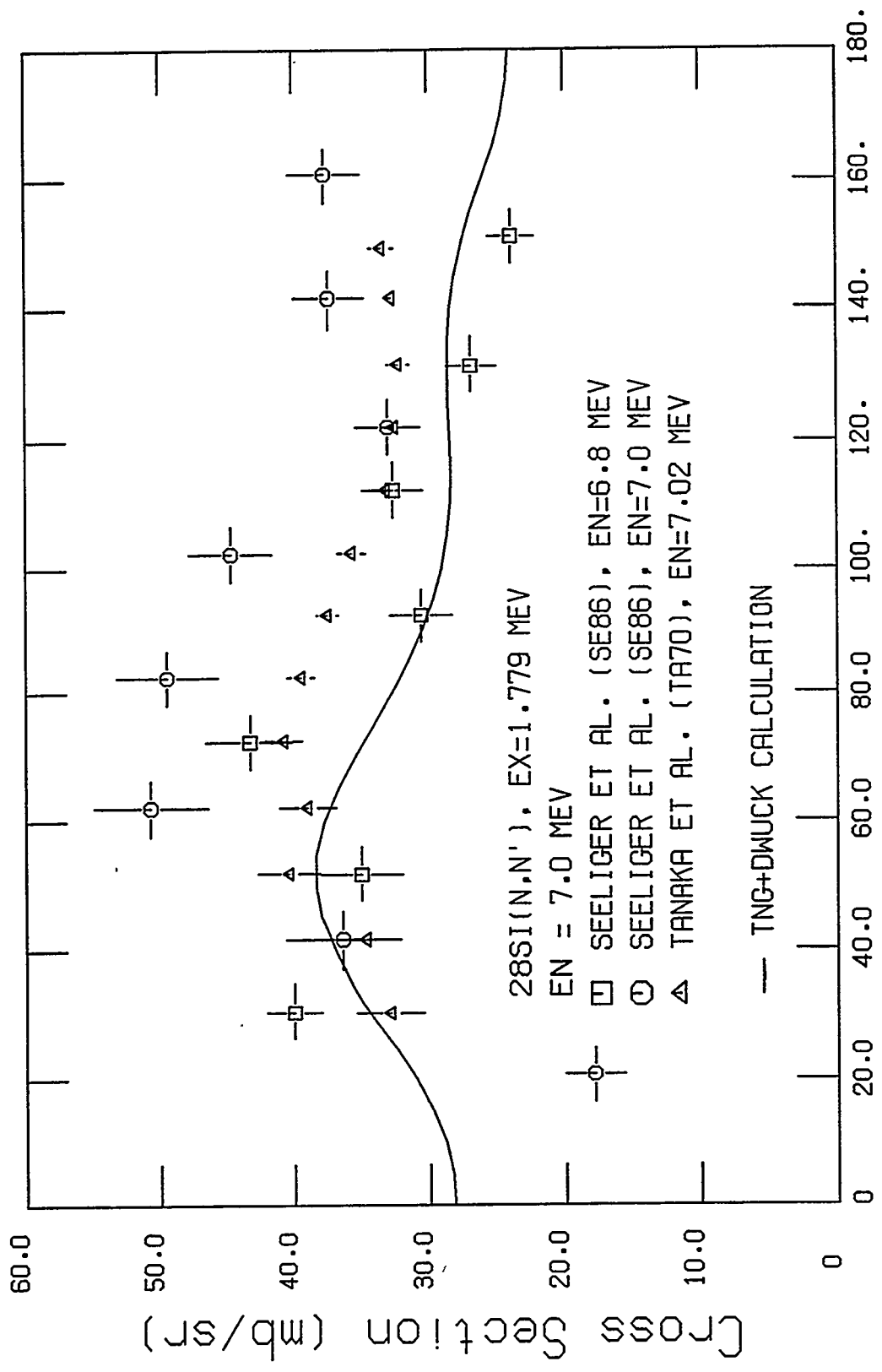

Fig. 39. Comparison of calculated and experimental differential cross sections for exciting the 1.779-MeV level at E_n = 7.0 MeV.

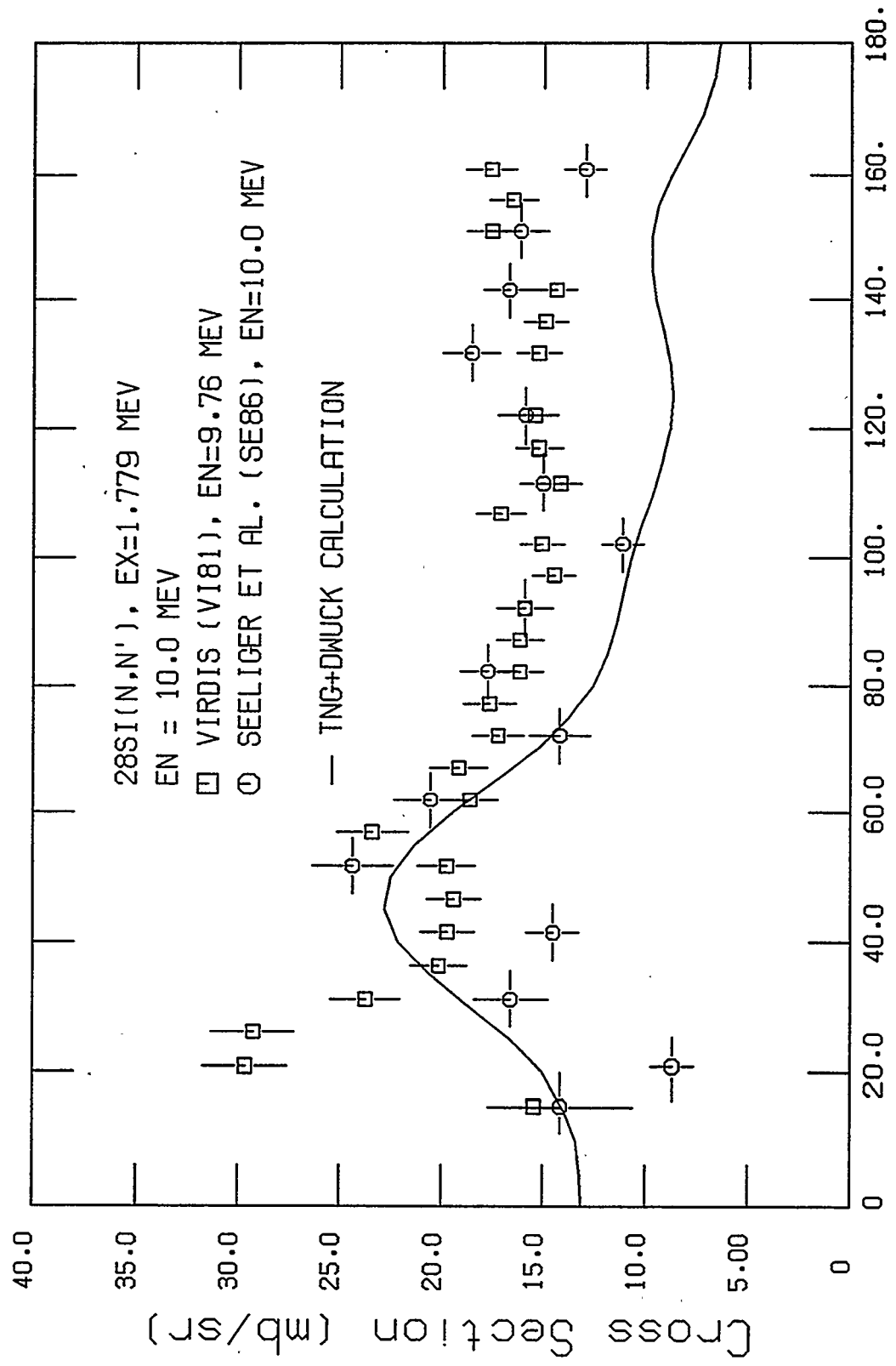

Fig. 40. Comparison of calculated and experimental differential cross sections for exciting the 1.779-MeV level at E_n = 10.0 MeV.

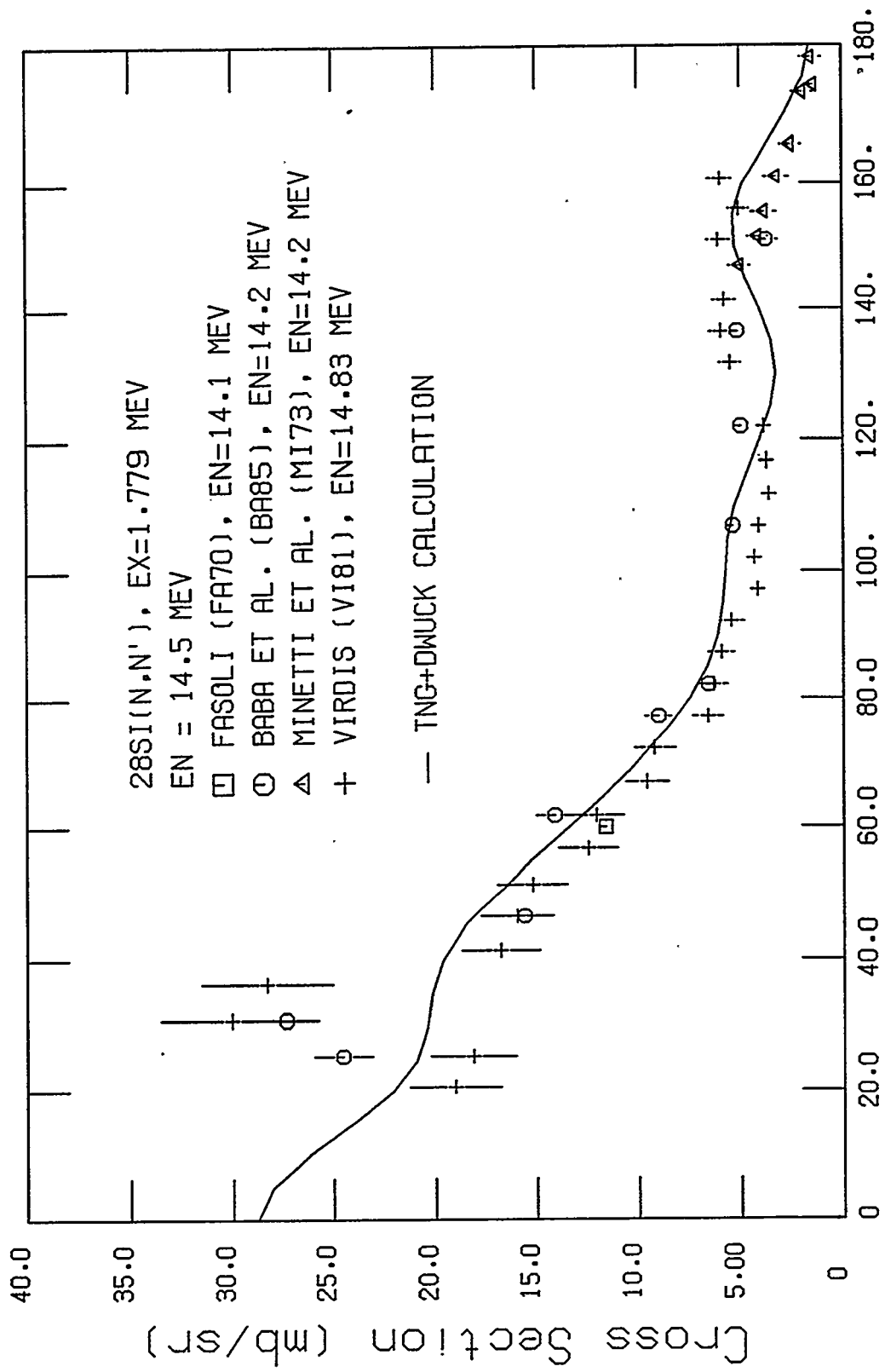

Fig. 41. Comparison of calculated and experimental differential cross sections for exciting the 1.779-MeV level at $E_n = 14.5$ MeV.

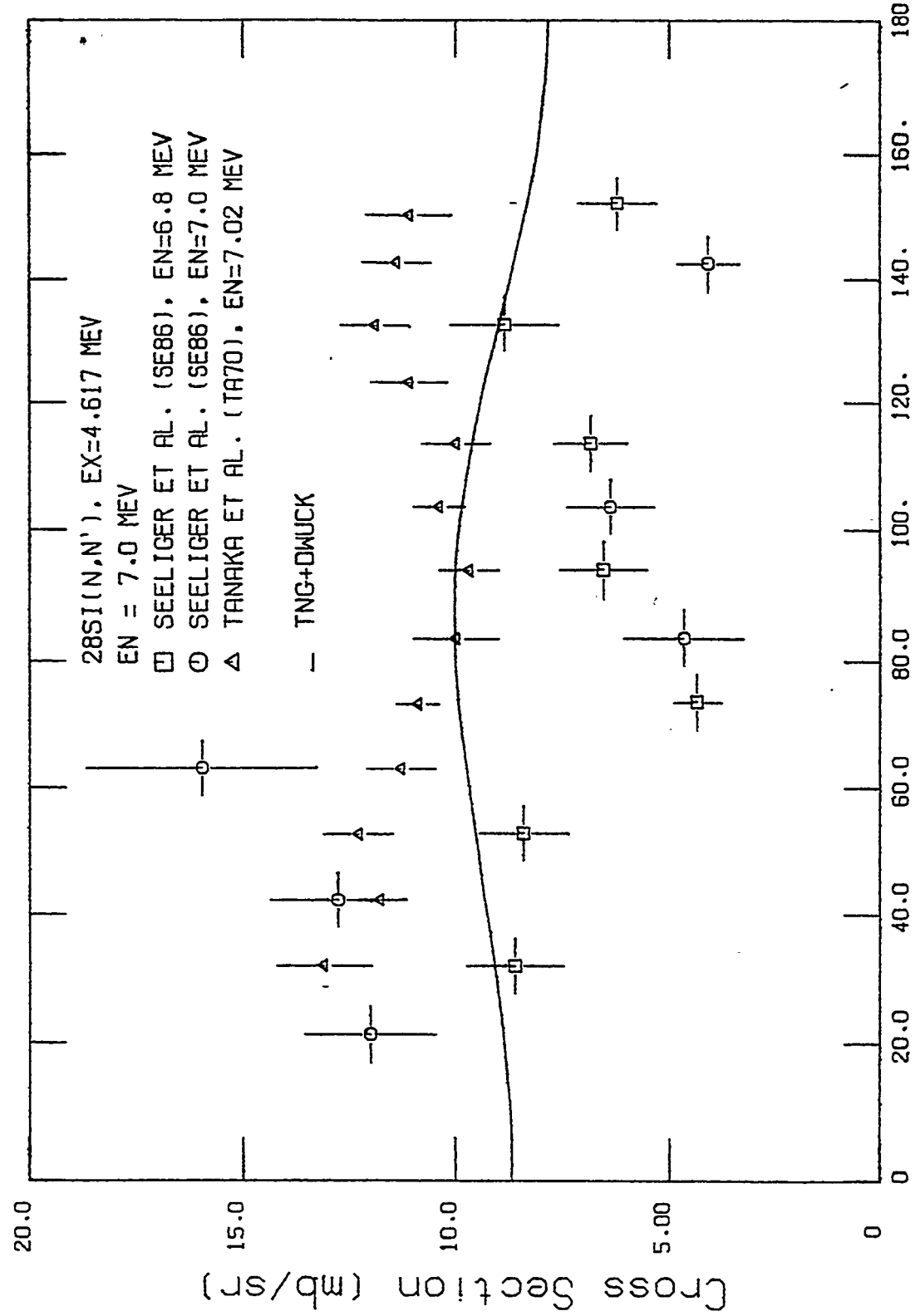

Fig. 42. Comparison of calculated and experimental differential cross sections for exciting the 4.617-MeV level at E_n = 7.0 MeV.

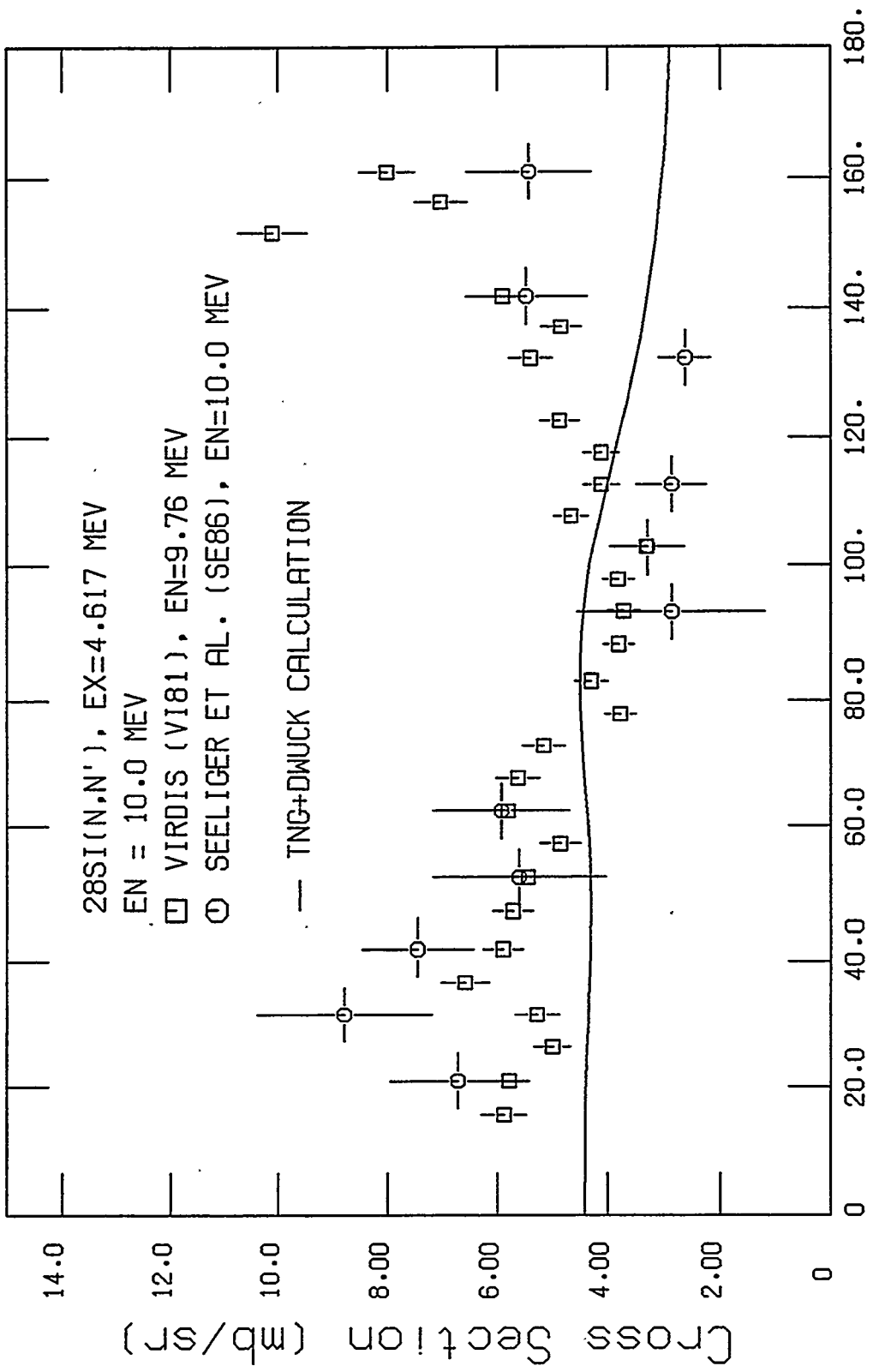

Fig. 43. Comparison of calculated and experimental differential cross sections for exciting the 4.617-MeV level at E_n = 10.0 MeV.

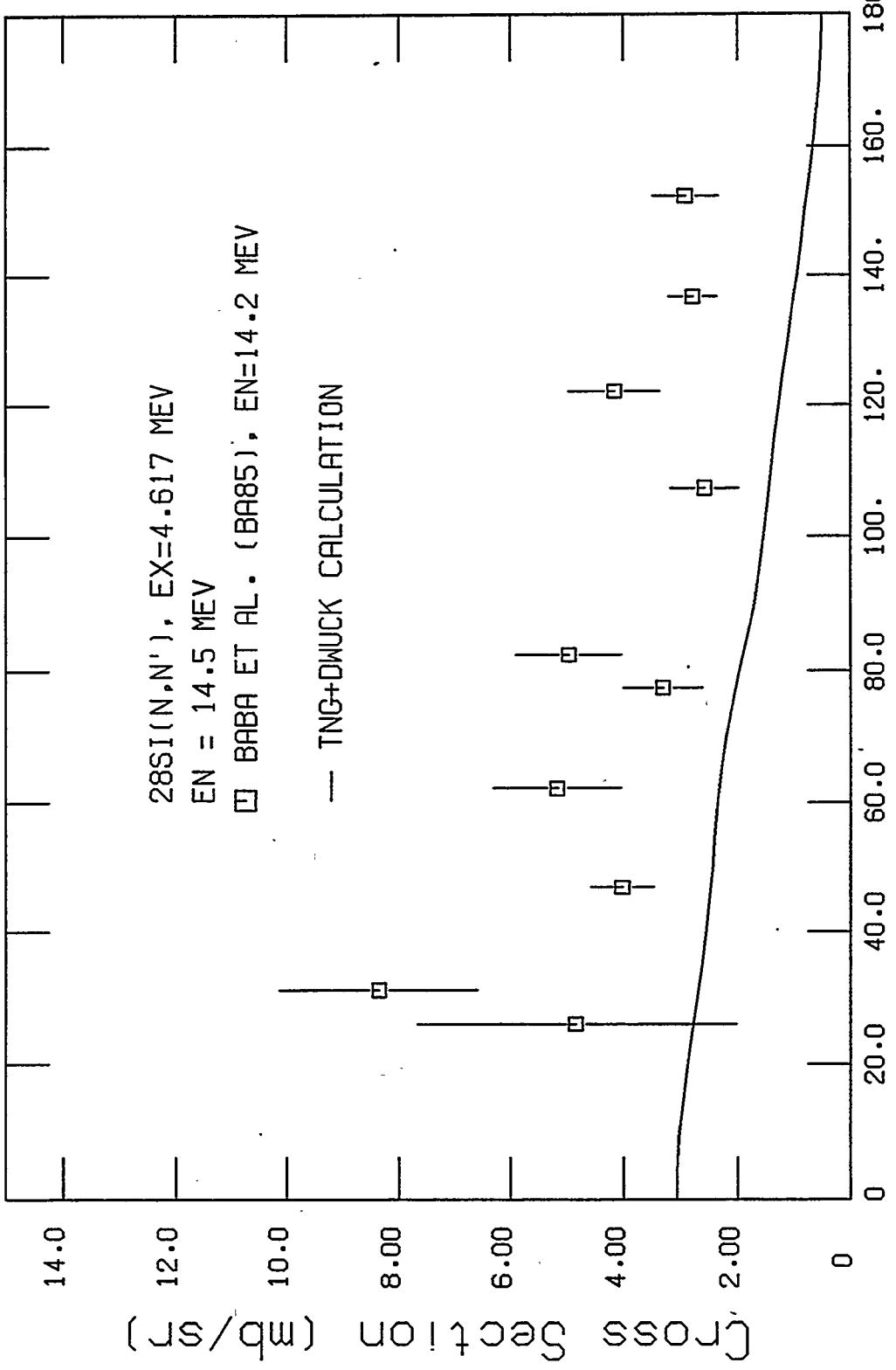

Fig. 44. Comparison of calculated and experimental differential cross sections for exciting the 4.617-MeV level at E_n = 14.5 MeV.

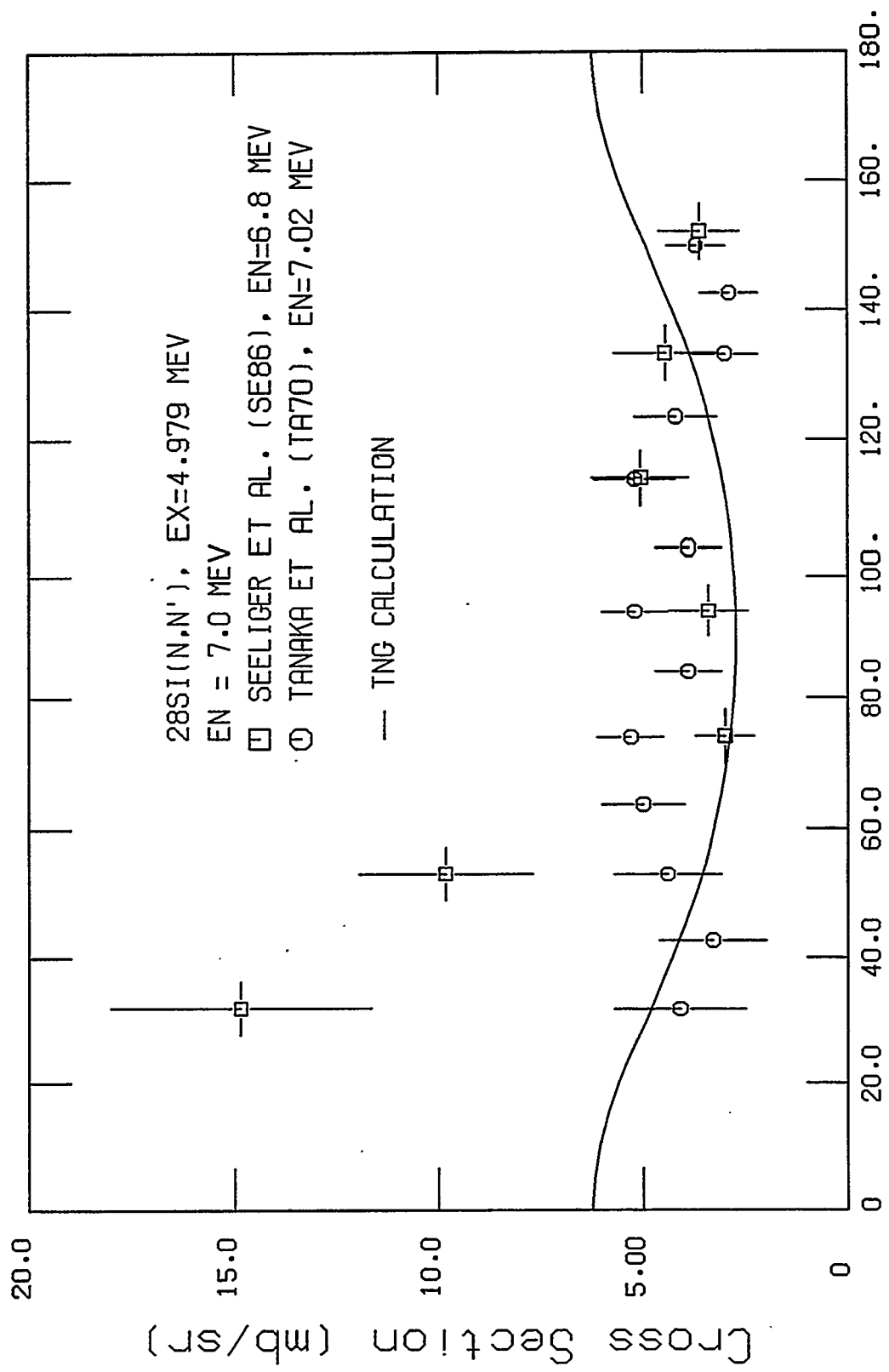

Fig. 45. Comparison of calculated and experimental differential cross sections for exciting the 4.979-MeV level at $E_n = 7.0$ MeV.

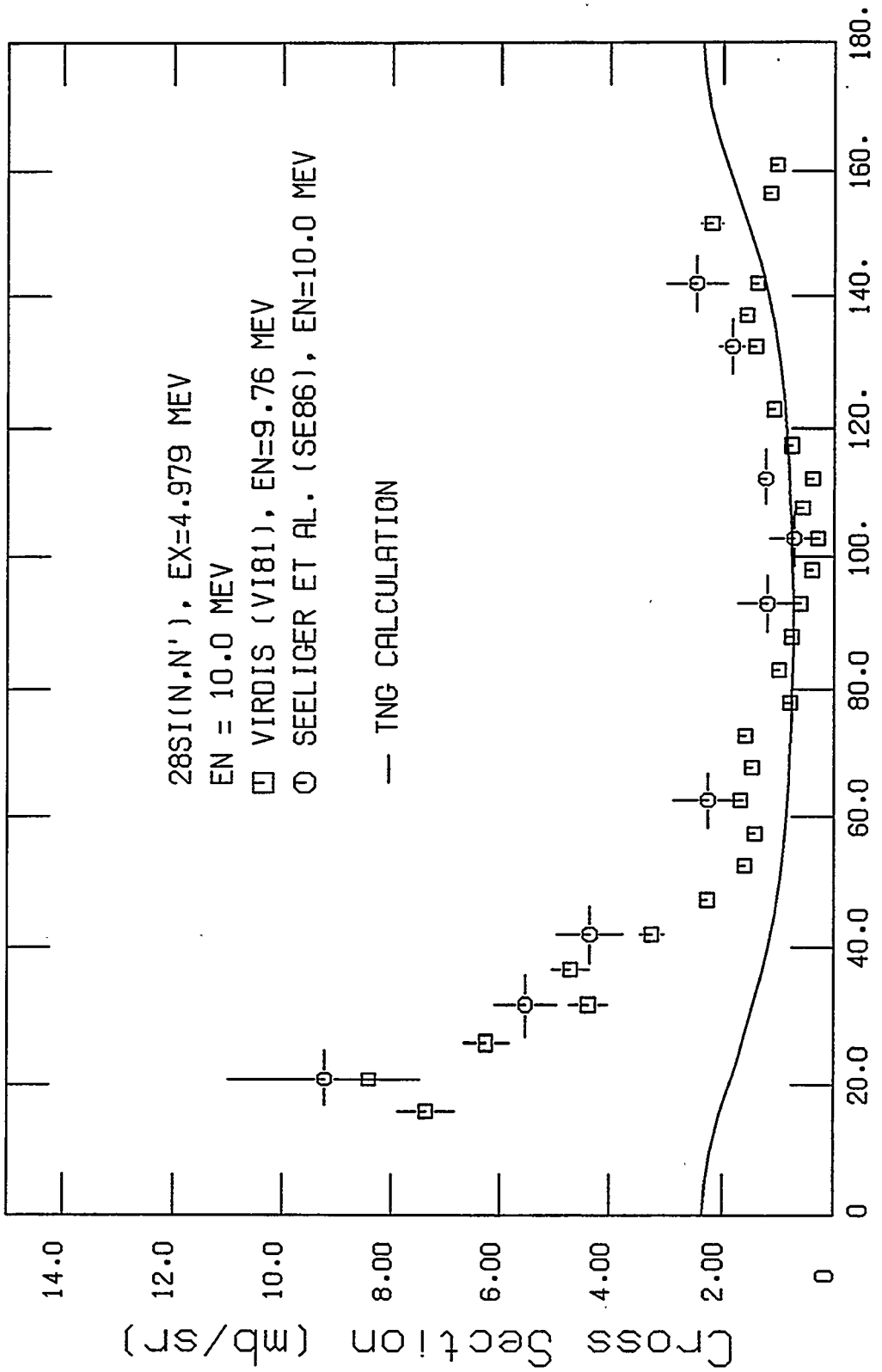

Fig. 46. Comparison of calculated and experimental differential cross sections for exciting the 4.979-MeV level at E_n = 10.0 MeV.

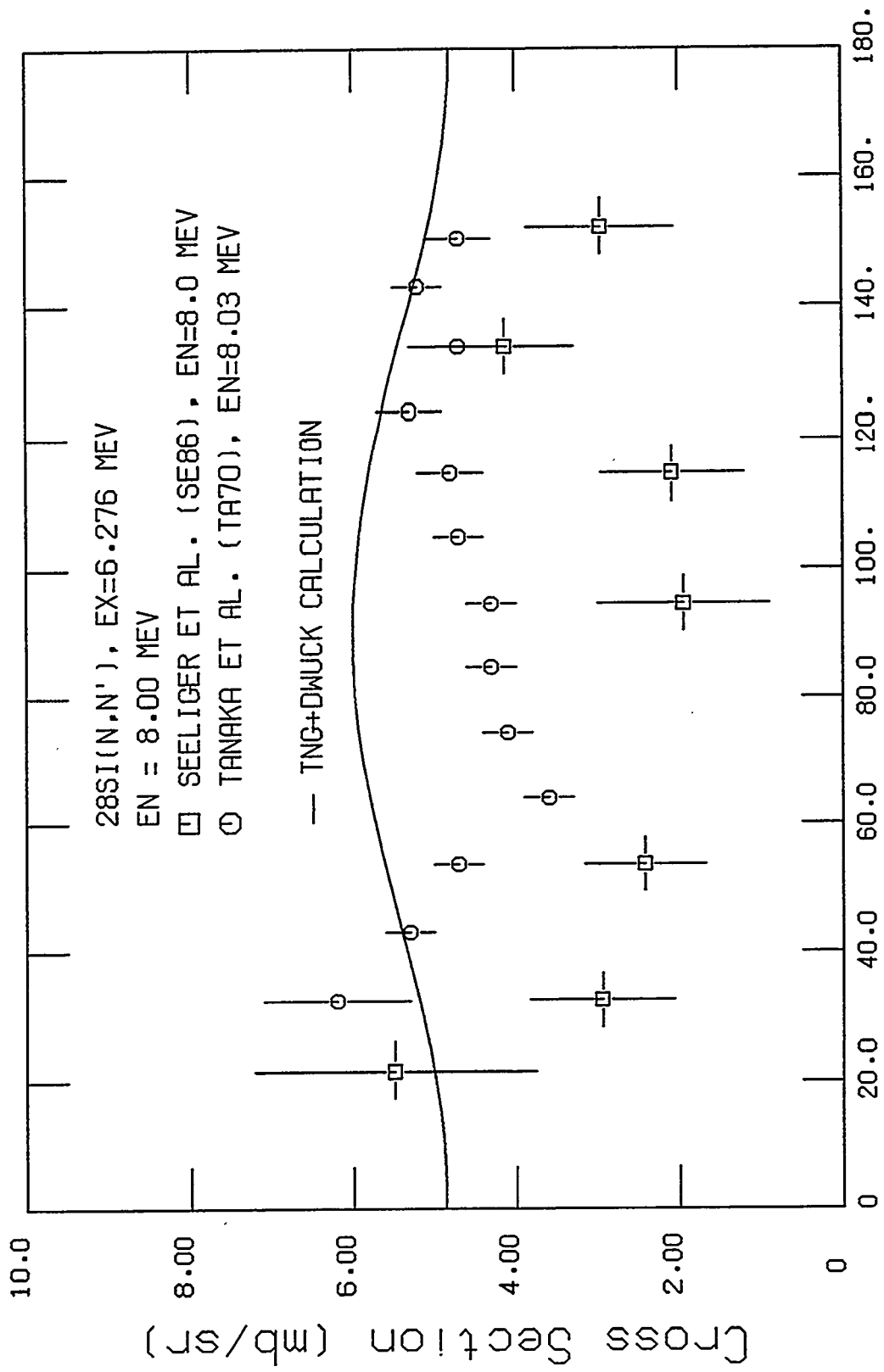

Fig. 47. Comparison of calculated and experimental differential cross sections for exciting the 6.276-MeV level at E_n = 8.0 MeV.

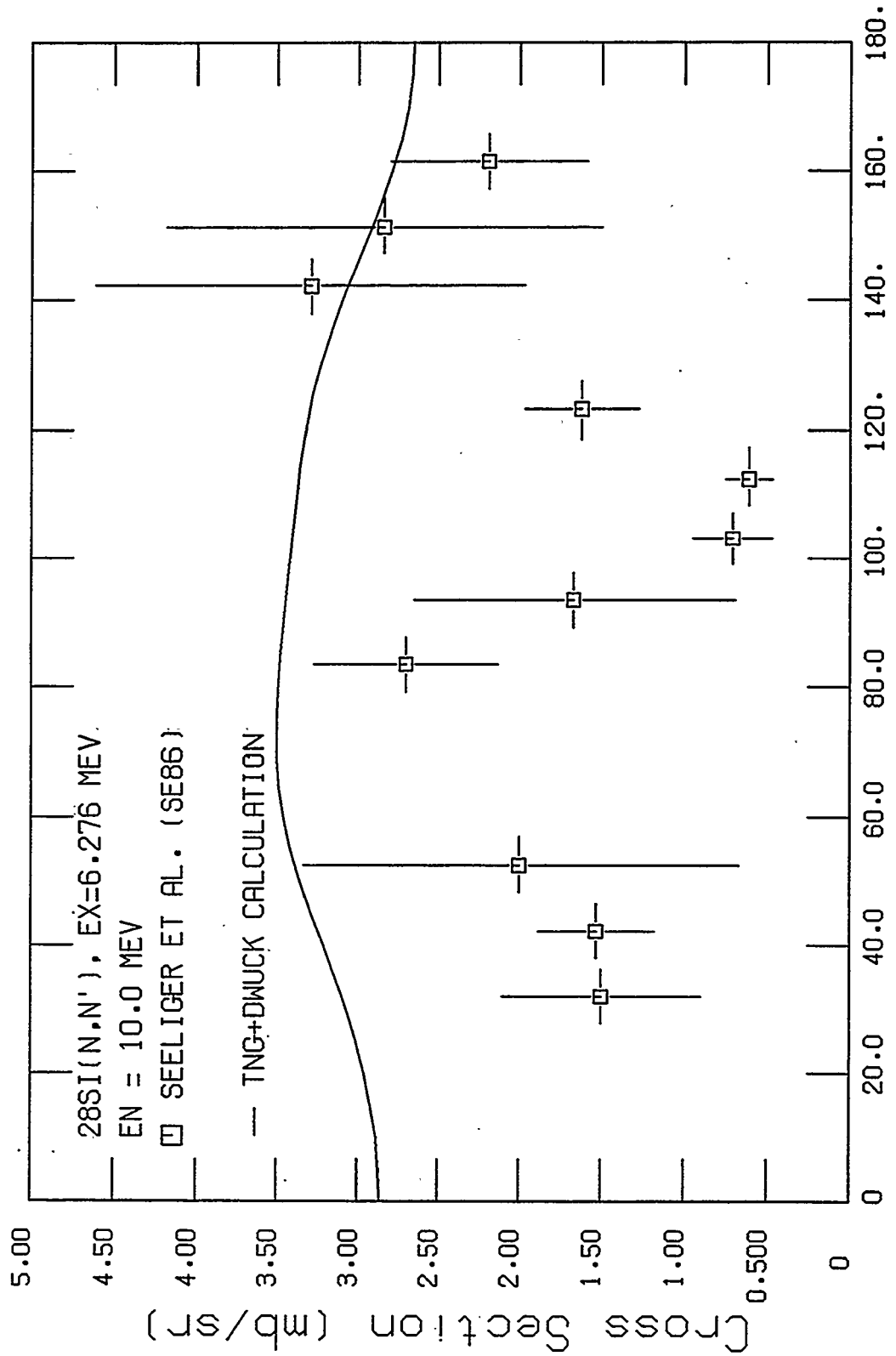

Fig. 48. Comparison of calculated and experimental differential cross sections for exciting the 6.276-MeV level at E_n = 10.0 MeV.

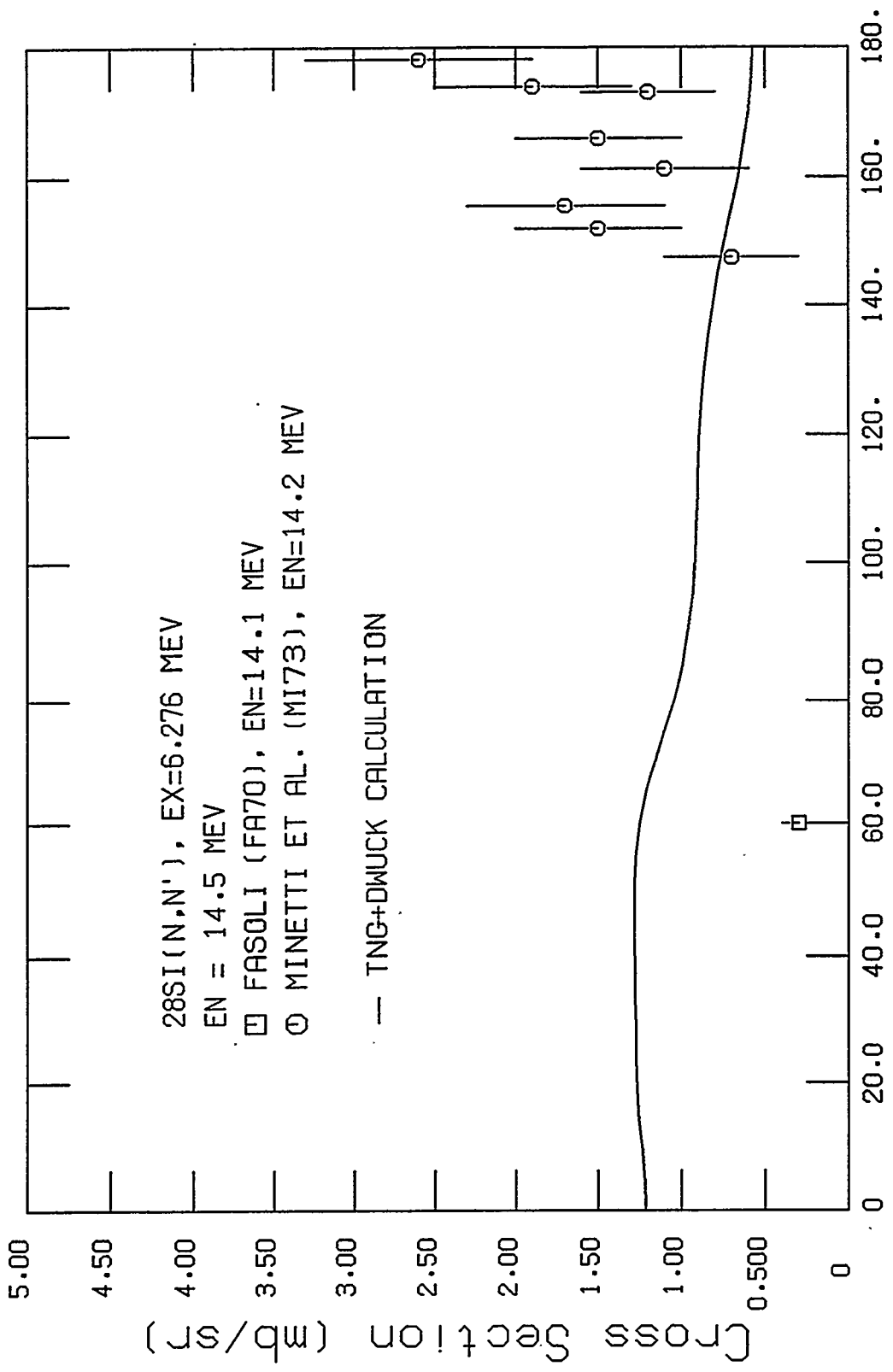

Fig. 49. Comparison of calculated and experimental differential cross sections for exciting the 6.276-MeV level at E_n = 14.5 MeV.

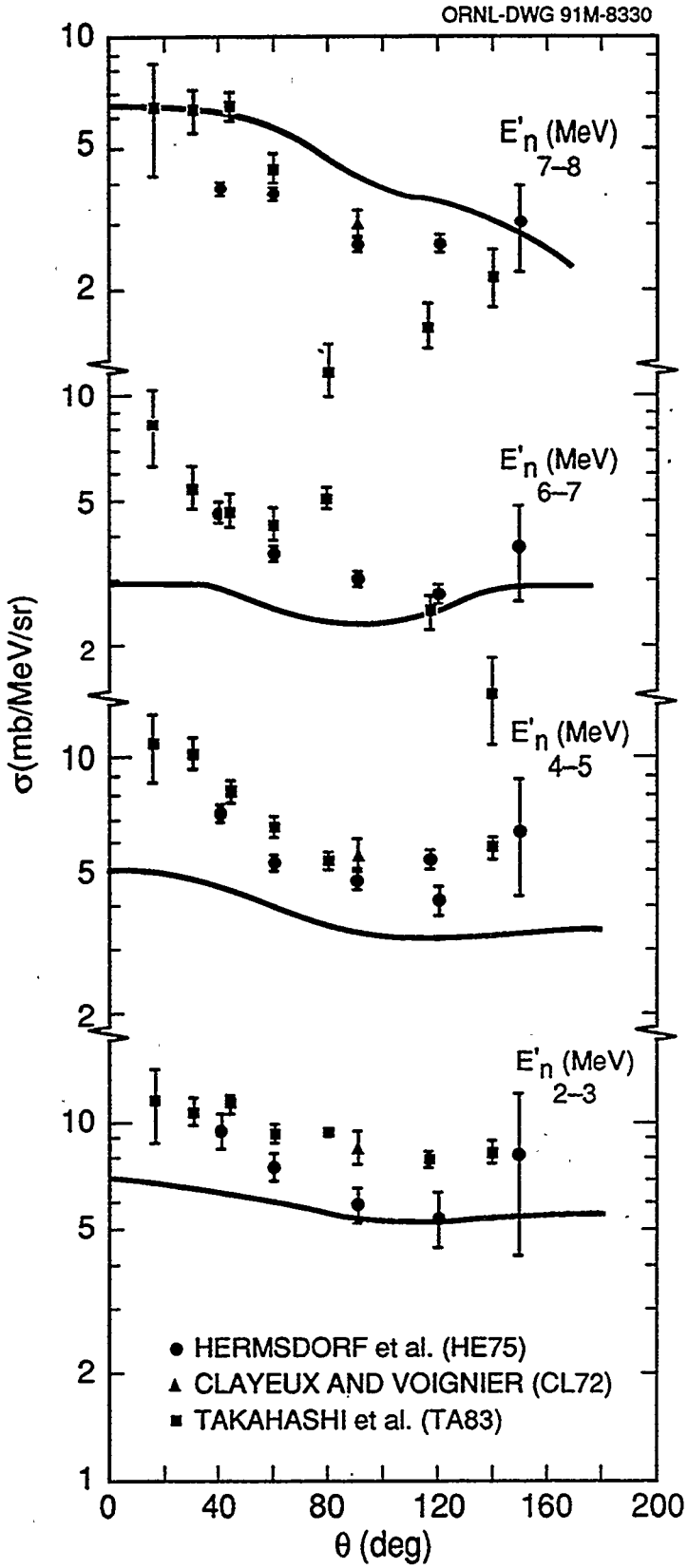

Fig. 50. Comparison of calculated and experimental cross sections for angular spectra of outgoing neutrons for ^{28}Si.

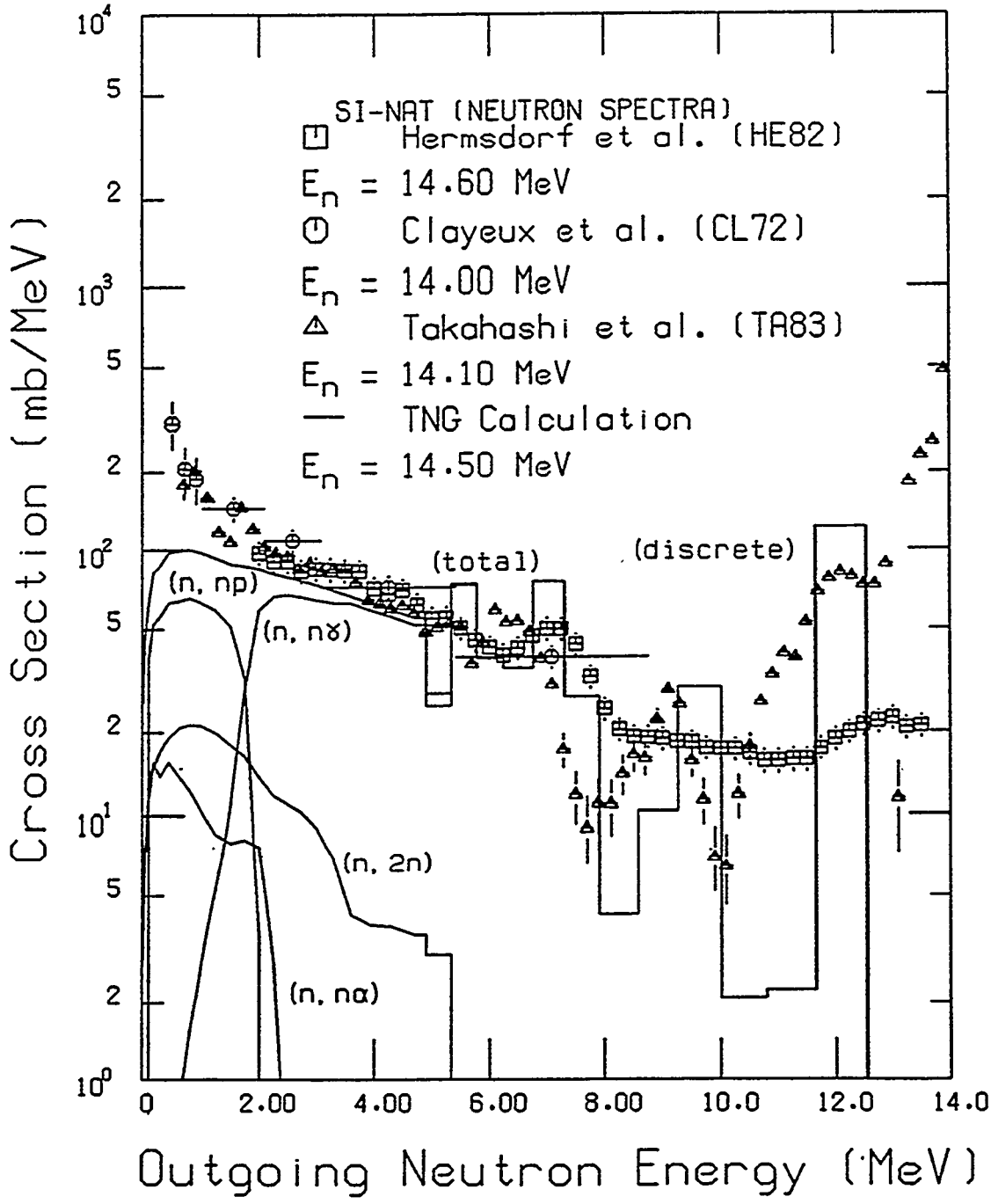

Fig. 51. Neutron emission spectra from the TNG calculation compared with experimental data. Contributions from the various neutron-producing components are shown (they sum to the total). The curves labeled (n,np) and n,nα) include the (n,pn) and (n,αn) components, respectively.

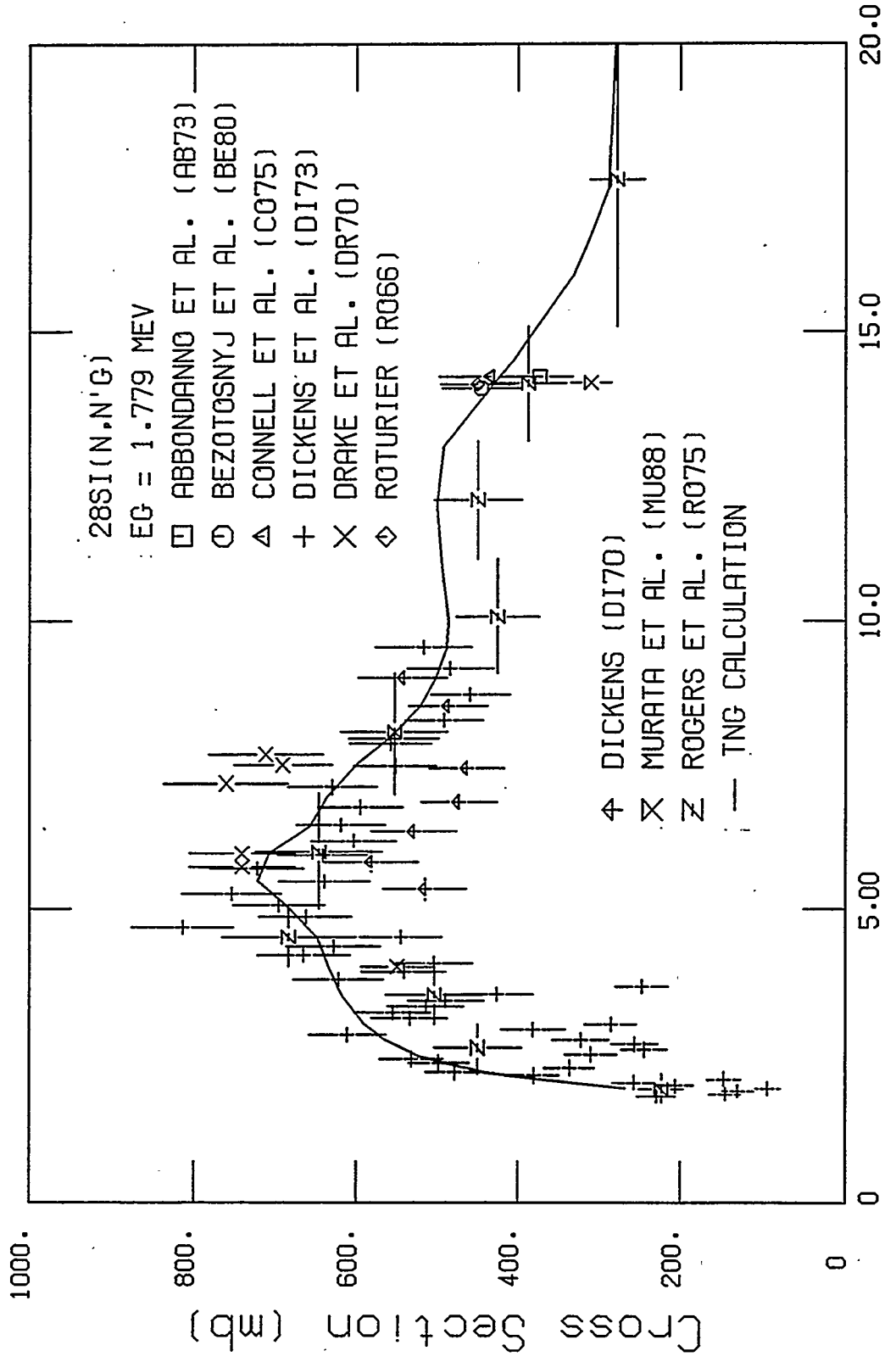

Fig. 52. Comparison of calculated and experimental cross sections for the production of the 1.779 MeV gamma ray from ^{28}Si.

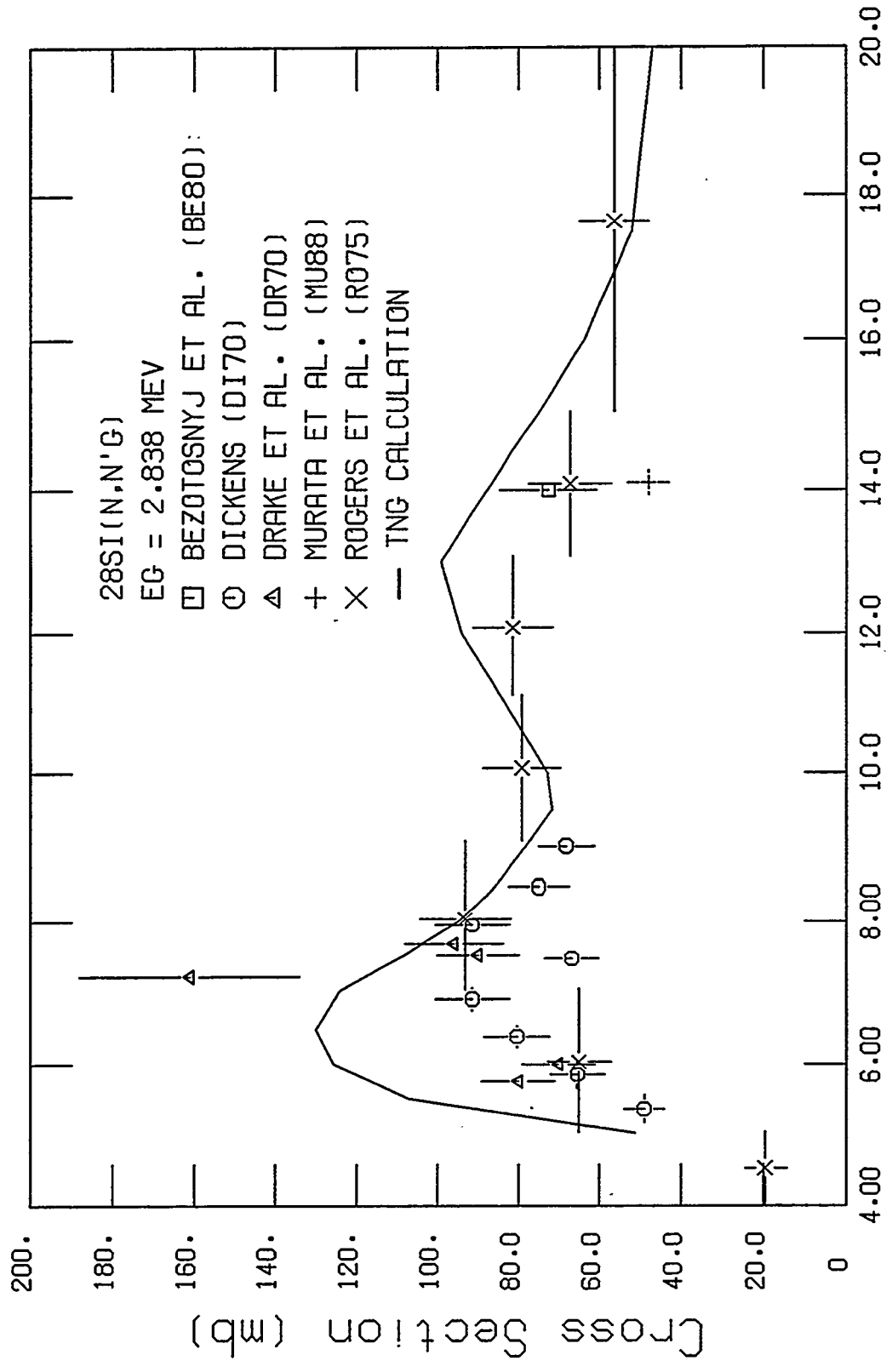

Fig. 53. Comparison of calculated and experimental cross sections for the production of the 2.838 MeV gamma ray from ^{28}Si.

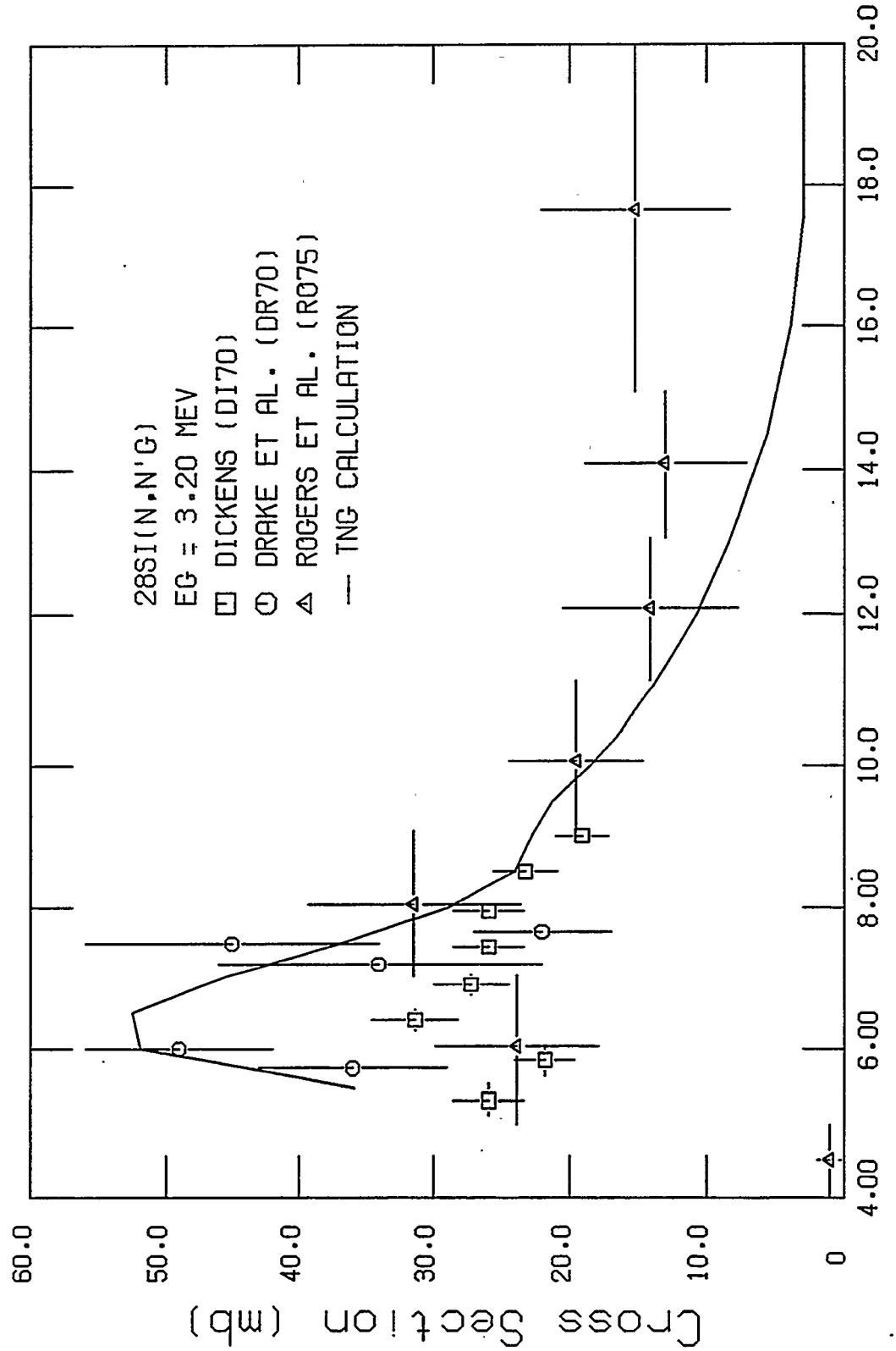

Fig. 54. Comparison of calculated and experimental cross sections for the production of the 3.2 MeV gamma ray from ^{28}Si.

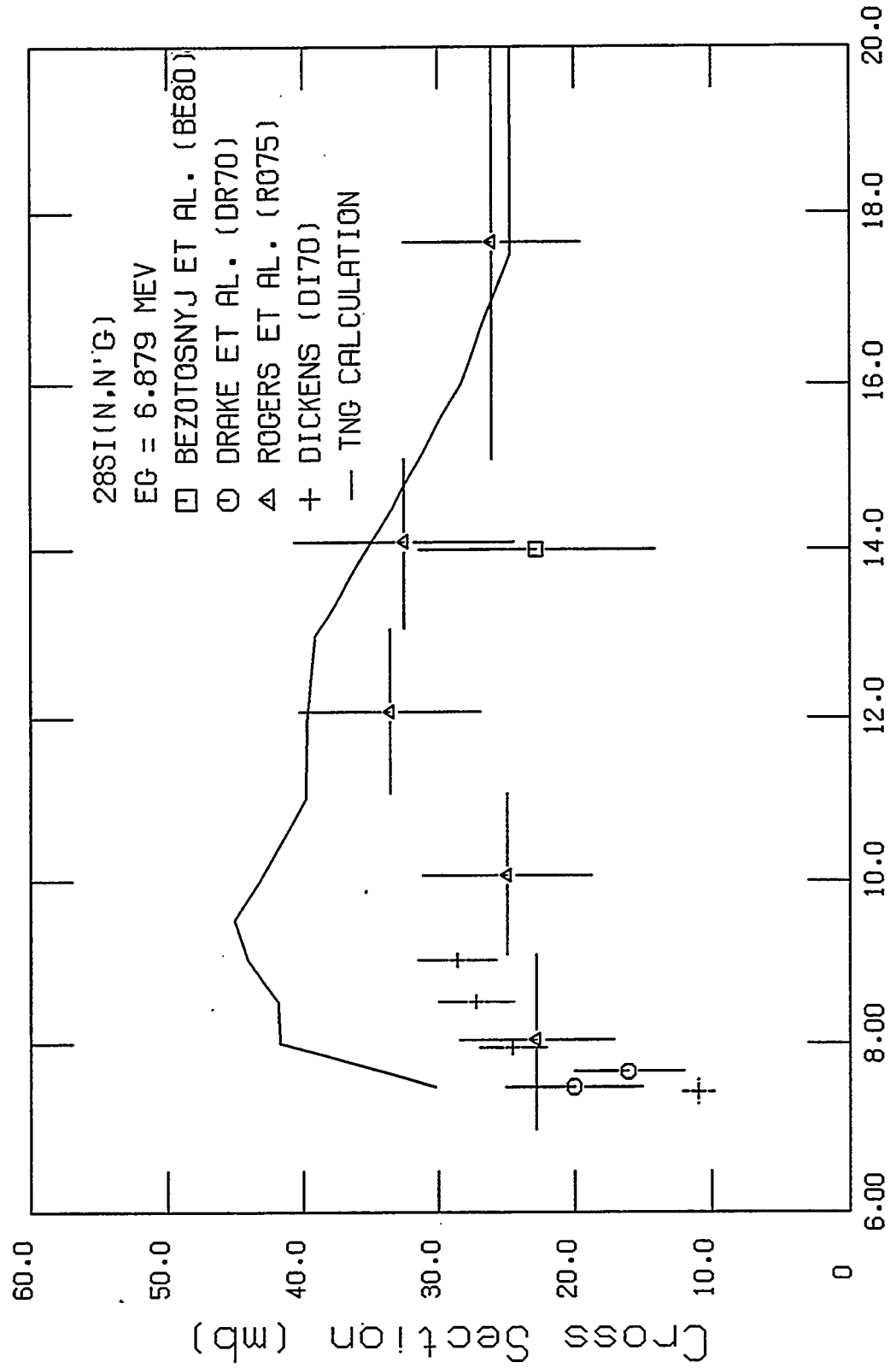

Fig. 55. Comparison of calculated and experimental cross sections for the production of the 6.879 MeV gamma ray from ^{28}Si.

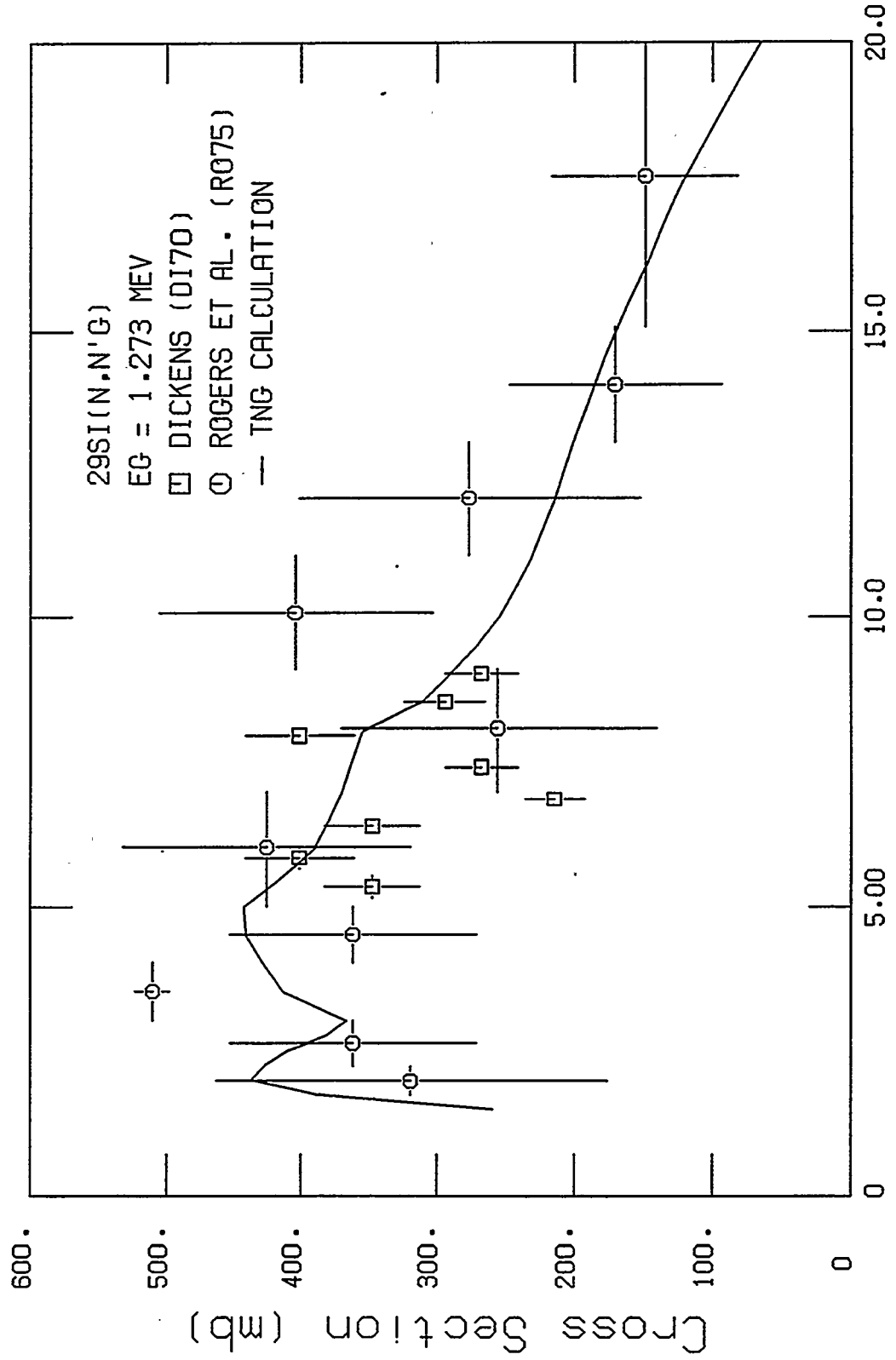

Fig. 56. Comparison of calculated and experimental cross sections for the production of the 1.273 MeV gamma ray from ^{29}Si.

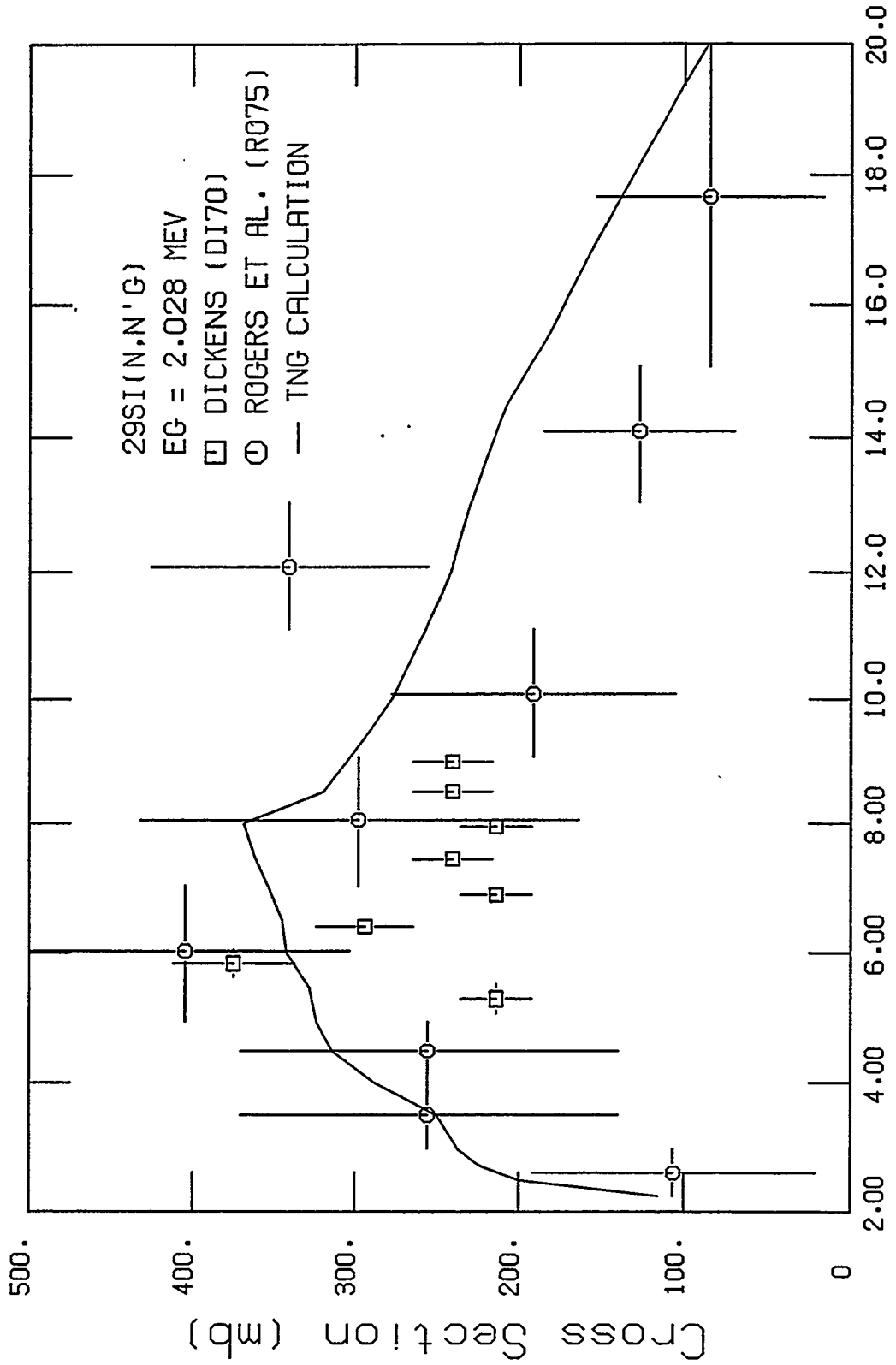

Fig. 57. Comparison of calculated and experimental cross sections for the production of the 2.028 MeV gamma ray from ^{29}Si.

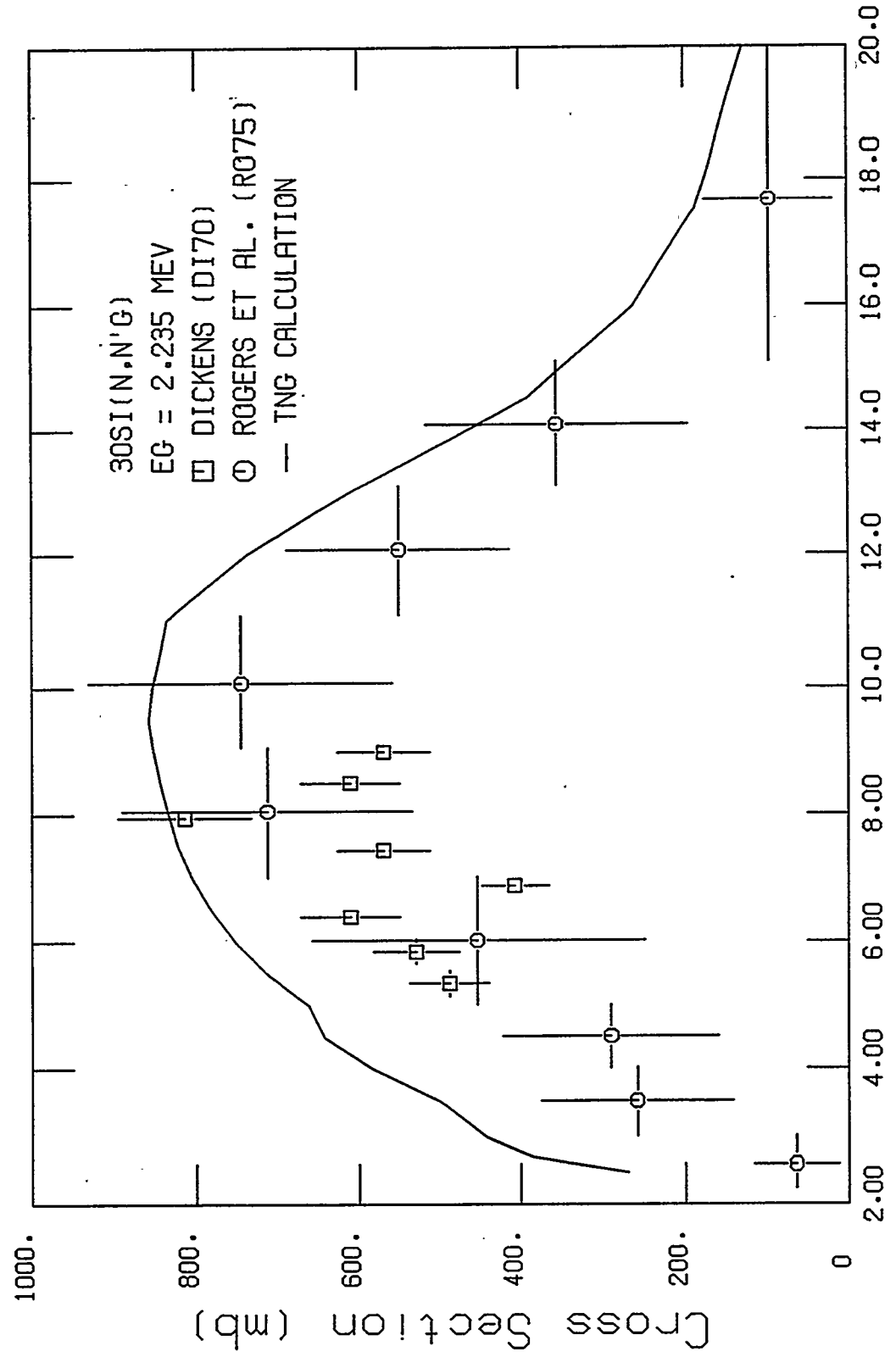

Fig. 58. Comparison of calculated and experimental cross sections for the production of the 2.235 MeV gamma ray from ^{30}Si.

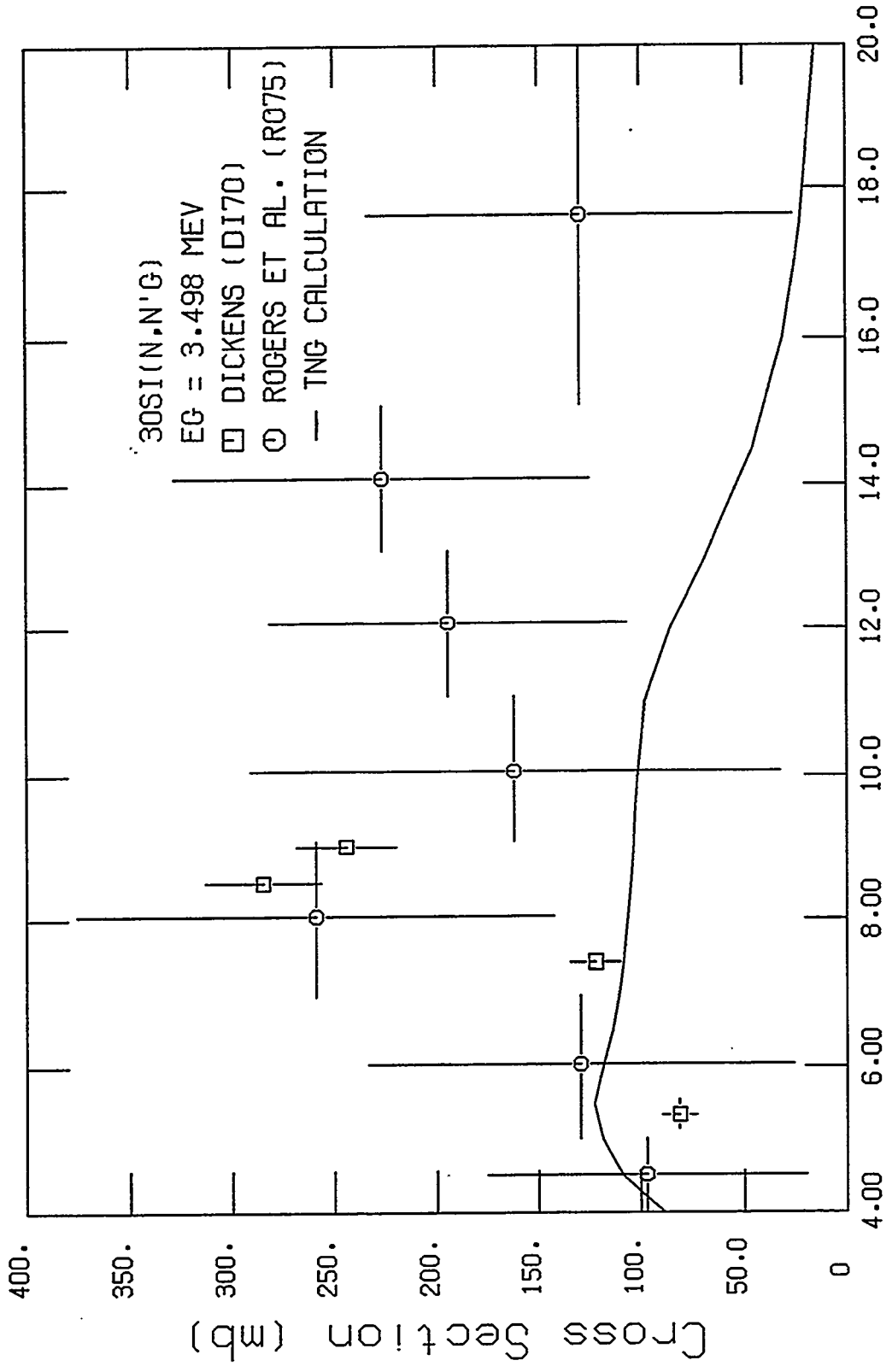

Fig. 59. Comparison of calculated and experimental cross sections for the production of the 3.498 MeV gamma ray from ^{30}Si.

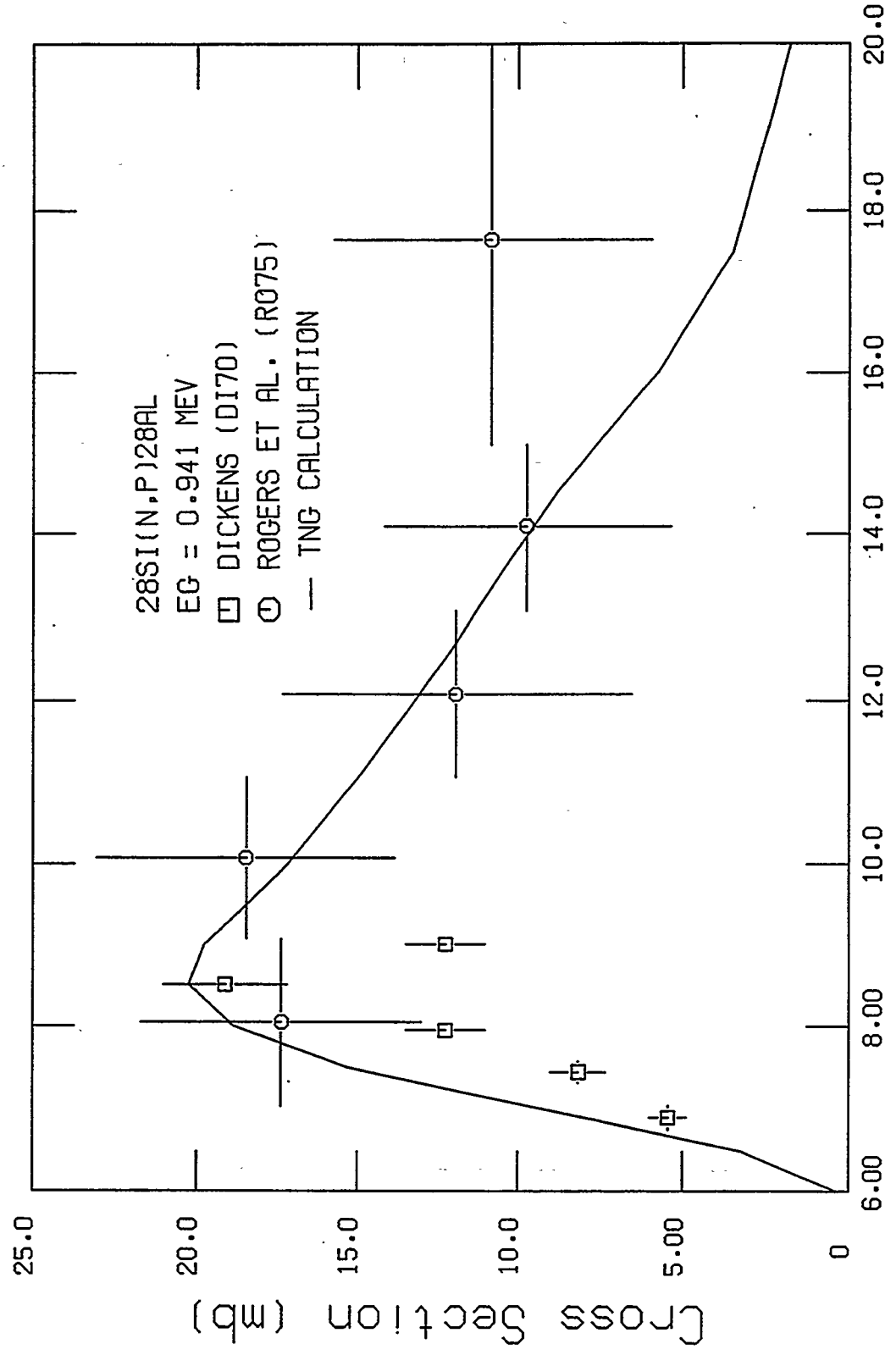

Fig. 60. Comparison of calculated and experimental cross sections for the production of the 0.941 MeV gamma ray from the (n,p) reaction for ^{28}Si.

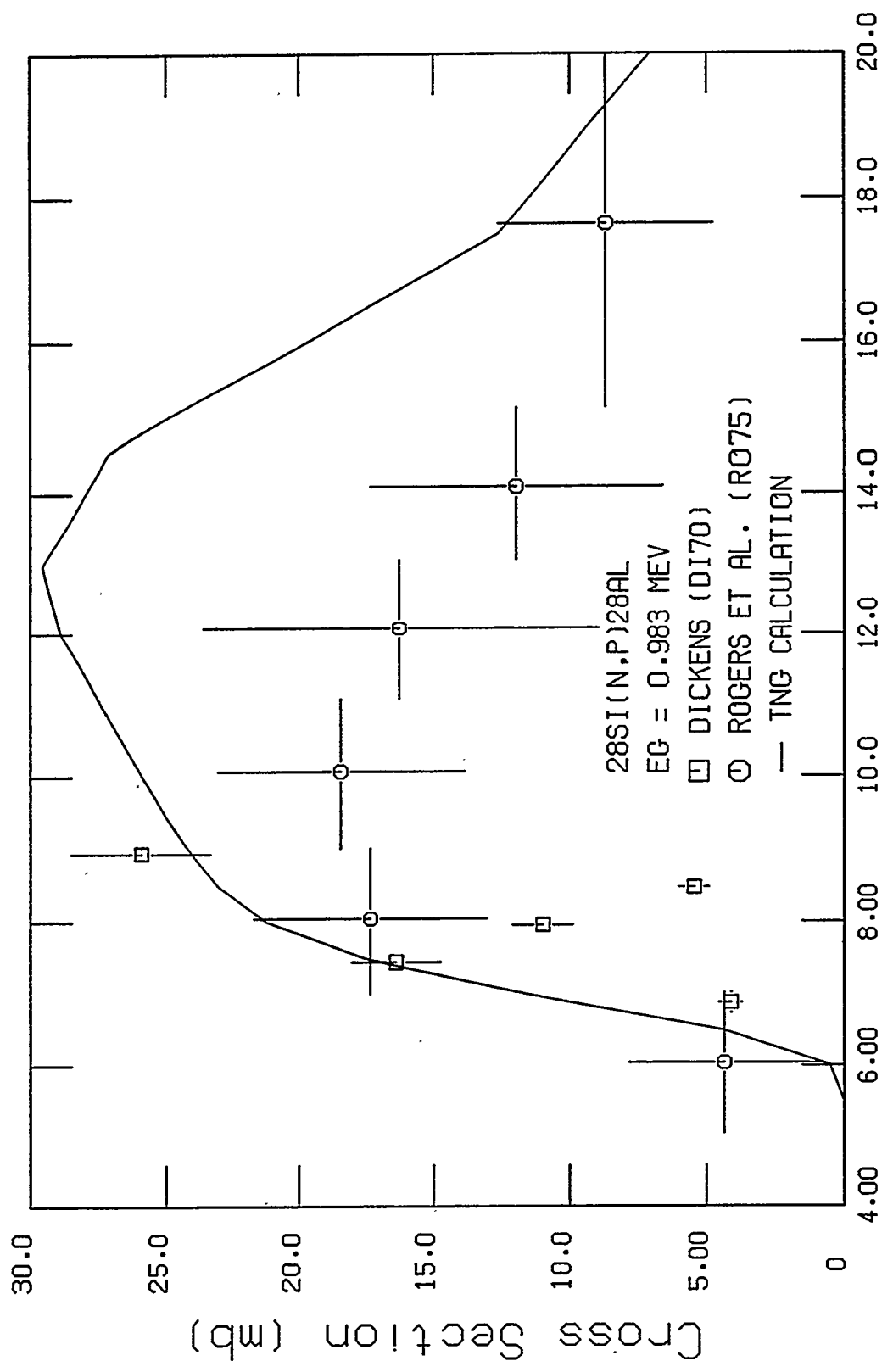

Fig. 61. Comparison of calculated and experimental cross sections for the production of the 0.983 MeV gamma ray from the (n,p) reaction for ^{28}Si.

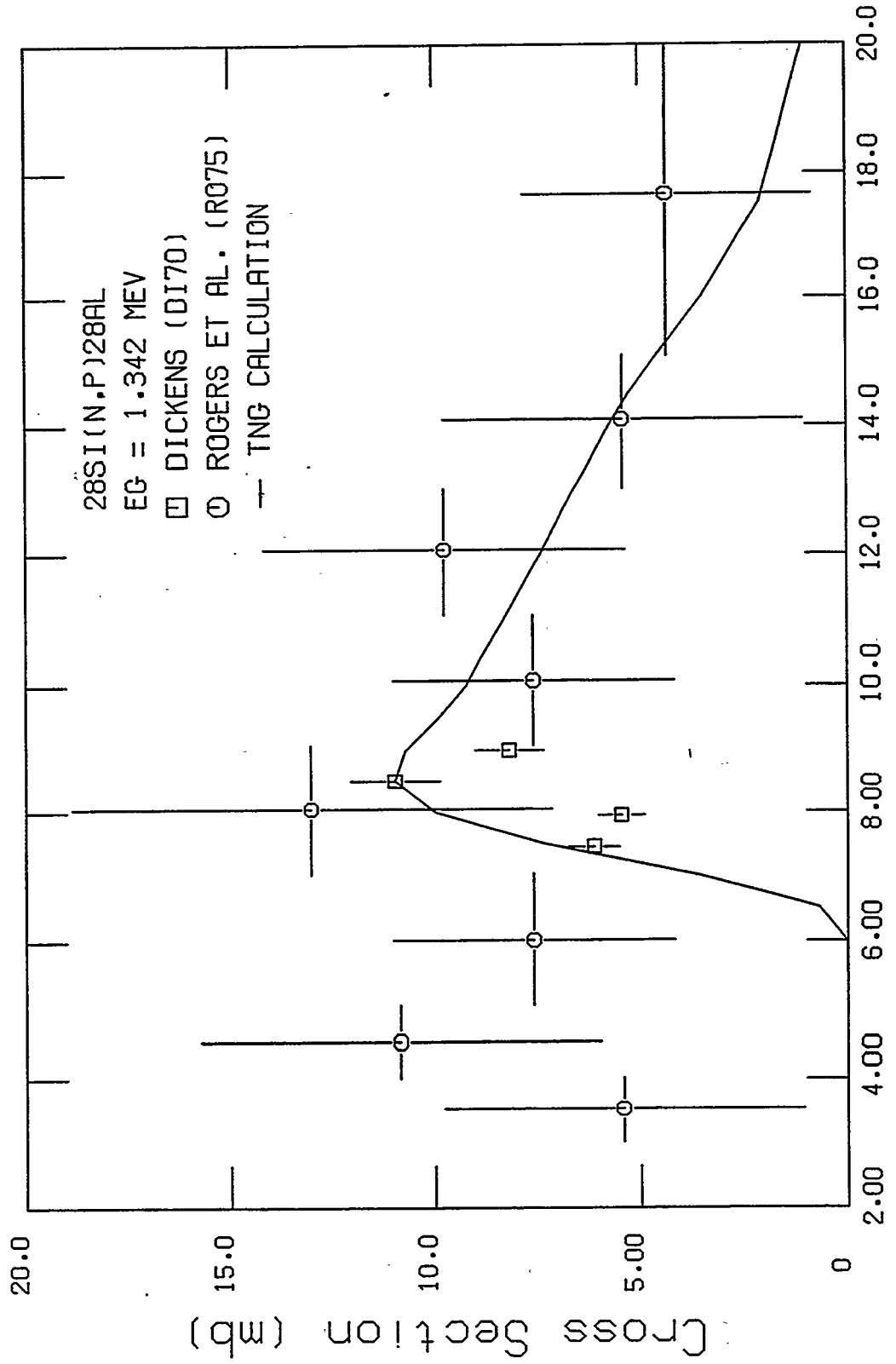

Fig. 62. Comparison of calculated and experimental cross sections for the production of the 1.342 MeV gamma ray from the (n,p) reaction for ^{28}Si.

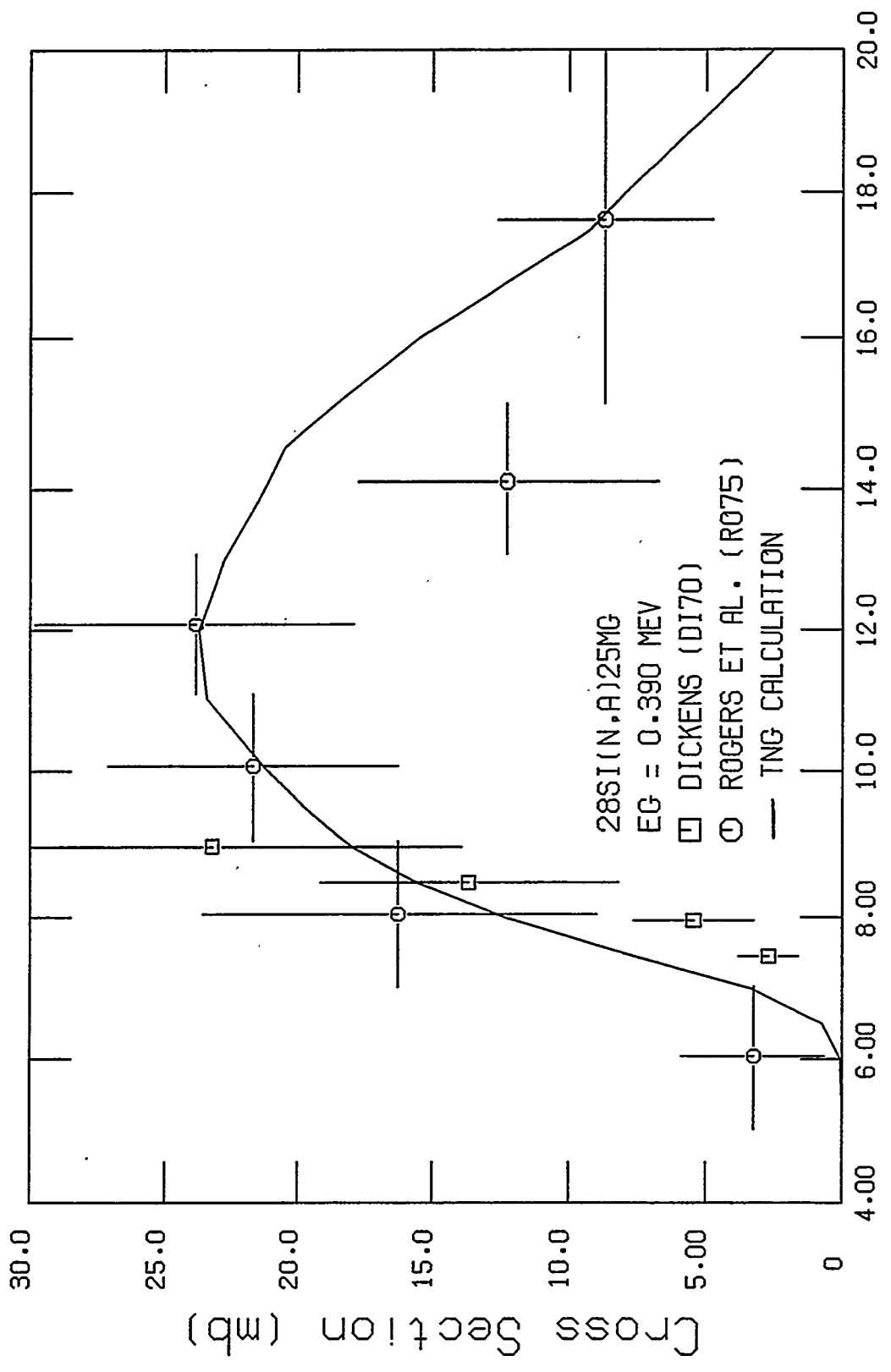

Fig. 63. Comparison of calculated and experimental cross sections for the production of the 0.390 MeV gamma ray from the (n,α) reaction for ^{28}Si.

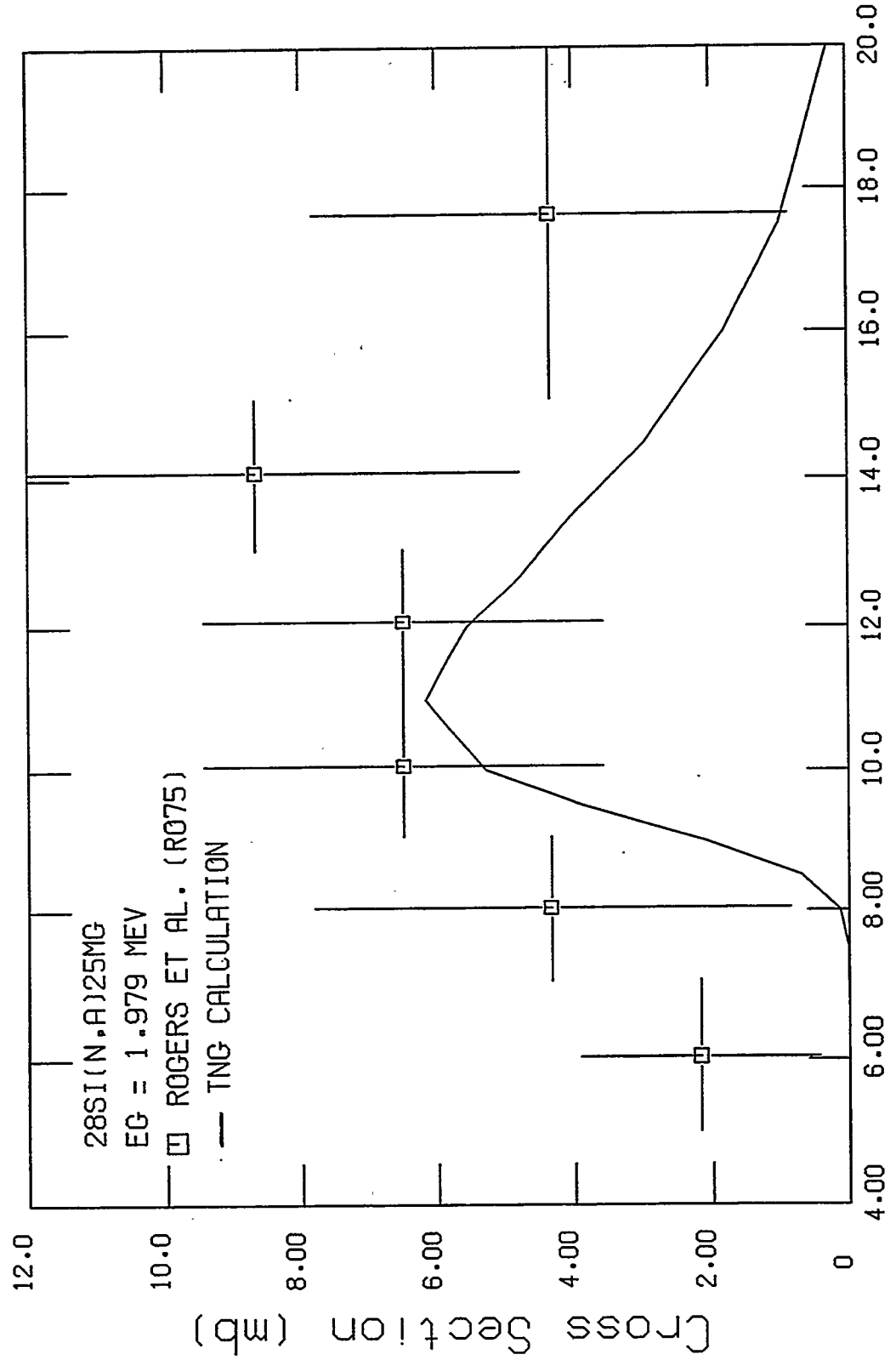

Fig. 64. Comparison of calculated and experimental cross sections for the production of the 1.979 MeV gamma ray from the (n,α) reaction for ^{28}Si.

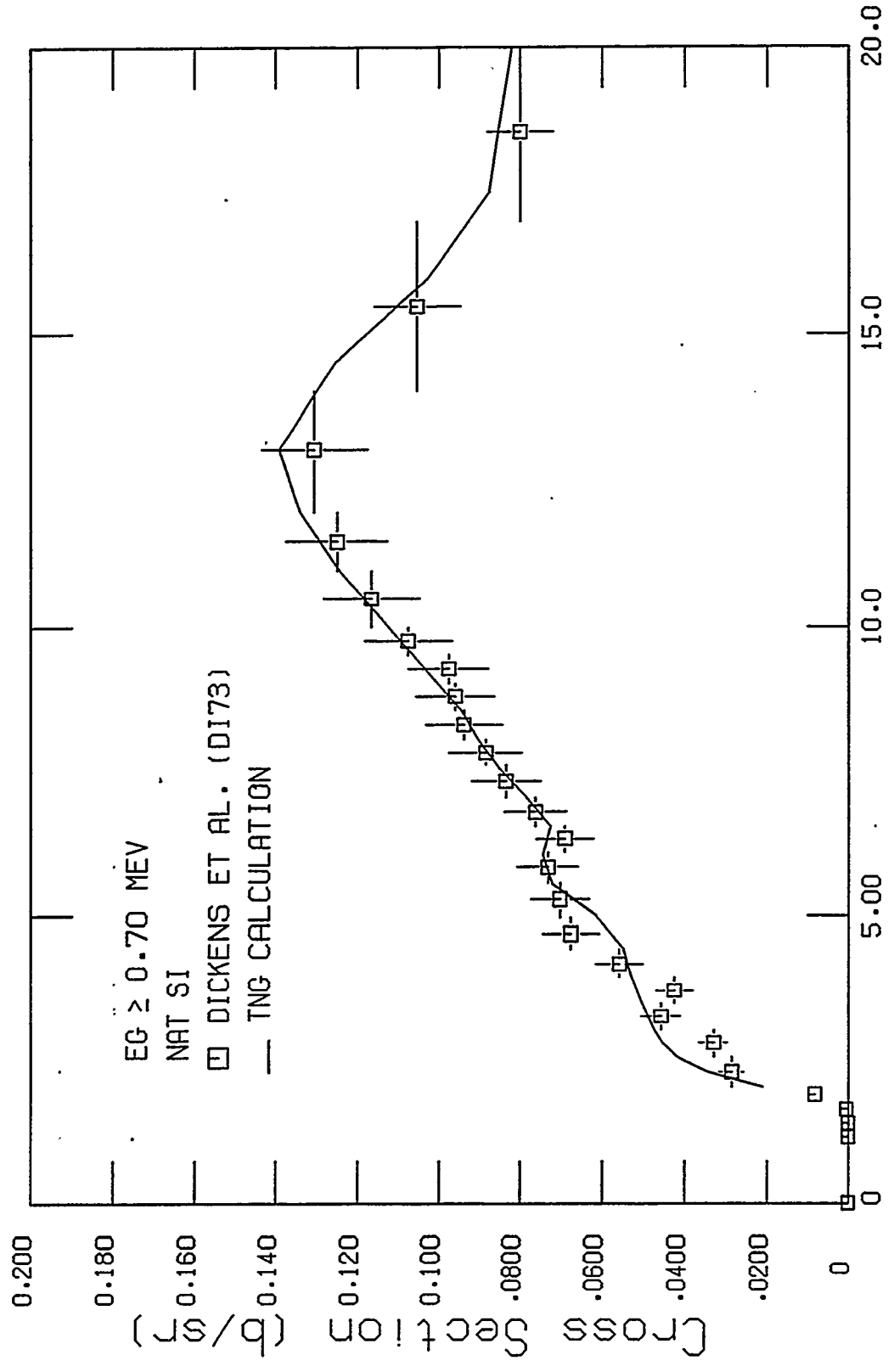

Fig. 65. Comparison of calculated and experimental integrated yield of secondary gamma rays with $E_\gamma \geq 0.7$ MeV as a function of incident neutron energies.

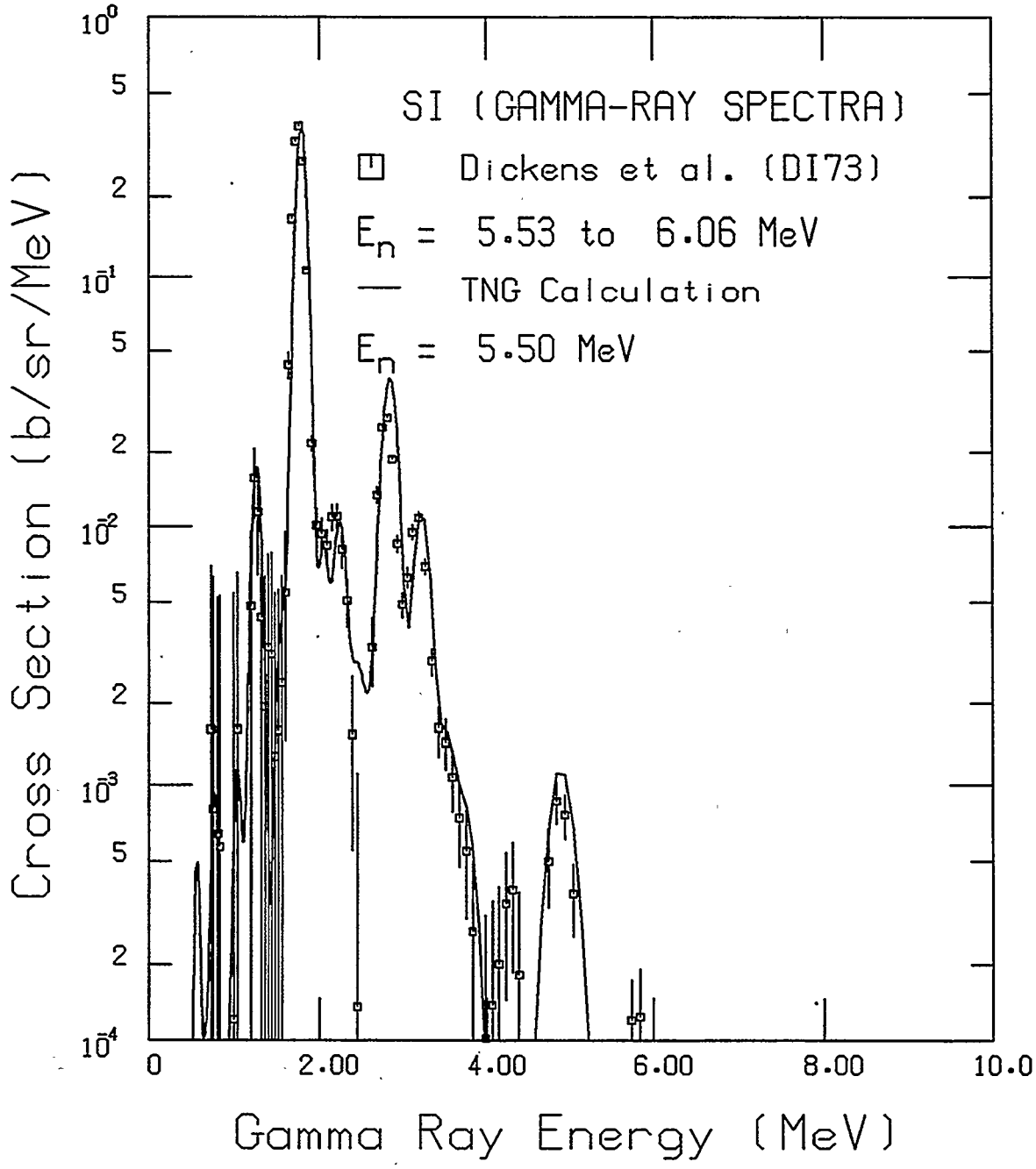

Fig 66. Secondary gamma-ray spectra vs gamma-ray energy from the TNG calculation (incident energy E_n = 5.5 MeV) compared with the data of Dickens et al. (DI73).

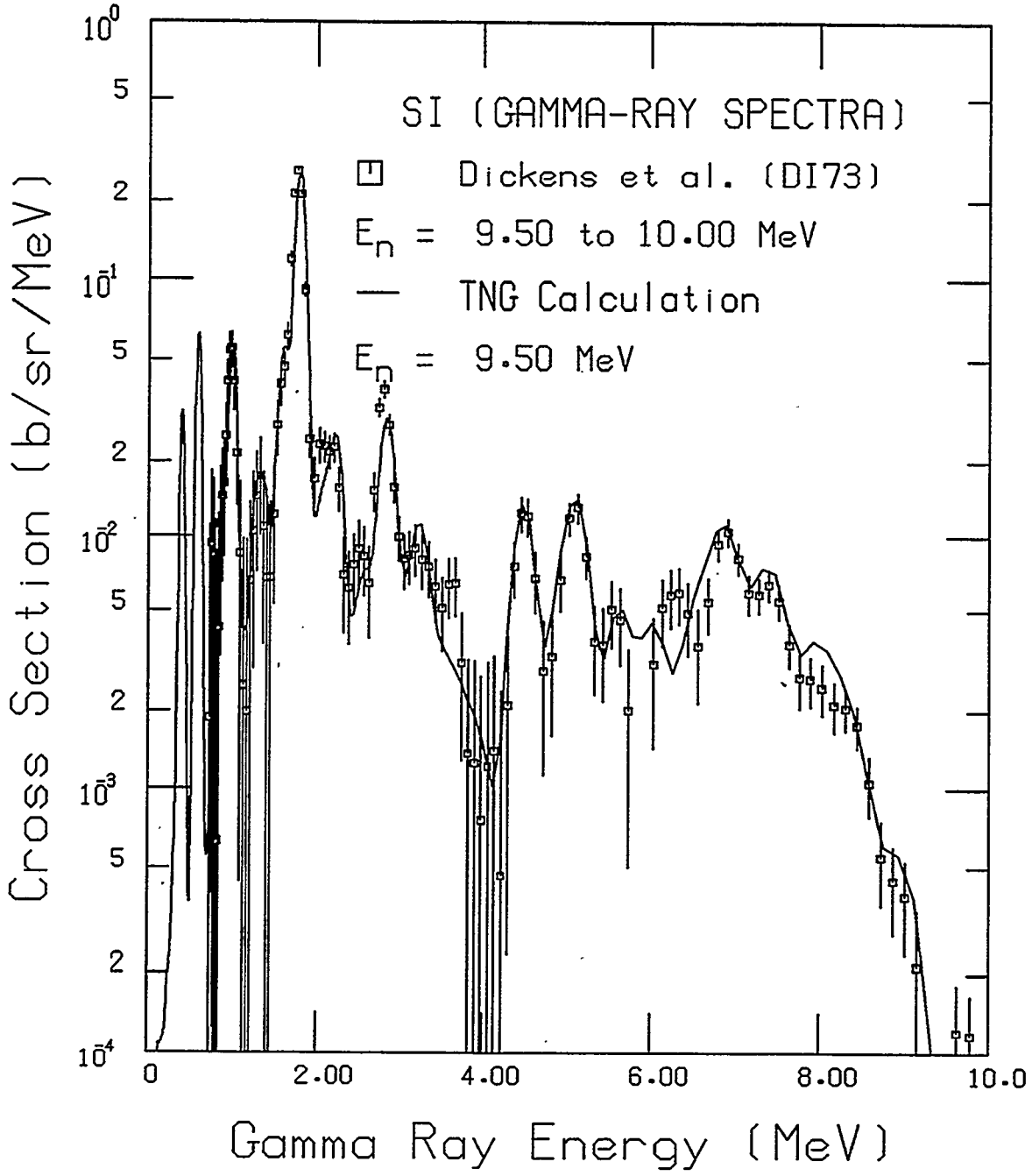

Fig 67. Secondary gamma-ray spectra vs gamma-ray energy from the TNG calculation (incident energy E_n = 9.5 MeV) compared with the data of Dickens et al. (DI73).

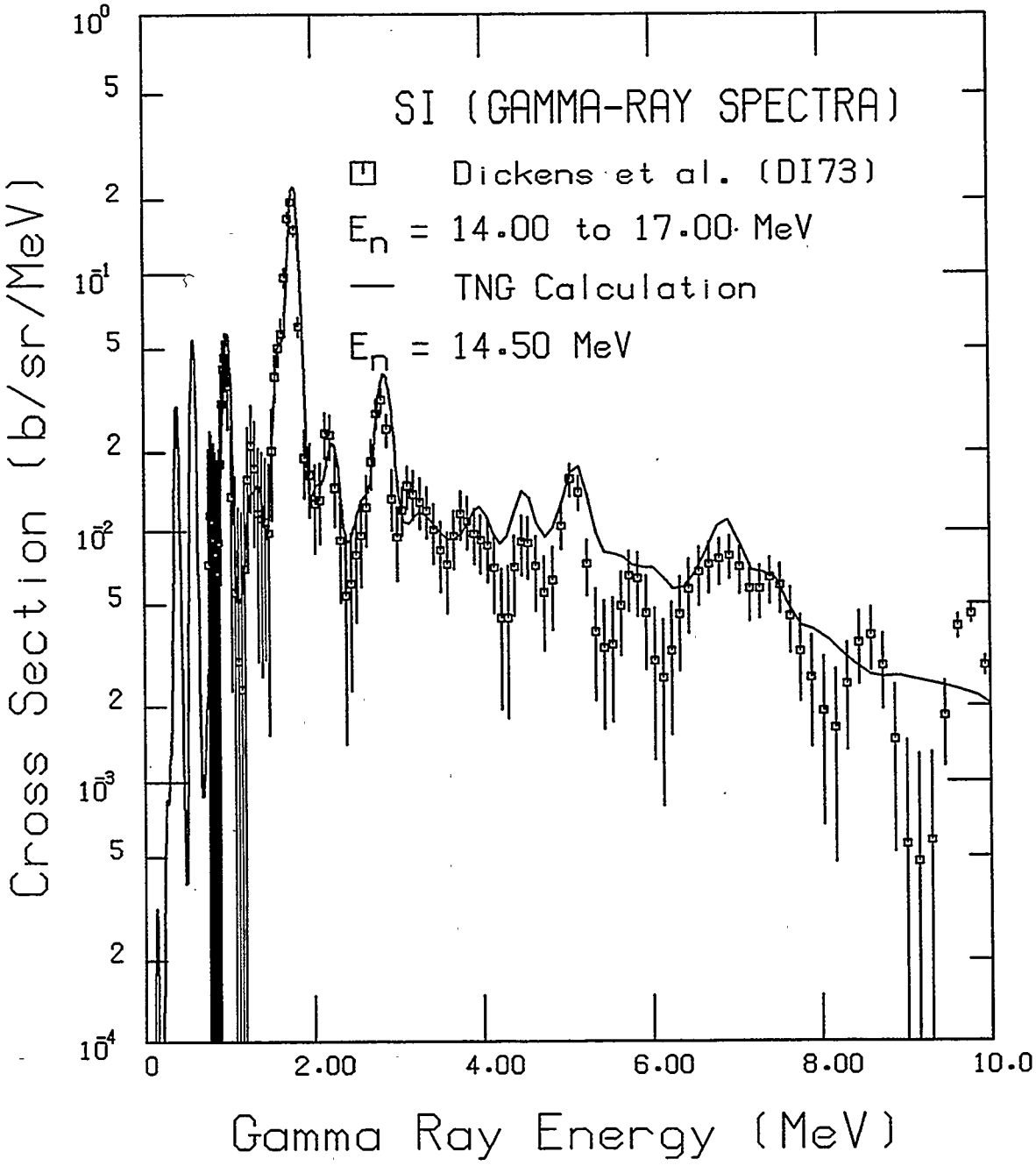

Fig. 68. Secondary gamma-ray spectra vs gamma-ray energy from the TNG calculation (incident energy E_n = 14.5 MeV) compared with the data of Dickens et al. (DI73).

ORNL/TM-11825

INTERNAL DISTRIBUTION

1. F. E. Bertrand
2. C. Y. Fu
3-7. D. M. Hetrick
8. C. M. Hopper
9. D. T. Ingersoll
10. M. A. Kuliasha
11-15. D. C. Larson
16-20. N. M. Larson
20-24. L. C. Leal
25. R. W. Roussin
26. R. M. Westfall
27. J. E. White
28. R. Q. Wright
29. Central Research Library
30-31. Laboratory Records (OSTI)
32. Laboratory Records - RC

EXTERNAL DISTRIBUTION

S. E. Berk, Office of Energy Research Reactors and Systems Radiation, ER-5333, U.S. Department of Energy, 1000 Independence Ave. SW, Washington, DC 20585

Dr. E. T. Cheng, TSI Research Corp., 225 Stevens Ave., Suite 203, Solana Beach, CA 92075

D. Cabrilla, U.S. Department of Energy, EM-23, 1000 Independence Avenue, Washington DC 20585-0002

C. Dunford, Bldg. 197D, National Nuclear Data Center, Brookhaven National Laboratory, Upton, NY 11973

S. Ganesan, Head, Nuclear Data Section, Indira Gandhi Centra for Atomic Research, Kalpakkam 603 102, Tamilnadu, India

R. E. MacFarlance, Los Alamos National Laboratory, T2, MS342, Los Alamos, NM 87545

C. I. Nordborg, OECD/NEA, Le Seine St-Germain 12, Boulevard Iles, 92130 Issy-les-Moulineaux, France

Nuclear Data Center, Japan Atomic Energy Research Institute, Tokaimura, Nakagun, Ibaraki-ken 319-11 Japan

Dr. Phillip G. Young, Group T-2, MS B-243, Los Alamos National Laboratory, Los Alamos, NM 87545